Modulation of Mesenchymal Stem Cell Invasion into Decellularized Engineered Tissues

A DISSERTATION

SUBMITTED TO THE FACULTY OF

UNIVERSITY OF MINNESOTA

BY

Nathan Kyle Weidenhamer

IN PARTIAL FULFILLMENT OF THE REQUIREMENTS

FOR THE DEGREE OF

DOCTOR OF PHILOSOPHY

Robert T. Tranquillo, Advisor

June 2013

Acknowledgements

The completion of this dissertation, and all the work leading up to it, was a challenging and rewarding journey. It would not have been possible to complete this journey without a strong support system. I was fortunate enough to have the support of family, friends, colleagues, and mentors, whom I would like to thank here.

I would like to thank my advisor, Dr. Bob Tranquillo. He has provided excellent support in my development as a researcher and has trained me to think about problems critically and in great depth. I can only hope that someday I will be able to think as quickly on my feet as he is able to. I'd also like to thank my advisory committee members, Dr. Dave Odde, Dr. Paolo Provenzano, and Dr. James McCarthy for their feedback and guidance along the way.

Next, I would like to thank my friends and colleagues. My girlfriend, Anna, helped greatly with my transition to Minnesota life, and has always been supportive of my work. She has been patient with me through frustrating times and long hours, and shared my successes as well. I would like to acknowledge my good friends Arun Saini, Jared Hierman, Keith Jamison, and Faisal Hadi, who were always willing to share ideas (and beers). I would like to thank Sandy Johnson, Dr. Zeeshan Syedain, Dr. Justin Weinbaum, and the rest of the Tranquillo lab, who were instrumental in getting me acclimated to a new lab, training me on new techniques (and scolding me when I did things incorrectly), and helping me brainstorm and plan my experiments. I would like to thank my undergraduate students, Ben Hinton, Fluvio Lobo, and Nathan Klair. I wish you the best of luck with your future plans. Again, I really appreciate all your friendship, advice, and comraderie.

Finally, I would like to thank my family. My parents played an instrumental role in my education. As teachers themselves, they understood the importance of an education to my future, and were both encouraging and strict when it came to my studies. They sacrificed a lot to send me to college, support me throughout college, and help me through my transition to the Midwest and beyond. I will always be grateful for their support.

Abstract

Mechanical forces play an important role in shaping the organization and alignment of the extracellular matrix (ECM) in developing and mature tissues, where the organization gives the tissue its unique functional properties. This dissertation will discuss research that is fundamental to the understanding of the interaction of cells with the extracellular matrix (ECM), a concept that is vital to creating functional engineered tissues, such as arteries and heart valves. The work presented is divided into two main focus areas; the influence of mechanical forces on the development of cell and ECM alignment and the influence of ECM alignment and culture conditions on cell invasion.

The first focus area developed a novel method to create and stretch tubular cell sheets by seeding neonatal dermal fibroblasts (nHDF) onto a rotating silicone tube. Fibroblasts proliferated to create a confluent monolayer around the tube and a collagenous, isotropic tubular tissue over 4 weeks of static culture. These silicone tubes with overlying tubular tissue constructs were mounted into a cyclic distension bioreactor and subjected to cyclic circumferential stretch at 5% strain, 0.5 Hz for 3 weeks. Tissue subjected to cyclic stretch compacted axially over the silicone tube in comparison to static controls, leading to a circumferentially-aligned tissue with higher membrane stiffness and maximum tension. In a subsequent study, the tissue constructs were constrained against axial compaction during cyclic stretching. The resulting alignment of fibroblasts and collagen was perpendicular (axial) to the stretch direction (circumferential). When the cells were devitalized with sodium azide before stretching, similarly constrained tissue did not develop strong axial alignment. This work suggests that both mechanical stretching and mechanical constraints are important in determining tissue organization, and that this organization is dependent on an intact cytoskeleton.

The second focus area explored the influence of ECM alignment and culture conditions on human mesenchymal stem cell (hMSC) invasion into decellularized tissues. These studies showed that the soluble factors insulin and ascorbic acid promote the invasion of hMSCs into decellularized engineered tissues. We speculate that this is due to an increase in motility and proliferation of hMSCs when exposed to these factors. Furthermore, hMSC invasion into aligned and non-aligned matrices was not different, although there was a difference in cell orientation between aligned and non-aligned matrices. Finally, we show that, regardless of culture conditions or ECM alignment, hMSCs appear to be differentiating toward a myofibroblast-like phenotype.

Table of Contents

List of Tables

List of Figures

Chapter 1: Introduction

The purpose of this introduction is to orient the reader to the clinical unmet need that motivates research in vascular tissue engineering, summarize design criteria for these replacements, and summarize the basic concept of tissue engineering and relevant advances in the field. More detailed background pertaining to the specific research goals of this thesis are covered in individual chapters.

Background and Overview

Cardiovascular diseases are the leading cause of death in the United States and account for over $500B in direct and indirect health care costs.[1] Although there are many different classifications and causes of cardiovascular disease, the work of the Tranquillo Group has focused on the pursuit of functional replacements for key cardiovascular structures, such as the *coronary arteries* and *heart valves*.

Myocardial infarction (MI) results from the interruption of blood flow to the myocardium due to the occlusion of a coronary artery. If left untreated, the lack of nutrient and oxygen supply to the myocardium can result in necrosis of the cells in the infarcted region, affecting the heart's ability to pump effectively. Perfusion can be restored by placing a stent to open the lumen of the affected coronary artery, or by bypassing the blocked coronary artery with a segment of another artery or vein, a procedure known as coronary bypass grafting (CABG).

The American Heart Association estimates that the incidence of MI in America is 935,000 patients, with approximately 416,000 of these patients needing a CABG

procedure to re-establish blood flow to the coronary arteries.[1] Autologous vessels, such as the saphenous vein (SV) and internal mammary artery (IMA), are the current gold-standard for CABG. However, many patients do not have a suitable vessel due to disease or a previous harvest. Synthetic materials such as expanded polytetrafluoroethylene (ePTFE) and Dacron tend to fail due to acute thrombosis or intimal hyperplasia.[2] The poor success of synthetic materials and the lack of supply of autologous vessels for CABG have motivated our work in the development of a tissue-engineered artery.

Heart valves allow for unidirectional blood flow in the heart. For example, the tricuspid and mitral valves control the flow of blood from the atria to the ventricles of the heart. Similarly, the pulmonary and aortic valves control the flow of blood from the ventricles to the pulmonary and systemic circulation, respectively. Heart valves can become dysfunctional with age and disease, resulting in regurgitation and/or stenosis. If left untreated, valve disease can lead to left ventricular hypertrophy and heart failure.

Every year, more than 100,000 patients in the US need to have a dysfunctional valve replaced with a mechanical or bioprosthetic valve.[3] Both mechanical and bioprosthetic valves have advantages and disadvantages. Mechanical valves have a high durability, but require lifelong anticoagulation to prevent thromboembolism. Bioprosthetic valves do not require long term anticoagulation, but have less durability than mechanical valves, and are prone to calcification and degradation. In addition, both mechanical and bioprosthetic valves are acellular and do not repair, remodel, or grow with the patient. For a complete comparison of the advantages and disadvantages of mechanical, bioprosthetic, and tissue engineered valves, see the review by Mendelson and Shoen.[4] The ability of a prosthetic heart valve to grow is particularly important for

pediatric patients, who may require several heart valve replacements. The inability of current valve replacements to repair, remodel, and grow has motivated our work in tissue-engineered heart valves.

This dissertation will discuss research that is fundamental to the understanding of the interaction of cells with the extracellular matrix (ECM), a concept that is vital to creating functional engineered tissues, such as arteries and heart valves. The work presented is divided into two main focus areas; the influence of mechanical forces and geometric constraints on the development of cell and ECM alignment and the influence of ECM alignment on cell invasion.

Native Tissues

Arteries

Structure

Arteries are the conduits that carry oxygenated blood from the left-side of the heart to the organs of the body. Evaluating an artery in cross-section demonstrates that it is composed of three major layers: the *tunica intima*, the *tunica media*, and the *tunica adventitia* (see Figure 1-1).[5] Each of these layers has its own role in governing the overall function of the artery. An ideal tissue-engineered artery would be able to recapitulate the form and function of these three layers.

The *tunica intima* is comprised of endothelial cells (ECs) and their associated basement membrane. The primary functions of the healthy *tunica intima* is to provide a thromboresistant surface, to regulate diffusion of molecules across the wall of the blood vessel, and to secrete factors that regulate vascular tone and thromboresistance.[6]

The *tunica media* is the largest layer of a muscular artery, and is composed of circumferentially-aligned smooth muscle cells (SMCs) surrounded by a dense ECM composed of aligned collagen, elastin, and proteoglycans. The function of the *tunica media* is to provide mechanical support for the artery against the pressure generated during the cardiac cycle. The SMCs of the *tunica media* are responsible for maintaining vascular tone by contracting or relaxing in response to various factors. SMCs can also synthesize ECM in response to vascular injury.[7]

Figure 1-1: Schematic of native artery structure. The three main layers of the muscular artery are the *tunica intima*, *tunica media*, and *tunica advenitia*.[5]

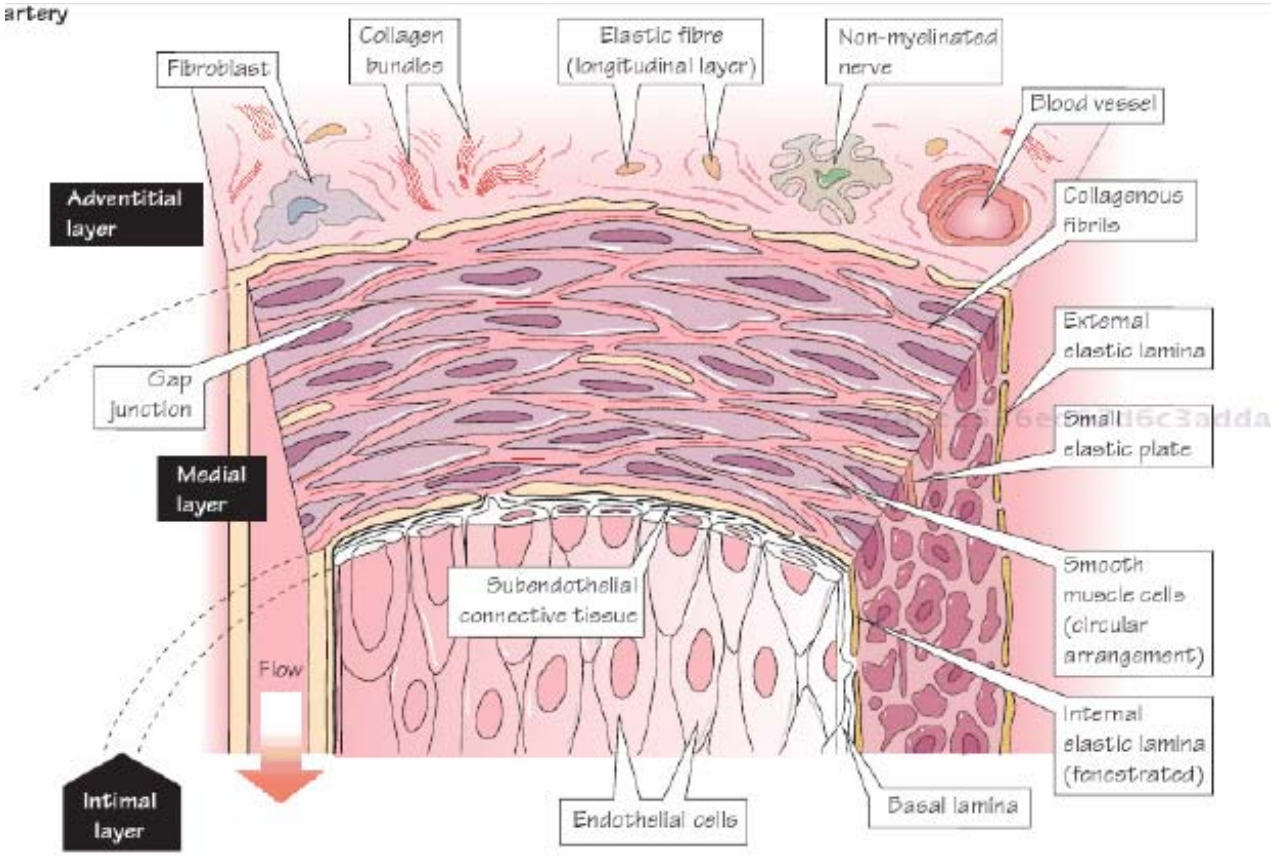

The *tunica adventitia* is the outermost layer of the artery, and is composed of fibroblasts and nerves surrounded by ECM. The collagen-rich ECM of the adventitia prevents overexpansion of the artery during the cardiac cycle and anchors the artery to other nearby structures.

Mechanical Properties

Arteries are exposed to time-varying pressure and shear stress due to the pulsatile nature of blood flow. As such, an artery must be able to withstand these loads without failure or permanent deformation (dilatation). The mechanics of the artery are primarily governed by the circumferentially-aligned collagen and elastin in the arterial wall. The mechanical properties of the artery are anisotropic and non-linear.[8] For example, the ultimate tensile strength (UTS) and Young's modulus of a ovine femoral artery are ~3.5 times higher in the circumferential direction than in the radial direction[9]. Furthermore, it is thought that the ECM of the *tunica media* largely dominates the mechanical response of the artery, except under large extensions, where there is a substantial contribution from the ECM of the *tunica adventitia.*[10,11]

Each ECM component within these layers has its own, unique mechanical contribution that determines the overall mechanical response of the artery. For example, collagen provides the high tensile strength of the artery and engages at higher strains, whereas elastin provides the compliance of the artery at low strain.[10,12] The properties of collagen and elastin proteins will be briefly discussed below.

Collagen

Collagen is the primary load-bearing protein in the human body. The load-bearing capacity of collagen is provided by its ability to form a hierarchy of increasingly organized structures. Collagen is a trimer formed from the assembly of individual collagen polypeptide chains into a stable triple-helix configuration. The mechanical and thermal stability of collagen is attributed to the high percentage of glycine residues in the polypeptides, which permits the close "bundling" of the triple-helix, as well as facilitates hydrogen-bonding with other collagen molecules to form collagen fibrils and fibers.[13,14]

Collagen is processed within the cell as its inactive form, procollagen. After transcription, proline residues are hydroxylated by the enzyme prolyl-4-hydroxylase (P4H) in the presence of the co-factor ascorbic acid (vitamin C), and procollagen is secreted by the cell. After secretion, the extracellular cleavage of the N- and C-terminal ends allows for rapid self-assembly of collagen into fibrils. Finally, collagen fibrils can be stabilized via cross-linking. This cross-linking is facilitated by the enzyme lysyl oxidase to form mature insoluble, collagen fibers.

Elastin

Elastin provides an artery with its compliance, and prevents vascular dilation (creep) from occurring in response to cyclic loading. It is thought that the elastic recoil of elastin fibers is provided by hydrophobic interactions between elastin monomers, which prefer to aggregate when not under strain.[13] Elastin is secreted by the cell as its globular form, tropoelastin. Although less understood, it is thought that a series of complex interactions with proteins such as fibrillins, fibulins, micro-fibril associated-glycoproteins (see Wagenseil and Mecham for a complete review) facilitate alignment,

cross-linking by lysyl oxidase, and assembly of insoluble elastin on microfibrils.[15] Fibrillar elastin in tissue-engineered arteries and valves is often minimal, and improving the production of elastin is an active area of research.

Design Criteria for Tissue Engineered Arteries

A tissue engineered artery should closely mimic the structure and function of the native artery. It should have a *tunica intima* consisting of a stable endothelium with associated basement membrane to provide a non-thrombogenic and non-immunogenic surface. Upon implantation, there should be little platelet adhesion/activation and no acute thrombus formation. Furthermore, there should be no adverse tissue remodeling due to a chronic immune response. It should have a *tunica media* and *tunica intima* composed of smooth muscle cells and fibroblasts surrounding a dense ECM of collagen and elastin. Ideally, these cells should be able to repair and remodel the existing ECM and respond to physiological signals. The mechanical properties of this ECM should match that of a native artery, including the compliance, burst pressure, and suture retention strength. The tissue engineered artery should be able to be handled and manipulated by a surgeon, as well as be free from contamination upon implantation. See Table 1-1 for an estimate of mechanical design criteria with literature references.

Design Criteria	Role/Measurement	Requirement
Non-thrombogenic, non-immunogenic, sterile	A vascular graft must not initiate the formation of a thrombus and must not cause inflammation or an improper immune response. The graft must remain patent and without stenosis.	Non-thrombogenic: confluent endothelial cell layer formed in vivo. Long term patency Non-immunogenic: No signs of chronic inflammation Sterile: Free from microbial contamination
Compliance (%)	Compliance mismatch is associated with intimal hyperplasia and stenosis in vascular grafts.[16] Defined as the change in diameter under a given change in pressure.	3.5% (ovine femoral)[9] 11.5% (human IMA)[17]
Burst Pressure (mmHg)	A vascular graft must not be at risk of failure in vivo. Burst pressure is an indicator of in vivo performance. Defined as the maximum pressure at which the graft fails at a given axial stretch.	1300 mmHg (ovine carotid)[16] 1600 mmHg (human SV)[17] 2500 mmHg (ovine femoral)[9] 3200 mmHg (human IMA)[17]
Suture Retention (g-force)	Measure of the ability of a surgeon to handle the graft and suture it in place. Defined as the amount of force necessary to pull a suture through the graft	138 g (human IMA)[17]

Table 1-1: Design criteria for vascular grafts

Heart Valves

Structure

Heart valves allow for unidirectional blood flow in the heart. There are four valves in the human heart. The tricuspid and mitral valves control the flow of blood from the atria to the ventricles of the heart. Similarly, the pulmonary and aortic valves control

the flow of blood from the ventricles to the pulmonary and systemic circulation, respectively.

Since our goal is to create a tissue-engineered aortic valve, we will limit our discussion about the structure and mechanics of the heart valve to the aortic valve. The aortic valve consists of 3 valve leaflets, the commissures, and the valve root. The valve leaflets are the structures that move during the cardiac cycle, opening during systole to allow flow, and closing during diastole (coaptation). The valve leaflets are connected to each other and the valve root at points known as commissures.

The valve leaflet consists of three layers: the *ventricularis*, the *fibrosa*, and the *spongiosa*.[4,18] The *ventricularis* is the layer closest to the inflow surface (ventricular side) and is composed primarily of elastin. The *spongiosa* is the middle-layer of the valve leaflet and is composed primarily of glycosaminoglycans (GAGs). The *fibrosa* is the layer closest to the outflow surface (aortic side) and is composed primarily of collagen. See Figure 1-2 for macroscopic and microscopic views of the aortic valve. The leaflet contains valvular interstitial cells (VICs) in the interior and valvular endothelial cells (VECs) covering the surface of the valve leaflet. As in arteries, endothelial cells are primarily responsible for maintaining a non-thrombogenic surface and regulating diffusion of solutes. However, there are differences in gene expression and response to shear stress between valvular endothelial cells and aortic endothelial cells.[19,20] VICs are mesenchymal cells that are responsible for secreting and degrading ECM in the valve leaflet.

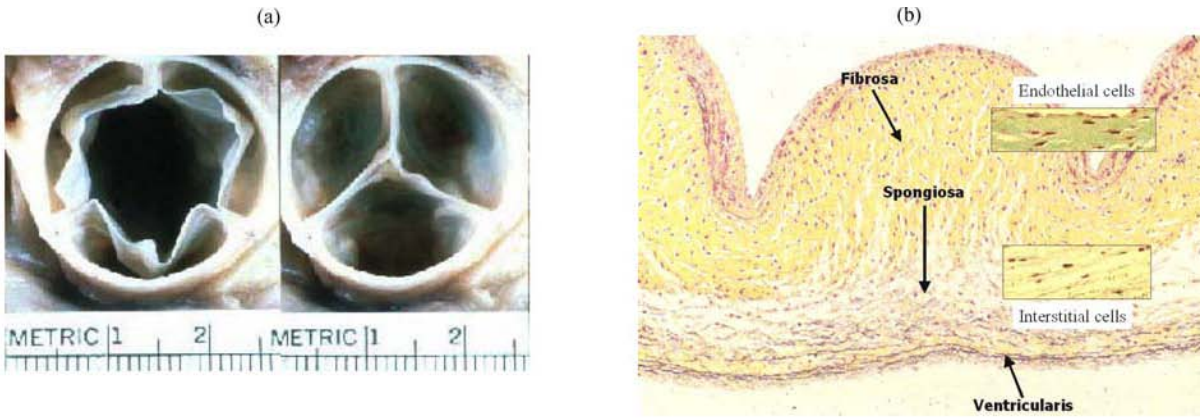

Figure 1-2: Macroscopic and microscopic view of the aortic valve (A) The aortic valve during systole (left) and diastole (right). (B) Histology of the aortic valve leaflet showing the three main layers: *ventricularis*, the *fibrosa*, and the *spongiosa*.[4]

Mechanical Properties

Like arteries, valve leaflets are exposed to time-varying stresses due to the pulsatile nature of the blood flow. The valve leaflets must be able to open rapidly during systole and close securely (without regurgitation) during diastole. Like arteries, the ECM of the leaflet largely determines its mechanical properties. For comment on the individual contribution of collagen and elastin to mechanical properties, see the discussion for the mechanical properties of arteries.

Depending on the time during the cardiac cycle and the location on the leaflet, the leaflet may experience tensile or compressive stresses, as well as shear stress.[4] For example, the *ventricularis* is subjected to tensile stresses during systole. Since the *ventricularis* is primarily composed of elastic fibers, it has high flexibility under low strain, allowing for easy opening of the valve. During systole, the *fibrosa* is subjected to compressive forces. Therefore, the collagen fibers in the *fibrosa* are relaxed (crimped) during systole and support load during diastole. It is thought that the recoil of elastic fibers of the *ventricularis* support the rapid closing of the valve leaflets during diastole.

Finally, the *spongiosa* primarily supports the shear stresses generated during the flexure of the leaflet.

The overall mechanics of the aortic valve are non-linear and anisotropic. The aortic valve is stiffer in the circumferential direction, when compared to the radial direction. At the physiological membrane tension of 60 N/m (true stress of 200 kPa for a leaflet of 300 μm thickness), Christie and Barratt-Boyes found the radial stretch ratio for unfixed porcine aortic valve leaflets to be 1.75 and the circumferential stretch ration to be 1.12.[21] This data is supported by the work of Stella *et al.*, who found the stretch ratio of porcine aortic valve leaflets at the same membrane tension to be ~1.60 in the radial direction, and ~1.20 in the circumferential direction.[22] The uniaxial Young's modulus of the native aortic valve is 15 MPa in the circumferential direction and 2.5 MPa in the radial direction[23]. The uniaxial ultimate tensile strength (UTS) of the native valve is 1.1 MPa in the circumferential direction and 0.6 MPa in the radial direction.[23]

Design Criteria for Tissue Engineered Heart Valves

A tissue engineered aortic valve should closely mimic the structure and function of the native aortic valve. It should be completely coated with a stable endothelium with associated basement membrane to provide a non-thrombogenic and non-immunogenic surface. Upon implantation, there should be little platelet adhesion/activation and no acute thrombus formation. Furthermore, there should be no adverse tissue remodeling due to a chronic immune response. It should have an internal structure similar to the *ventricularis, spongiosa,* and, *fibrosa* of the valve leaflet, being composed of mesenchymal cells (VICs or others) surrounding a dense ECM of collagen and elastin. Ideally, these cells should be able to repair and remodel the existing ECM and not be

prone to calcification. The flexibility of the leaflet should match that of the native valve leaflet and it should be able to withstand many cycles of repeated loaded (assuming a heart rate of 60 bpm, ~30 million cycles per year) The tissue engineered valve should be able to be handled and manipulated by a surgeon, as well as be free from contamination upon implantation

Design Criteria	Role/Measurement	Requirement
Non-thrombogenic, non-immunogenic, sterile	A heart valve must not initiate the formation of a thrombus and must not cause inflammation or an improper immune response.	Non-thrombogenic: confluent endothelial cell layer formed in vivo. Non-immunogenic: No signs of chronic inflammation, free of calcification Sterile: Free from microbial contamination
Flexibility/Stiffness	A heart valve should have similar flexibility in both the circumferential and radial direction to ensure proper performance in vivo. This can be evaluated by achieving the proper stretch ratios at physiological stress levels.	Circumferential stretch ratio of 1.6-1.7 at 60 N/m tension Radial stretch ration of 1.1-1.2 at 60 N/m tension[21,22] Circumferential Young's modulus of ~15 MPa and radial Young's modulus of ~2.5 MPa[23]
Ultimate Tensile Strength (UTS)	A heart valve must not be at risk of failing at physiological loads. This can be measured by measuring the stress at uniaxial failure in each direction	Circumferential UTS of 1.1MPa and radial UTS of 0.6MPa[23]
Fatigue Life	A heart valve must be able to maintain its mechanical properties over many loading cycles.	Maintains flexibility and UTS after many loading cycles (~30 million per year)
Suture Retention (g-force)	Measure of the ability of a surgeon to handle the valve and suture it in place. Defined as the amount of force necessary to pull a suture through the graft material	138 g (human IMA)[17]

Table 1-2: Design criteria for aortic valves

Vascular Tissue Engineering

Tissue engineering seeks to utilize the principles of the life sciences and engineering to create functional replacements for diseased or damaged tissues.[24] Although there are many strategies for engineering artery and valve replacements, they can generally be categorized as follows: (1) Post-cellularized approaches: a decellularized native tissue or biomaterial scaffold is implanted *in vivo* without cells, and relies on environmental signals to recruit host cells, which will degrade and replace the biomaterial scaffold with cell-produced ECM, (2) Pre-cellularized approaches: the appropriate cells are placed within or onto a biomaterial scaffold and cultured *in vitro*, with the biomaterial scaffold being degraded and replaced with cell-produced ECM, (3) the appropriate cells are placed cultured *in vitro* and stimulated to secrete their own ECM, building a 3D structure that can be implanted, avoiding the need for biomaterial degradation. Figure 1-3 outlines the key differences between these techniques.

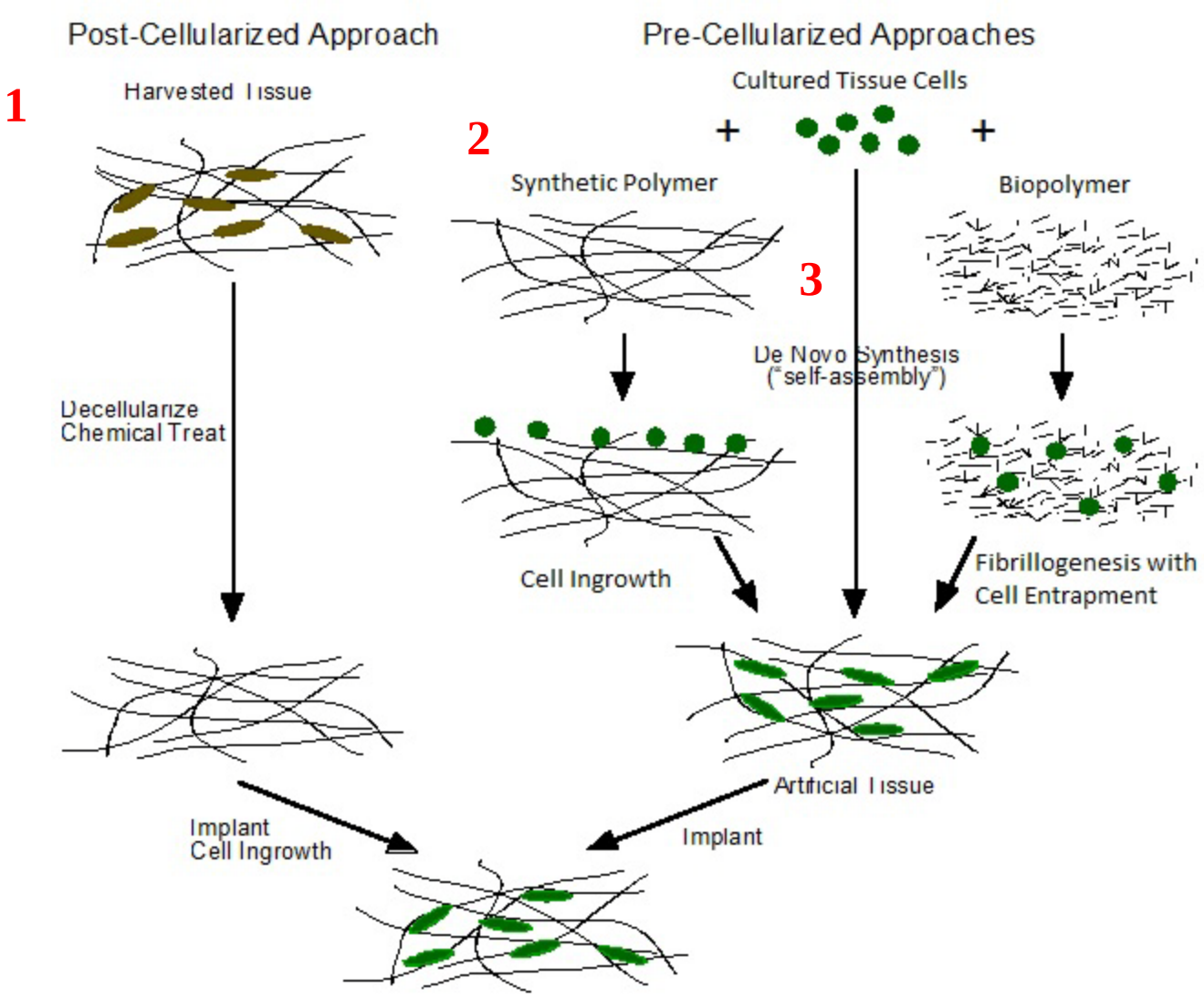

Figure 1-3: Approaches to Tissue Engineering. (1) Post-cellularized approaches: a decellularized native tissue or biomaterial scaffold is implanted *in vivo* without cells, which will degrade and replace the biomaterial scaffold with cell-produced ECM (2) Pre-cellularized approaches: the appropriate cells are placed within or onto a biomaterial scaffold and cultured *in vitro*, with the biomaterial scaffold being degraded and replaced with cell-produced ECM, (3) the appropriate cells are placed cultured *in vitro* and stimulated to secrete their own ECM, building a 3D structure that can be implanted, avoiding the need for biomaterial degradation.

The main similarity between these approaches is the interactions between cells with the biomaterial scaffold and environmental cues. The following sections will briefly

discuss the interaction between cells, scaffolds, and signals in the context of vascular tissue engineering.

Cells

Fibroblasts/Smooth Muscle Cells

Fibroblasts are cells of mesenchymal origin that are responsible for the synthesis of ECM in connective tissues. When cultured in the presence of vitamin C, fibroblasts upregulate the synthesis and deposition of insoluble collagens.[25–27] Vitamin C is necessary for the formation of a stable collagen triple helix, but it has also been shown to upregulate collagen gene expression in fibroblasts,[28–30] suggesting that vitamin C influences fibroblast behavior at pre-translational as well as post-translational mechanisms.

Similar to fibroblasts, arterial smooth muscle cells are cells of mesenchymal origin that are responsible for ECM synthesis in the artery, as well as regulating vascular tone. Like fibroblasts, smooth muscle cells can be stimulated to synthesize secrete insoluble collagens in response to vitamin C.[28,31] Smooth muscle cells also express a variety of proteins essential for the contractile response, including α-smooth muscle actin (αSMA), calmodulin, calponin, and smooth muscle myosin heavy chain (SM-MHC).

The ability of fibroblasts and smooth muscle to secrete collagen in culture makes them a promising cell source for vascular tissue engineering. Fibroblasts derived from human skin (dermal fibroblasts, NHDF) and cells derived from the venous circulation (myofibroblast and smooth muscle cells) are commonly used. These cells have been used for vascular tissue engineering in several different approaches, including, but not limited

to, encapsulation in fibrin, [9,32–36] seeding onto synthetic scaffolds,[37–41] the "de novo" synthesis approach,[42–45] and hybrid approaches utilizing fibrin encapsulation and synthetic scaffolds.[46–48]

Mesenchymal Stromal Cells

Mesenchymal stromal cells (MSCs) are multipotent cells derived from the bone marrow, adipose tissue, and other sources. MSCs are an attractive cell source for tissue engineering because they are easily harvested from the bone marrow or fat tissue, replacing the need for a skin biopsy or vein harvest. The ability to expand rapidly in culture, differentiate into multiple lineages, and to modulate the immune response are also appealing properties of MSCs.

The International Society for Cellular Therapy defines the MSC as a cell that is plastic-adherent, expresses the surface markers CD105, CD73, and CD90, and does not express the hematopoietic markers CD45, CD34, CD14 or CD11b, CD79α or CD19, and the MHC class II antigen HLA-DR.[49] MSCs must also be able to differentiate into osteoblasts, adipocytes, and chondroblasts *in vitro*. While many other surface antigens have been proposed to be markers of the MSC phenotype (CD271+, CD146+, Stro-1+),[50] no one marker uniquely defines the MSC phenotype[51]. Therefore, the ability to differentiate is considered the most stringent criteria, and will be discussed in more detail.

Differentiation

MSCs must be able to differentiate osteoblasts, adipocytes, and chondroblasts *in vitro*. MSCs have also been shown to differentiate into other lineages including fibroblast,[52] smooth muscle cells,[53–55] and endothelial cells.[56] The ability of MSCs to

differentiate into these three mesenchymal lineages was first demonstrated by Pittenger *et.al.*[57] In this study, the differentiation capacity of clonal populations of bone-marrow derived MSCs was evaluated. Adipogenic differentiation of a cell monolayer was induced with dexamethasone, insulin, indomethacin, and 3-isobutyl-1-methylxanthine (IBMX) and evaluated by the uptake of a lipophilic dye (Oil Red O). Osteogenic differentiation was of a cell monolayer was induced with dexamethasone, vitamin C, β-glycerophosphate and evaluated by the staining of calcium deposits (Alizarin Red). Chondrogenic differentiation of a micro-mass pellet was induced with dexamethasone, vitamin C, and TGF-β3 and evaluated by the accumulation of proteoglycans (Alcian Blue). Of the 6 colonies tested, all 6 were capable of osteogenic differentiation, 5 were capable of adipogenic differentiation, and 3 were capable of chondrogenic differentiation. Since this landmark paper, these tests for differentiation have become routine characterization of MSCs.

Immunomodulatory Properties

MSCs have been shown to be immunomodulatory, both *in vitro* and *in vivo*. MSCs do not express MHCII, suggesting that they do not act as a professional antigen-presenting cells.[58] In addition MSCs do not express the costimulatory molecules CD80 and CD86 necessary to illicit a T-cell response. Both autologous and allogeneic human MSCs have been show to be capable of suppressing T-lymphocyte activation and proliferation *in vitro.*[59–61] This immunouppression occurred even in the presence of the appropriate costimulatory molecules CD28 and CD3,[60] or when the MSCs are physically separated from the T-lymphocytes,[59,60] suggesting that MSC suppress the immune response via soluble factors. In addition to the *in vitro* work, allogeneic MSCs have been

transplanted in humans undergoing hematopoietic stem cell transplantation as a means of reducing the effects of graft-versus-host disease (GVHD). The transplants were found to be safe and to reduce the frequency of severe GVHD.[62–64]

Use in Vascular Tissue Engineering

MSCs are potential candidates as a cell-source for tissue engineering since they are capable of differentiating into the lineages found in the native artery or valve, have been shown to be tolerated by the immune system, and are greatly expandable in culture. Several research groups have been interested in the use of MSCs in vascular tissue engineering applications.

MSCs have been used in the fabrication of tissue engineered heart valves by seeding expanded MSCs onto a PGA/P4HB[65] or PLLA[66] scaffold in the geometry of a trileaflet valve. After several weeks of bioreactor culture, the MSCs secreted substantial amounts of collagen and expressed αSMA and vimentin, indicating they had differentiated into a fibroblast-like phenotype. Furthermore, the valve leaflets had uniaxial mechanical properties that were similar to native leaflets. This approach has since been abandoned for heart valve tissue engineering, in favor for direct cell seeding of bone-marrow mononuclear cells prior to implantation, which is thought to be more clinically applicable.[67,68]

MSCs have also been used as matrix-producing cells in tissue engineered arteries. Gong *et. al.*created optimized conditions for culturing MSCs seeded onto PGA scaffolds[69]. The optimized conditions consisted of a proliferation phase, where the MSCs were exposed to 10 ng/ml PDGF-BB in the absence of cyclic stretch and a differentiation

phase, where the MSCs were exposed to 1 ng/ml TGF-β1with cyclic stretch. This optimized protocol led to a more uniform cell distribution throughout the tissue and a collagen content that was 50% of a human native artery, suggesting that MSCs can be used to create tissue-engineered arteries if exposed to the right conditions. MSCs have also been explored as matrix-producing cells in fibrin-based scaffolds[70] and decellularized scaffolds.[71]

The properties of MSCs have also been used to improve the thrombogenicity of vascular grafts. Pre-seeding PLLA scaffolds with MSCs reduced intimal hyperplasia and thrombus formation when grafts were placed in the carotid position of athymic rats for 60 days[72]. The authors suspect that although the MSCs are not retained in the graft long term, the initial presence of the MSCs recruits host cells and prevent early thrombosis, possibly due to the expression of heparan sulfate proteoglycans on the surface of MSCs.

Scaffolds

Polymer Scaffolds

Polymer scaffolds are commonly used in vascular tissue engineering. These polymers are designed to have the fiber size, porosity, and microstructure that mimic the native ECM, degrade at a rate similar to the rate of tissue growth, and provide adequate mechanical properties during the tissue maturation phase. Polyglycolic acid (PGA), its copolymer poly(lactic-co-glycolic acid) (PLGA), and other polyesters are the most frequently used polymers in the literature. These polymers degrade via hydrolysis at the ester bonds, and the degradation rate can be tuned by varying the proportions of monomers.

The Niklason group has developed a tissue engineered artery that consists of SMCs seeded onto a tubular PGA scaffold. They have been able to show that, after 8 weeks of bioreactor culture, cells infiltrate the scaffold and secrete ECM to levels approximately 65% of native.[38,73] Although some PGA polymer remains at the end of the culture time, the graft was composed primarily of SMCs and collagen. These grafts have been successfully implanted into baboons as an arteriovenous shunt[74] and in dogs and pigs as a coronary bypass for 6 months.[66,67] Other groups have developed hybrid approaches to vascular tissue engineering, in which a polylactide (PLA) scaffold is seeded with vascular cells encapsulated within a fibrin carrier. These studies demonstrated uniform cellularity throughout the tissue and collagen content approximately 40% of native after only 3 weeks of bioreactor culture.[46] These grafts have been successfully implanted into the carotid artery of sheep for 6 months.[47]

Another strategy is to skip the *in vitro* culture period by implanting the grafts immediately, with or without cell-seeding. This approach has been used with the degradable scaffolds poly(glycerol sebacate) (PGS)[75] and poly-l-lactide ε-caprolactone (P(CL/LA)).[76] In this case, graft remodeling is thought to occur via an acute inflammatory response, where host macrophages initially invade the tissue, and secrete signals that recruit vascular cells to the graft tissue.[77] The scaffold eventually degrades, leaving a remodeled ECM behind.

Biological Scaffolds

Another option for creating a tissue engineering scaffold is by encapsulating cells in a biopolymer such as collagen or fibrin. Collagen was the first biopolymer scaffold to be investigated, with the seminal work of Weinberg and Bell in 1986.[78] Weinberg and

Bell created a tissue engineered blood vessel (TEBV) by encapsulating bovine smooth muscle cells (SMCs, inner layer) and bovine fibroblasts (outer layer) in a collagen gel. After a culture period of compaction and remodeling, the lumen of the neoartery was then seeded with endothelial cells. Unfortunately, these grafts were unable to withstand arterial pressures. The remodeling of cell-seeded collagen gels has been explored extensively,[79–81] but the mechanical properties required for implantation in the arterial circulation were never achieved. Since then, fibrin has been the preferred scaffold due to its enhanced ability to promote extracellular matrix remodeling.[33,36] Currently, our lab produces tissue engineered arteries and heart valves by entrapping human neonatal dermal fibroblasts (nHDF) or ovine fibroblasts (oDF) in a fibrin gel, which contract and degrades the fibrin matrix while secreting collagen. Constraints imposed on the gel allow for contraction in the radial and axial direction, creating circumferential alignment of the secreted collagen fibers.[36] Improvements in culture conditions[82–84] and mechanical conditioning[9,32,83,85] have led to the development of implantable, fibrin-based arteries[9] and heart valves.[86]

Decellularized/Recellularized Scaffolds

Decellularized heart valves and blood vessels ideally have the prerequisite mechanical properties, ECM content/composition and organization to act as suitable replacements for damaged native tissue. It has been shown that detergent decellularization is an effective technique for removing the majority of cells from the native tissue and has little effect on the collagen/elastin content or burst pressure, although subtle changes to the collagen microstructure may occur.[87–89] However,

nonviable tissue is prone to degradation and calcification and is incapable of growing and remodeling with the patient.[90] Therefore, there is a motivation to ensure adequate recellularization of decellularized tissues.

To date, rapid *in vivo* recellularization of decellularized native tissue has proven difficult. Sheep pulmonary valves that had been decellularized with detergents showed limited *in vivo* recellularization in the valve leaflet after 20 weeks of implantation in juvenile sheep, although there was significant cell infiltration in the valve cusp.[91] The recellularization potential of decellularized porcine pulmonary valves was improved by conjugation of an anti-CD133 antibody to the decellularized tissue. However, significant recellularization was not seen until 3 months,[92] In addition, unpublished results from our own experience with decellularized tissue-engineered vascular grafts suggest that complete recellularization of the graft takes longer than 3 months *in vivo*.

The limited *in vivo* recellularization of decellularized tissue motivates exploring a period of *in vitro* recellularization. Syedain et. al. showed decellularized tissue-engineered leaflet mimics were capable of complete recellularization with MSCs in only 3 weeks of *in vitro* culture.[93] Iop et. al. showed similar recellularization potential with MSCs seeded onto decellularized porcine and human pulmonary leaflets.[94] However, the variables that influence the *in vitro* recellularization potential, such as decellularization protocol, cell culture conditions, and scaffold alignment have yet to be explored.

Cell Sheets ("De Novo Synthesis")

The development of cell-derived tissue from extended culture of plated cells, also known as a "cell sheet," is a popular tissue engineering strategy. Utilizing this approach,

mesenchymal cells such as fibroblasts,[44,95,96] smooth muscle cells,[44,54,97] and mesenchymal stem cells[54,98] have been cultured and stimulated to secrete a collagenous extracellular matrix. After several weeks of culture, the resulting tissue sheet of nominal thickness 20 μm can be removed from the substrate by mechanical peeling or with a temperature change[99] and layered to form thicker, mechanically-robust tissues. Cell sheet technology has been widely used in the development of engineered tissues such as blood vessels, myocardium, cornea, esophagus and trachea.[100]

The use of layered cell sheets to create tissue engineered blood vessels is arguably the most successful technique. After being described by L'Heureux in 1998,[44] the technology has been spun out into a company (Cytograft) and the technology is currently undergoing clinical trials for use as an arteriovenous shunt.[101] Although lacking physiological cell and ECM alignment, these grafts have been shown to be extraordinarily strong; having burst pressures greater than 3000 mmHg[17].

Signals

Growth Factors

Growth factors and supplements are widely used in tissue engineering to increase the proliferation and matrix deposition of fibroblasts and vascular smooth muscle cells. The most commonly used growth factor to increase collagen deposition and organization in fibroblasts and vascular smooth muscle cells is TGF-β1. TGF- β1 is known to be a potent regulator of vascular phenotype and is often associated with the late stages of wound healing, in which the provisional matrix is replaced with mature collagen and contracted to seal the wound.[102] In fibrin-based TEBVs, TGF-β1 has been shown to

increase the collagen content of constructs. The increase in collagen content resulted in a corresponding increase in mechanical properties of the constructs.[33,82,84] One consequence of TGF-β1 stimulation, however, is a decrease in cell proliferation and a shift to a more contractile phenotype. While this response is desirable for the vasoactive response to pharmacological stimulation, it can also lead to over-compaction of the scaffold, which shortens the maturation period of the construct.[103,104] It has also been found that stimulation with TGF-β1 counteracts the benefits derived from cyclic mechanical stretch through inhibition of the p38 signaling pathway.[105]

Alternatively, epidermal growth factor (EGF) can be used to increase mechanical properties without the effects of decreased cell proliferation and increased contractility. Grouf et al. showed that supplementation with 5 ng/ml EGF led to a slight increase in collagen content in fibrin-based constructs in comparison to 1 ng/ml TGF- β1 (49% versus 33% with respect to no growth factor control).[106] EGF also increased cell numbers by 17% and reduced alpha-smooth muscle actin (αSMA) expression, a marker of contractile phenotype.

Mechanical Stimulation / Bioreactors

Mechanical stimulation via bioreactor culture is a common strategy employed to increase the functional properties of engineered tissue. Vascular tissues are constantly subjected to pulsatile flow, leading to time-dependent stresses (both normal and shear stress) and transmural flow Engineers have attempted to mimic the *in vivo* environment by designing systems that can wholly or partially mimic the flow and pressure profiles experienced by the tissue.

Pulsatile flow bioreactors have been shown to increase the mechanical properties of tissue-engineered vascular grafts and valves. These improvements have been shown in bioreactors that allow for transmural flow through the tissue wall[9,38,107] and in bioreactors that do not allow for transmural flow (fluid flow or air pressure is applied through an impermeable tube leading to cyclic circumferential stretch only).[32,85,103,108] These data suggest that both nutrient transport and mechanical stimulation of the vascular cells is important in determining the tissue response to mechanical stimulation.

References

1. Lloyd-Jones D, Adams RJ, Brown TM, et al. Heart Disease and Stroke Statistics—2010 Update. *Circulation*. 2010;121(7):e46–e215.

2. Conte MS. The ideal small arterial substitute: a search for the Holy Grail? *FASEB J*. 1998;12(1):43–45.

3. Vesely I. Heart Valve Tissue Engineering. *Circulation Research*. 2005;97(8):743–755.

4. Mendelson K, Schoen FJ. Heart Valve Tissue Engineering: Concepts, Approaches, Progress, and Challenges. *Ann Biomed Eng*. 2006;34(12):1799–1819.

5. Aaronson PI (Philip I. *The cardiovascular system at a glance*. 4th ed. Chichester, West Sussex ; Malden, MA: Wiley-Blackwell; 2013.

6. Van Hinsbergh VWM. The endothelium: vascular control of haemostasis. *European Journal of Obstetrics & Gynecology and Reproductive Biology*. 2001;95(2):198–201.

7. Owens GK, Kumar MS, Wamhoff BR. Molecular Regulation of Vascular Smooth Muscle Cell Differentiation in Development and Disease. *Physiol. Rev.* 2004;84(3):767–801.

8. Von Maltzahn WW, Warriyar RG, Keitzer WF. Experimental measurements of elastic properties of media and adventitia of bovine carotid arteries. *J Biomech*. 1984;17(11):839–847.

9. Syedain ZH, Meier LA, Bjork JW, Lee A, Tranquillo RT. Implantable arterial grafts from human fibroblasts and fibrin using a multi-graft pulsed flow-stretch bioreactor with noninvasive strength monitoring. *Biomaterials*. 2011;32(3):714–722.

10. Dobrin PB. Mechanical properties of arteries. *Physiol Rev*. 1978;58(2):397–460.

11. Humphrey JD. *Cardiovascular Solid Mechanics*. 2nd ed. New York, NY: Springer-Verlag; 2002.

12. Bank AJ, Wang H, Holte JE, et al. Contribution of Collagen, Elastin, and Smooth Muscle to In Vivo Human Brachial Artery Wall Stress and Elastic Modulus. *Circulation*. 1996;94(12):3263–3270.

13. Alberts B, Johnson A, Lewis J, et al. *Molecular Biology of the Cell*. 4th ed. New York, NY: Garland Science; 2002.

14. Gelse K, Pöschl E, Aigner T. Collagens—structure, function, and biosynthesis. *Advanced Drug Delivery Reviews*. 2003;55(12):1531–1546.

15. Wagenseil JE, Mecham RP. New insights into elastic fiber assembly. *Birth Defects Research Part C: Embryo Today: Reviews*. 2007;81(4):229–240.

16. Crapo PM, Wang Y. Physiologic compliance in engineered small-diameter arterial constructs based on an elastomeric substrate. *Biomaterials*. 2010;31(7):1626–1635.

17. Konig G, McAllister TN, Dusserre N, et al. Mechanical properties of completely autologous human tissue engineered blood vessels compared to human saphenous vein and mammary artery. *Biomaterials*. 2009;30(8):1542–1550.

18. Schoen FJ, Hoerstrup SP. Chapter II.6.10 - Heart Valve Tissue Engineering. In: Buddy D. Ratner, Allan S. Hoffman, Frederick J. Schoen and Jack E. LemonsA2 - Buddy D. Ratner ASH, Jack E. Lemons, eds. *Biomaterials Science (Third Edition)*. Academic Press; 2013:1246–1261.

19. Butcher JT, Penrod AM, García AJ, Nerem RM. Unique Morphology and Focal Adhesion Development of Valvular Endothelial Cells in Static and Fluid Flow Environments. *Arterioscler Thromb Vasc Biol*. 2004;24(8):1429–1434.

20. Butcher JT, Tressel S, Johnson T, et al. Transcriptional profiles of valvular and vascular endothelial cells reveal phenotypic differences: influence of shear stress. *Arterioscler. Thromb. Vasc. Biol.* 2006;26(1):69–77.

21. Christie GW, Barratt-Boyes BG. Mechanical properties of porcine pulmonary valve leaflets: How do they differ from aortic leaflets? *The Annals of Thoracic Surgery*. 1995;60(suppl_2):S195.

22. Stella JA, Liao J, Sacks MS. Time-dependent biaxial mechanical behavior of the aortic heart valve leaflet. *Journal of Biomechanics*. 2007;40(14):3169–3177.

23. Robinson PS, Johnson SL, Evans MC, Barocas VH, Tranquillo RT. Functional Tissue-Engineered Valves from Cell-Remodeled Fibrin with Commissural Alignment of Cell-Produced Collagen. *Tissue Engineering Part A*. 2008;14(1):83–95.

24. Langer R, Vacanti JP. Tissue Engineering. *Science*. 1993;260(5110):920–926.

25. Freiberger H, Grove D, Sivarajah A, Pinnell SR. Procollagen I Synthesis in Human Skin Fibroblasts: Effect of Culture Conditions on Biosynthesis. *J Invest Dermatol*. 1980;75(5):425–430.

26. Grinnell F, Fukamizu H, Pawelek P, Nakagawa S. Collagen processing, crosslinking, and fibril bundle assembly in matrix produced by fibroblasts in long-term cultures supplemented with ascorbic acid. *Experimental Cell Research*. 1989;181(2):483–491.

27. Levene CI, Bates CJ. Ascorbic Acid and Collagen Synthesis in Cultured Fibroblasts. *Annals of the New York Academy of Sciences*. 1975;258(Second Conference on Vitamin C):288–306.

28. Davidson JM, LuValle PA, Zoia O, Quaglino D, Giro M. Ascorbate Differentially Regulates Elastin and Collagen Biosynthesis in Vascular Smooth Muscle Cells and Skin Fibroblasts by Pretranslational Mechanisms. *Journal of Biological Chemistry*. 1997;272(1):345–352.

29. Kurata S, Hata R. Epidermal growth factor inhibits transcription of type I collagen genes and production of type I collagen in cultured human skin fibroblasts in the presence and absence of L-ascorbic acid 2-phosphate, a long-acting vitamin C derivative. *J. Biol. Chem.* 1991;266(15):9997–10003.

30. Kurata S-I, Senoo H, Hata R-I. Transcriptional Activation of Type I Collagen Genes by Ascorbic Acid 2-Phosphate in Human Skin Fibroblasts and Its Failure in Cells from a Patient with α2(I)-Chain-Defective Ehlers-Danlos Syndrome. *Experimental Cell Research*. 1993;206(1):63–71.

31. De Clerck Y A, Jones P A. The effect of ascorbic acid on the nature and production of collagen and elastin by rat smooth-muscle cells. 1980.

32. Syedain ZH, Tranquillo RT. Controlled Cyclic Stretch Bioreactor for Tissue-Engineered Heart Valves. *Biomaterials*. 2009;30(25):4078–4084.

33. Grassl ED, Oegema TR, Tranquillo RT. Fibrin as an alternative biopolymer to type-I collagen for the fabrication of a media equivalent. *Journal of Biomedical Materials Research*. 2002;60(4):607–612.

34. Balguid A, Mol A, Van Vlimmeren MAA, Baaijens FPT, Bouten CVC. Hypoxia Induces Near-Native Mechanical Properties in Engineered Heart Valve Tissue. *Circulation*. 2009;119(2):290–297.

35. Flanagan TC, Cornelissen C, Koch S, et al. The in vitro development of autologous fibrin-based tissue-engineered heart valves through optimised dynamic conditioning. *Biomaterials*. 2007;28(23):3388–3397.

36. Grassl ED, Oegema TR, Tranquillo RT. A fibrin-based arterial media equivalent. *Journal of Biomedical Materials Research Part A*. 2003;66A(3):550–561.

37. Iwasaki K, Kojima K, Kodama S, et al. Bioengineered Three-Layered Robust and Elastic Artery Using Hemodynamically-Equivalent Pulsatile Bioreactor. *Circulation*. 2008;118(14_suppl_1):S52–57.

38. Niklason LE, Gao J, Abbott WM, et al. Functional Arteries Grown in Vitro. *Science*. 1999;284(5413):489–493.

39. Niklason LE, Abbott W, Gao J, et al. Morphologic and mechanical characteristics of engineered bovine arteries. *Journal of Vascular Surgery*. 2001;33(3):628–638.

40. Gui L, Zhao L, Spencer RW, et al. Development of Novel Biodegradable Polymer Scaffolds for Vascular Tissue Engineering. *Tissue Engineering Part A*. 2011;17(9-10):1191–1200.

41. Mol A, Rutten MCM, Driessen NJB, et al. Autologous Human Tissue-Engineered Heart Valves Prospects for Systemic Application. *Circulation*. 2006;114(1 suppl):I–152–I–158.

42. Gauvin R, Guillemette MD, Galbraith T, et al. Mechanical Properties of Tissue-Engineered Vascular Constructs Produced Using Arterial or Venous Cells. *Tissue Engineering Part A*. 2011. Available at: http://dx.doi.org/10.1089/ten.TEA.2010.0613.

43. Gauvin R, Ahsan T, Larouche D, et al. A Novel Single-Step Self-Assembly Approach for the Fabrication of Tissue-Engineered Vascular Constructs. *Tissue Engineering Part A*. 2010;16(5):1737–1747.

44. L'heureux N, Paquet S, Labbe R, Germain L, Auger FA. A completely biological tissue-engineered human blood vessel. *FASEB J*. 1998;12(1):47–56.

45. L'Heureux N, Dusserre N, Konig G, et al. Human tissue-engineered blood vessels for adult arterial revascularization. *Nat Med*. 2006;12(3):361–365.

46. Tschoeke B, Flanagan TC, Koch S, et al. Tissue-Engineered Small-Caliber Vascular Graft Based on a Novel Biodegradable Composite Fibrin-Polylactide Scaffold. *Tissue Engineering Part A*. 2009;15(8):1909–1918.

47. Koch S, Flanagan TC, Sachweh JS, et al. Fibrin-polylactide-based tissue-engineered vascular graft in the arterial circulation. *Biomaterials*. 2010;31(17):4731–4739.

48. Tschoeke B, Flanagan TC, Cornelissen A, et al. Development of a Composite Degradable/Nondegradable Tissue-engineered Vascular Graft. *Artificial Organs*. 2008;32(10):800–809.

49. Dominici M, Le Blanc K, Mueller I, et al. Minimal criteria for defining multipotent mesenchymal stromal cells. The International Society for Cellular Therapy position statement. *Cytotherapy*. 2006;8(4):315–317.

50. Pevsner-Fischer M, Levin S, Zipori D. The Origins of Mesenchymal Stromal Cell Heterogeneity. *Stem Cell Rev and Rep*. 2011;7(3):560–568.

51. Alt E, Yan Y, Gehmert S, et al. Fibroblasts share mesenchymal phenotypes with stem cells, but lack their differentiation and colony-forming potential. *Biology of the Cell*. 2011;103:197–208.

52. Lee CH, Shah B, Moioli EK, Mao JJ. CTGF directs fibroblast differentiation from human mesenchymal stem/stromal cells and defines connective tissue healing in a rodent injury model. *J Clin Invest*. 2010;120(9):3340–3349.

53. Gong Z, Calkins G, Cheng E, Krause D, Niklason LE. Influence of Culture Medium on Smooth Muscle Cell Differentiation from Human Bone Marrow–Derived Mesenchymal Stem Cells. *Tissue Engineering Part A*. 2009;15(2):319–330.

54. Williams C, Xie AW, Emani S, et al. A Comparison of Human Smooth Muscle and Mesenchymal Stem Cells as Potential Cell Sources for Tissue-Engineered Vascular Patches. *Tissue Engineering Part A*. 2012;18(9-10):986–998.

55. Kurpinski K, Lam H, Chu J, et al. Transforming Growth Factor-β and Notch Signaling Mediate Stem Cell Differentiation into Smooth Muscle Cells. *STEM CELLS*. 2010;28(4):734–742.

56. Janeczek Portalska K, Leferink A, Groen N, et al. Endothelial Differentiation of Mesenchymal Stromal Cells. *PLoS One*. 2012;7(10).

57. Pittenger MF, Mackay AM, Beck SC, et al. Multilineage Potential of Adult Human Mesenchymal Stem Cells. *Science*. 1999;284(5411):143–147.

58. Nauta AJ, Fibbe WE. Immunomodulatory properties of mesenchymal stromal cells. *Blood*. 2007;110(10):3499–3506.

59. Nicola MD, Carlo-Stella C, Magni M, et al. Human bone marrow stromal cells suppress T-lymphocyte proliferation induced by cellular or nonspecific mitogenic stimuli. *Blood*. 2002;99(10):3838–3843.

60. Tse WT, Pendleton JD, Beyer WM, Egalka MC, Guinan EC. Suppression of allogeneic T-cell proliferation by human marrow stromal cells: implications in transplantation. *Transplantation*. 2003;75(3):389–397.

61. Le Blanc K, Tammik L, Sundberg B, Haynesworth SE, Ringdén O. Mesenchymal Stem Cells Inhibit and Stimulate Mixed Lymphocyte Cultures and Mitogenic Responses Independently of the Major Histocompatibility Complex. *Scandinavian Journal of Immunology*. 2003;57(1):11–20.

62. Le Blanc K, Rasmusson I, Sundberg B, et al. Treatment of severe acute graft-versus-host disease with third party haploidentical mesenchymal stem cells. *The Lancet*. 2004;363(9419):1439–1441.

63. Lazarus HM, Koc ON, Devine SM, et al. Cotransplantation of HLA-Identical Sibling Culture-Expanded Mesenchymal Stem Cells and Hematopoietic Stem Cells in Hematologic Malignancy Patients. *Biology of Blood and Marrow Transplantation*. 2005;11(5):389–398.

64. Baron F, Lechanteur C, Willems E, et al. Cotransplantation of Mesenchymal Stem Cells Might Prevent Death from Graft-versus-Host Disease (GVHD) without Abrogating Graft-versus-Tumor Effects after HLA-Mismatched Allogeneic Transplantation following Nonmyeloablative Conditioning. *Biology of Blood and Marrow Transplantation*. 2010;16(6):838–847.

65. Hoerstrup SP, Kadner A, Melnitchouk S, et al. Tissue Engineering of Functional Trileaflet Heart Valves From Human Marrow Stromal Cells. *Circulation*. 2002;106(12 suppl 1):I–143–I–150.

66. Ramaswamy S, Gottlieb D, Engelmayr GC, et al. The Role of Organ Level Conditioning on the promotion of Engineered Heart Valve Tissue Development In-Vitro Using Mesenchymal Stem Cells. *Biomaterials*. 2010;31(6):1114.

67. Weber B, Scherman J, Emmert MY, et al. Injectable living marrow stromal cell-based autologous tissue engineered heart valves: first experiences with a one-step intervention in primates. *Eur Heart J*. 2011;32(22):2830–2840.

68. Emmert MY, Weber B, Wolint P, et al. Stem Cell–Based Transcatheter Aortic Valve Implantation: First Experiences in a Pre-Clinical Model. *JACC: Cardiovascular Interventions*. 2012;5(8):874–883.

69. Gong Z, Niklason LE. Small-diameter human vessel wall engineered from bone marrow-derived mesenchymal stem cells (hMSCs). *FASEB J*. 2008;22(6):1635–1648.

70. O'Cearbhaill ED, Murphy M, Barry F, McHugh PE, Barron V. Behavior of Human Mesenchymal Stem Cells in Fibrin-Based Vascular Tissue Engineering Constructs. *Ann Biomed Eng*. 2010;38(3):649–657.

71. Zhao Y, Zhang S, Zhou J, et al. The development of a tissue-engineered artery using decellularized scaffold and autologous ovine mesenchymal stem cells. *Biomaterials*. 2010;31(2):296–307.

72. Hashi CK, Zhu Y, Yang G-Y, et al. Antithrombogenic property of bone marrow mesenchymal stem cells in nanofibrous vascular grafts. *Proceedings of the National Academy of Sciences*. 2007;104(29):11915 –11920.

73. Dahl S, Rhim C, Song Y, Niklason L. Mechanical Properties and Compositions of Tissue Engineered and Native Arteries. *Annals of Biomedical Engineering*. 2007;35(3):348–355.

74. Dahl SLM, Kypson AP, Lawson JH, et al. Readily Available Tissue-Engineered Vascular Grafts. *Sci Transl Med*. 2011;3(68):68ra9–68ra9.

75. Wu W, Allen RA, Wang Y. Fast degrading elastomer enables rapid remodeling of a cell-free synthetic graft into a neo-artery. *Nat Med*. 2012;18(7):1148–1153.

76. Brennan MP, Dardik A, Hibino N, et al. Tissue engineered vascular grafts demonstrate evidence of growth and development when implanted in a juvenile animal model. *Ann Surg*. 2008;248(3):370–377.

77. Roh JD, Sawh-Martinez R, Brennan MP, et al. Tissue-engineered vascular grafts transform into mature blood vessels via an inflammation-mediated process of vascular remodeling. *Proc Natl Acad Sci U S A*. 2010;107(10):4669–4674.

78. Weinberg C, Bell E. A blood vessel model constructed from collagen and cultured vascular cells. *Science*. 1986;231(4736):397–400.

79. Seliktar D, Black R, Vito R, Nerem R. Dynamic Mechanical Conditioning of Collagen-Gel Blood Vessel Constructs Induces Remodeling In Vitro. *Annals of Biomedical Engineering*. 2000;28(4):351–362.

80. L'Heureux N, Germain L, Labbé R, Auger FA. In vitro construction of a human blood vessel from cultured vascular cells: a morphologic study. *J. Vasc. Surg*. 1993;17(3):499–509.

81. Girton TS, Oegema TR, Grassl ED, Isenberg BC, Tranquillo RT. Mechanisms of Stiffening and Strengthening in Media-Equivalents Fabricated Using Glycation. *J. Biomech. Eng.* 2000;122(3):216–223.

82. Neidert MR, Lee ES, Oegema TR, Tranquillo RT. Enhanced fibrin remodeling in vitro with TGF-[beta]1, insulin and plasmin for improved tissue-equivalents. *Biomaterials*. 2002;23(17):3717–3731.

83. Swartz DD, Russell JA, Andreadis ST. Engineering of fibrin-based functional and implantable small-diameter blood vessels. *Am J Physiol Heart Circ Physiol*. 2005;288(3):H1451–1460.

84. Yao L, Swartz DD, Gugino SF, Russell JA, Andreadis ST. Fibrin-Based Tissue-Engineered Blood Vessels: Differential Effects of Biomaterial and Culture Parameters on Mechanical Strength and Vascular Reactivity. *Tissue Engineering*. 2005;11(7-8):991–1003.

85. Syedain ZH, Weinberg JS, Tranquillo RT. Cyclic distension of fibrin-based tissue constructs: Evidence of adaptation during growth of engineered connective tissue. *Proceedings of the National Academy of Sciences*. 2008;105(18):6537–6542.

86. Syedain Z, Lahti M, Johnson S, et al. Implantation of a Tissue-engineered Heart Valve from Human Fibroblasts Exhibiting Short Term Function in the Sheep Pulmonary Artery. *Cardiovascular Engineering and Technology*. 2011;2(2):101–112.

87. Gui L, Muto A, Chan SA, Breuer CK, Niklason LE. Development of Decellularized Human Umbilical Arteries as Small-Diameter Vascular Grafts. *Tissue Engineering Part A*. 2011;15(9):2665–2676.

88. Yazdani SK, Watts B, Machingal M, et al. Smooth Muscle Cell Seeding of Decellularized Scaffolds: The Importance of Bioreactor Preconditioning to Development of a More Native Architecture for Tissue-Engineered Blood Vessels. *Tissue Engineering Part A*. 2009;15(4):827–840.

89. Schaner PJ, Martin ND, Tulenko TN, et al. Decellularized vein as a potential scaffold for vascular tissue engineering. *Journal of Vascular Surgery*. 2004;40(1):146–153.

90. Schoen FJ, Levy RJ. Calcification of Tissue Heart Valve Substitutes: Progress Toward Understanding and Prevention. *The Annals of Thoracic Surgery*. 2005;79(3):1072–1080.

91. Quinn RW, Hilbert SL, Bert AA, et al. Performance and Morphology of Decellularized Pulmonary Valves Implanted in Juvenile Sheep. *The Annals of Thoracic Surgery*. 2011;92(1):131–137.

92. Jordan JE, Williams JK, Lee S-J, et al. Bioengineered self-seeding heart valves. *The Journal of Thoracic and Cardiovascular Surgery*. 2012;143(1):201–208.

93. Syedain ZH, Bradee AR, Kren S, Taylor DA, Tranquillo RT. Decellularized Tissue-Engineered Heart Valve Leaflets with Recellularization Potential. *Tissue Engineering Part A*. 2013;19(5-6):759–769.

94. Iop L, Renier V, Naso F, et al. The influence of heart valve leaflet matrix characteristics on the interaction between human mesenchymal stem cells and decellularized scaffolds. *Biomaterials*. 2009;30(25):4104–4116.

95. Dong-Youn Lee, Jun-Mo Yang, Park K-H. A dermal equivalent developed from fibroblast culture alone: Effect of EGF and insulin. *Wound Repair & Regeneration*. 2007;15(6):936–939.

96. Takahashi H, Nakayama M, Shimizu T, Yamato M, Okano T. Anisotropic cell sheets for constructing three-dimensional tissue with well-organized cell orientation. *Biomaterials*. 2011;32(34):8830–8838.

97. Isenberg BC, Backman DE, Kinahan ME, et al. Micropatterned cell sheets with defined cell and extracellular matrix orientation exhibit anisotropic mechanical properties. *Journal of Biomechanics*. 2012;45(5):756–761.

98. See EY-S, Toh SL, Goh JCH. Multilineage Potential of Bone-Marrow-Derived Mesenchymal Stem Cell Cell Sheets: Implications for Tissue Engineering. *Tissue Engineering Part A*. 2011;16(4):1421–1431.

99. Kumashiro Y, Yamato M, Okano T. Cell Attachment–Detachment Control on Temperature-Responsive Thin Surfaces for Novel Tissue Engineering. *Annals of Biomedical Engineering*. 2010;38(6):1977–1988.

100. Yang J, Yamato M, Shimizu T, et al. Reconstruction of functional tissues with cell sheet engineering. *Biomaterials*. 2007;28(34):5033–5043.

101. Wystrychowski W, Cierpka L, Zagalski K, et al. Case study: first implantation of a frozen, devitalized tissue-engineered vascular graft for urgent hemodialysis access. *J Vasc Access*. 2011;12(1):67–70.

102. Barrientos S, Stojadinovic O, Golinko MS, Brem H, Tomic-Canic M. Growth factors and cytokines in wound healing. *Wound Repair and Regeneration*. 2008;16(5):585–601.

103. Stegemann JP, Nerem RM. Phenotype Modulation in Vascular Tissue Engineering Using Biochemical and Mechanical Stimulation. *Annals of Biomedical Engineering*. 2003;31(4):391–402.

104. Stegemann JP, Nerem RM. Altered response of vascular smooth muscle cells to exogenous biochemical stimulation in two- and three-dimensional culture. *Experimental Cell Research*. 2003;283(2):146–155.

105. Syedain ZH, Tranquillo RT. TGF-Î²1 diminishes collagen production during long-term cyclic stretching of engineered connective tissue: Implication of decreased ERK signaling. *Journal of Biomechanics*. 2011;44(5):848–855.

106. Grouf JL, Throm AM, Balestrini JL, Bush KA, Billiar KL. Differential Effects of EGF and TGF-β1 on Fibroblast Activity in Fibrin-Based Tissue Equivalents. *Tissue Engineering*. 2007;13(4):799–807.

107. Bjork JW, Tranquillo RT. Transmural flow bioreactor for vascular tissue engineering. *Biotechnology and Bioengineering*. 2009;104(6):1197–1206.

108. Williams C, Wick TM. Perfusion Bioreactor for Small Diameter Tissue-Engineered Arteries. *Tissue Engineering*. 2004;10(5-6):930–941.

109. Isenberg BC, Tranquillo RT. Long-Term Cyclic Distention Enhances the Mechanical Properties of Collagen-Based Media-Equivalents. *Annals of Biomedical Engineering*. 2003;31(8):937–949.

Chapter 2: Influence of Cyclic Stretch on Cell and Collagen Alignment in Cell Sheets

Introduction

The development of cell-derived tissue from extended culture of plated cells, also known as a "cell sheet," is a popular tissue engineering strategy. Utilizing this approach, mesenchymal cells such as fibroblasts,[1–3] smooth muscle cells,[2,4,5] and mesenchymal stem cells[5,6] have been cultured and stimulated to secrete a collagenous extracellular matrix (ECM). After several weeks of culture, the resulting tissue sheet of nominal thickness 20 μm can be removed from the substrate by mechanical peeling or with a temperature change[7] and layered to form thicker, mechanically-robust tissues. Cell sheet technology has been widely used in the development of engineered tissues such as blood vessels, myocardium, cornea, esophagus and trachea.[8]

Since both the cells and ECM of cardiovascular tissues exhibit a characteristic alignment,[9] there is a need to develop techniques to generate alignment in cell sheets in order to confer the correct biological and mechanical properties. Techniques such as micro-patterning have been widely used to control cell behavior, influence tissue alignment, and dictate mechanical properties. Williams *et al.* found that 20 μm wide by 5 μm deep grooves on a fibronectin-coated PDMS substrate provided the appropriate environment to allow human mesenchymal stem cells to align with the grooves. Furthermore, tissues that were between 10-15 μm thick also showed alignment with the pattern direction.[4] Similarly, bovine aortic smooth muscle cells cultured on micro-patterned substrates showed alignment in the pattern direction, as well as a higher failure stress and stiffness in the pattern direction, indicating mechanical anisotropy.[4] However,

other studies show that the alignment of the tissue is only maintained in tissues under 20 μm thick, after which the cell layers could not sense the contact guidance cues presented by the patterned substrate, leading to an isotropic microstructure. This result suggests a limit to the number of cell layers that can sense the underlying substrate pattern.[10]

Mechanical strain has also been explored as a means to create alignment in cell sheets. Both static mechanical strain and cyclic mechanical strain have been considered. In one study, fibroblast cell sheets were physically constrained on two edges but allowed to freely compact inward along the other two edges for 21 days.[11] Over the course of the experiment, the cells and ECM aligned parallel to the constrained direction and showed a higher failure stress and stiffness in the aligned direction. Another study compared the difference between static stretch (as above) and cyclic stretch (10% stretch, 1 Hz) on the alignment and mechanical properties of similarly constrained fibroblast cell sheets.[12] This study found that both static stretch and cyclic stretch led to an alignment of the fibroblasts in the stretch direction, but that cyclic stretch improved mechanical anisotropy relative to static stretch. One difficulty in interpreting these studies comes from the fact that the cell sheets were permitted to compact in the direction that was not mechanically stretched. This makes it difficult to determine whether the source of alignment is due to the cells and ECM reorganizing in response to local mechanical strain, stress, and related effects, or if alignment is due to macroscopic compaction of the tissue and resultant reorientation of the cells and ECM.

In this study, we hypothesized that there is an interaction between cyclic mechanical stretch and the mechanical constraints placed on the tissue (i.e. preventing or allowing compaction) that ultimately determines the alignment of the cells and ECM. Since cell

sheets that are grown and stretched on a planar substrate peel off within a week (unpublished data), we decided to form the tissue around a distensible silicone tube since a tubular tissue cannot peel away from its substrate, permitting long-term stretching. In order to investigate the hypothesis, we developed three goals: 1) to develop a technique to seed fibroblasts uniformly onto a tubular substrate, 2) to modify our existing cyclic distention bioreactor[13,14] to accommodate silicone tubing on which a cell sheet is growing, and 3) to determine the influence of long-term cyclic stretch and mechanical constraints on cellular and ECM alignment.

Materials and Methods

Cell Culture

Neonatal human dermal fibroblast (nHDF, Clonetics) were maintained in a 50/50 mixture of Dulbecco's Modification of Eagle's Medium and Ham's F12 cell culture medium (DMEM/F12, Cellgro) supplemented with 15% fetal bovine serum (FBS, Thermo-Fisher Scientific), 100 U/ml penicillin, and 100 μg/ml streptomycin. Cells were incubated at 37°C in 100% humidity and 5% CO2, passaged at ~90% confluency, and harvested for use at passage 9.

Cell Seeding and Static Culture

nHDF were seeded directly onto a segment of 2 mm outer diameter silicone tubing (Vesta, Inc.) that was weighted with a PTFE-coated segment of stainless steel wire (McMaster-Carr) placed through the lumen. The silicone tubing was passively coated with 25 μg/ml of bovine fibronectin (Sigma) for 1 hr prior to cell seeding. The tubing was placed inside a vented 50 cc conical tube (TPP) with 5 ml of nHDF suspension in DMEM/F12 (3:1) with 10% FBS, 100 U/ml penicillin, and 100 μg/ml streptomycin. The

50 cc conical tube was placed horizontally into a CELLROLL System (Integra Biosciences AG) and set to roll at 2 rpm overnight (Figure 2.1a). After the rolling period, the cell-seeded tubing was placed into 6-well plates with a custom-made Teflon insert and maintained in DMEM/F12 (3:1) with 10% FBS, 100 U/ml penicillin, 100 μg/ml streptomycin, 50 μg/ml ascorbic acid (Sigma), 2 μg/ml insulin (Sigma), and 5 μg/ml epidermal growth factor (EGF, Calbiochem) for 4 weeks. Complete medium changes occurred 3 times weekly.

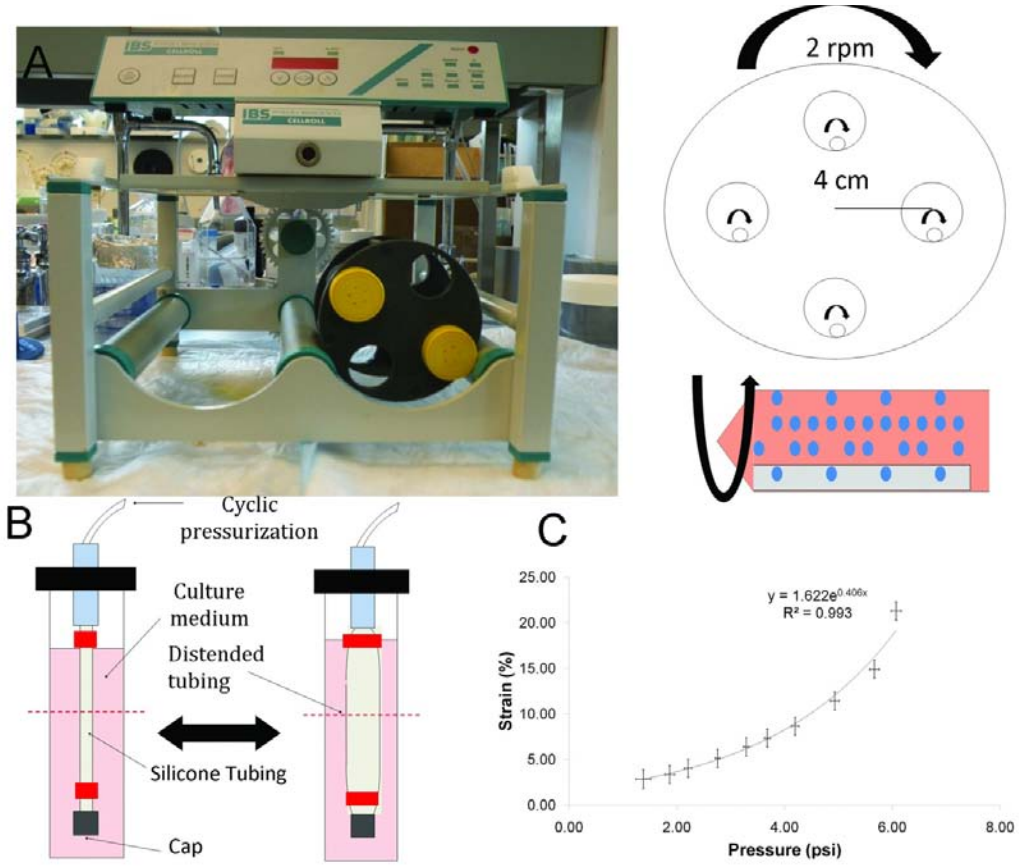

Figure 2.1: (A) Front view and schematic of the CellRoll system used to seed fibroblasts onto silicone tubing. 50 ml conical tubes were placed within the tubing rack and rolled at 2 rpm. The silicone tubing rolled within the 50 ml conical, allowing cells to settle onto the entire area of the tubing. (B) Diagram of the cyclic distension bioreactor used in this study. Silicone tubing is mounted, capped on one end, and subjected to cyclic air pressurization. Red segments indicate where constraints were applied and the dashed red line indicates the plane of histological sectioning.(C) Circumferential strain vs. pressure relation for the silicone tubing used in this study.

Bioreactor Culture

Cell-seeded silicone tubing was mounted into a customized cyclic distension bioreactor previously described,[13] by first sliding the tubing off of the PTFE-coated stainless steel wire (Figure 2.1b). In experiments where the tissue was constrained axially, a 2-0 silk suture (Fine Science Instruments) was tied at the ends of the tissue before sliding the tubing off of the wire. Once removed from the wire, the ends of the

tubing were tied to the barbed ends of a 1/8" male luer connector (Value Plastics Inc.). One end of the luer connector was plugged with a female luer cap and the other end was connected to a pressurized air line. The whole system was placed in a jar containing 60 ml of DMEM/F12 (3:1) with 10% FBS, 100 U/ml penicillin, 100 μg/ml streptomycin, 250 ng/ml Amphotericin B (Cellgro), 50 μg/ml ascorbic acid, 2 μg/ml insulin, and 5 μg/ml epidermal growth factor for 3 weeks, with 70% of the medium changed 3 times weekly. Cyclically-stretched samples were stretched as follows: the frequency and duty of the air cycle were controlled by a solenoid valve connected downstream of a pressure regulator. A laser micrometer was used to measure the diameter of the tube at different inlet air pressures, and a pressure–diameter correlation was recorded, which was used to (Figure 2.1c). The maximum circumferential strain (stretch) magnitude that could be applied reliably was 5%. For all studies, a 5% stretch magnitude and a stretch frequency of 0.5 Hz with 12.5% duty cycle, corresponding to a 0.25 sec stretch time in a 2 sec cycle period, were used. Static controls were mounted into bioreactors and not subjected to cyclic pressurization/stretch.

In order to determine the contribution of cells to any stretch-induced alignment, some samples were devitalized by treatment with sodium azide. 4 week-old cell-seeded tubing was treated with 0.5% sodium azide (Sigma), 10 mM EDTA (Sigma), 1 ug/ml Pepstatin A (Sigma), and 1 ug/ml Aprotinin (Sigma) for one week after being mounted in the bioreactor with sutures for axial constraint, but before stretching was initiated. After the azide treatment period, the tissue was maintained in DMEM with 10% FBS, 100 U/ml penicillin, 100 μg/ml streptomycin until harvest after 3 weeks of stretching. Cyclic stretch experiments were conducted as described above.

Collagen and Cell Quantification

Collagen content was quantified using a hydroxyproline assay previously described, assuming 7.46 mg of collagen per 1 mg of hydroxyproline.[15] The sample volume was calculated using the measured length, width, and thickness of the strips. The cell content was quantified with a modified Hoechst assay for DNA assuming 7.7 pg of DNA per cell.[16] Cell concentrations were calculated as the number of cells per unit volume using the measured dimensions of the strip. Live/Dead staining (Invitrogen) was conducted per the manufacturer's recommendations.

Polarized Light Imaging

Polarized light imaging was conducted as previously described.[17] Briefly, a fiber source (Technispec), focusing lens (Edmund Scientific) and computer-controlled rotation (Mill-Shaf Technologies) of a linear polarizer sheet (Edmund Scientific) provided wide-field illumination of a sample with linearly polarized light of variable transmission axes. Images were acquired in transmission mode at each of 20 rotation angles of the linear polarizer over the range of 0-180 degrees with a CCD device camera (Hitachi) and an effective circular analyzer made from a linear polarizer and a quarter-wave sheet (Oriel). Acquisition and image processing were done in Labview (National Instrument) and Matlab (MathWorks), respectively.

2D Fast Fourier Transform

Alignment of F-actin and collagen was determined using a 2D FFT method.[18] Briefly, a max-projection of the image was imported to ImageJ (NIH). The image was converted to 8-bit grayscale format, and the 2D FFT function was used to generate a FFT image. 2D FFT spectra displayed varying intensities that represented the magnitude of

different frequencies in the images. Isotropic images had circular spectra of bright pixels; anisotropic images had elliptical 2D FFT spectra shifted 90^o from the input image's preferred angle of orientation. This 90^o shift is due to the fact that the 2D FFT revealed rapid changes in pixel intensity, which occurred at high frequency perpendicular to the direction of cell or fiber alignment, while along the direction of cell or fiber alignment, little change was detected and the frequency was thus low. The oval-profile plugin (http://rsbweb.nih.gov/ij/plugins/oval-profile.html) was used to determine the intensity of the FFT as a function of angle over 180^o, with discrete sampling every 1^o. Intensity data was normalized to the minimum intensity and the peak angle was determined as the angle at which the intensity was maximum.

Uniaxial Mechanical Testing

Rings of tissue cut from each sample were tested for tensile properties. The dimensions of the sample were measured using calipers. The thickness of each sample was measured using a 50 g-force probe attached to a displacement transducer. Tissue rings were placed over two T-style grips, attached to the actuator arms and load cell of an Instron MicroBionix (Instron Systems) and straightened with an applied load of 0.005 N. This position was used as the reference length of the ring. Following 6 cycles of 0-10% strain conditioning at 2 mm/min, rings were stretched to failure at the same rate. True strain was calculated based on the natural log of length of the tissue over time divided by the initial length. The stress was calculated as force divided by the initial cross-sectional area. The tangent modulus (E) was determined as the slope of the linear region of the stress-strain curve prior to failure. The peak stress was defined as ultimate tensile strength

(UTS). Membrane stiffness and maximum tension were defined as E and UTS multiplied by thickness, respectively.

Tissue Processing &Histological Staining

Samples were fixed for 3 hrs in 4% paraformaldehyde at 4°C, infiltrated with a solution of 30% sucrose and 5% DMSO at 4C, frozen in OCT (Tissue-Tek) via slurry of pre-chilled isopentane in liquid N_2, and sectioned into 9 µm cross-sections. Samples were stained as follows:

After bringing slides to room temperature and rinsing for 5 min in PBS, slides were fixed for 20 min in formalin and rinsed in distilled water for 5 min. Slides were incubated with Bouin's solution (Sigma) for 1 hr at 56°C and rinsed in tap water for 5 min. Slides were then stained with Weigert's hematoxylin (Sigma) for 5 min and rinsed with distilled water for 5 min. Next, slides were stained with Beibrich Scarlet (Sigma)for 5 min and rinsed with distilled water for 5 min. Slides were then stained in phosphomolybdic acid/phosphotungstic acid solution (Sigma) for 5 min and immediately transferred to 2.5% Fast Green solution for 5 min. Finally, slides were dipped in 1% acetic acid for 1 min and dehydrated as described above for H&E. Slides were imaged with a color CCD camera.

Similarly, after bringing slides to room temperature and rinsing for 5 min in PBS, slides were fixed for 30 min in formalin and rinsed in distilled water for 5 min. Slides were stained with 1% Sirius Red in picric acid (Sigma) for 1 hr, washed in 0.5% acetic acid for 10 min and dehydrated as described above for H&E. Slides were imaged with a color CCD camera with the sample placed between crossed polarizers.

Immunostaining

For staining of tubular cell sheets, samples were left on the silicone tubing and fixed for 1 hr in 4% paraformaldehyde. Samples were cut into segments for histological staining, rinsed with PBS, and blocked in 5% normal donkey serum for 1 hr. Samples were incubated in 5 μg/ml rabbit anti-human collagen I (Novus) overnight at 4 ^{o}C, and rinsed in PBS. Samples were then incubated in 4 μg/ml donkey anti-rabbit Cy3 (Jackson) overnight at 4 ^{o}C. Samples were then permeabilized with 0.1% Triton-X for 1 hr, rinsed in PBS, and incubated in 15 μg/ml Oregon Green-conjugated phalloidin (Invitrogen) overnight at 4 ^{o}C. Samples were visualized with a Zeiss LSM 510 Meta Confocal microscope by taking z-stacks at a spacing of 3-5 μm. The image was "flattened" by taking the maximum projection of the z-stack. Each 500 μm x 500 μm image represents approximately 1% of the sample.

Statistics

For all experiments, n=3 or higher sample number was used, unless otherwise indicated. Statistical significance of differences between groups was determined using Student's t-test for two treatments and one-way ANOVA for more than two treatments with the Fisher's Least Significant Difference (LSD) post hoc test in GraphPad Prism® software for Windows. Kolmogorov-Smirnov tests were conducted in MATLAB®. Error bars in plots represent the standard error of the mean (SEM). Any reference to a difference in the Results and Discussion sections implies statistical significance at the level $p < 0.05$, unless otherwise indicated.

Results

Optimization of Growth Conditions

Culture conditions for growing cell sheets vary widely in the literature. In these studies, nHDF are typically cultured in a ratio of DMEM and Hams's F12, supplemented with 10-20% FBS. The medium always contains ascorbic acid (AA) to promote collagen synthesis, as well as other growth factors to promote cell proliferation. In order to determine the optimal growth media for our nHDF cell sheets, 0.5M nHDF were seeded onto fibronectin-coated silicone discs and cultured for 4 weeks in 3 different medias: DMEM + 10% FBS, DMEM/F12 (1:1) + 10% FBS, and D/F12 (3:1) +10% FBS. All medium contained 100 U/mL penicillin, 100 μg/mL streptomycin. Each of media was supplemented with 50 μg/ml AA to promote collagen synthesis.

Cells cultured in D/F12 (1:1) produced significantly less collagen when compared to DMEM and DMEM (3:1) (Figure 2.2a). Although there was an increasing trend in collagen content with cells cultured in D/F12 (3:1) when compared to DMEM, the difference was not statistically significant. Similar trends occurred with regards to cell proliferation. Cells cultured in D/F12 (1:1) proliferated less when compared to cells cultured in DMEM and DMEM (3:1) (Figure 2.2b). The collagen production per cell was significantly increased in cells cultured in D/F12 (3:1) when compared to D/F12, but no statistical difference was observed between D/F12 (3:1) and DMEM (Figure 2.2c).

A second experiment was designed to determine in the addition of 2 μg/ml insulin and 5 ng/ml epidermal growth factor (EGF) improved collagen production and proliferation in nHDF cell sheets, which have been shown to increase cellularity and collagen production in fibrin-based tissue equivalents (unpublished data). In order to

determine the optimal growth media for our nHDF cell sheets, 0.5M nHDF were seeded onto fibronectin-coated silicone discs and cultured for 4 weeks in 2 different medias: D/F12 (3:1) + 10% FBS + 50 µg/ml AA and D/F12 (3:1) + 10% FBS + 50 µg/ml AA + 2 µg/ml insulin + 5 ng/ml EGF. Although no statistical differences were found in collagen content and cellularity (Figure 2.2d,e), collagen production per cell was increased in the group containing insulin and EGF (Figure 2.2f).

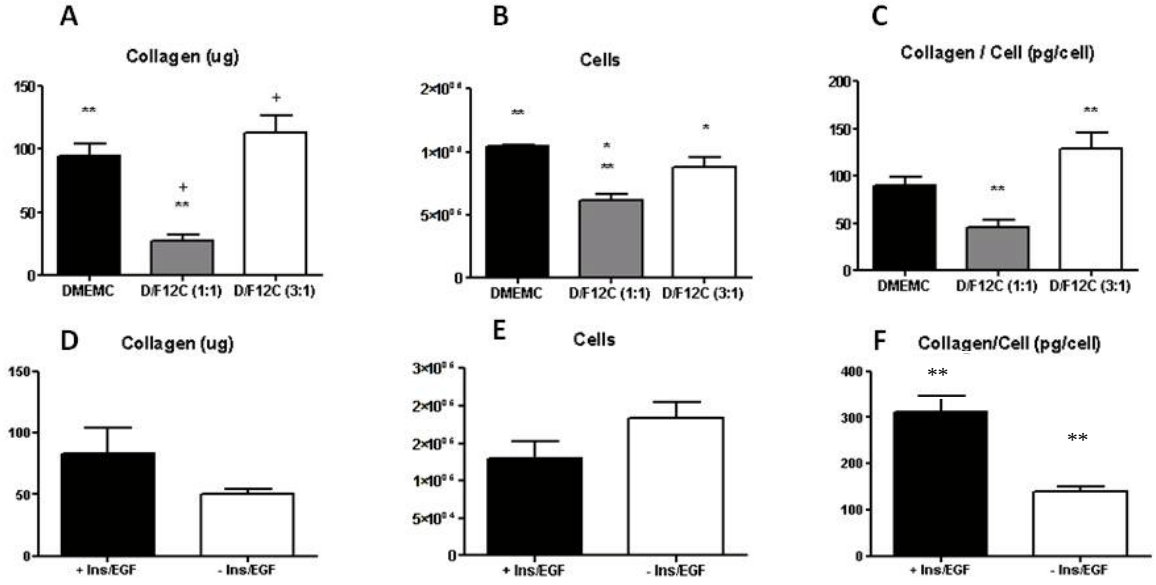

Figure 2.2: Optimization of culture conditions for nHDF cell sheets grown on silicone. (A-C) collagen content, cellularity, and collagen/cell for cell sheets grown in different basal media with 10% FBS and 50 µg/ml AA. (D-F) collagen content, cellularity, and collagen/cell for cell sheets grown in D/F12 (3:1) with 10% FBS and 50 µg/ml AA with or without 2µg/ml Insulin and 5 ng/ml EGF. Paired symbols indicate a statistical difference. * indicates $p < 0.05$, ** indicates $p<0.01$.

Cell-Seeding Optimization

The optimal seeding conditions were found by varying cell seeding density and the time spent in the CellRoll system. At harvest, the silicone tubing was cut into five segments of equal size and the number of adhered cells was quantified. A seeding density

of 1.0 M/ml yielded more adhered cells than a 0.4 M/ml seeding density, but was not statistically different than a 2.0 M/ml seeding density (Figure 2.3a). There was no statistical difference in the number of adhered cells between a 4 hr incubation time and an overnight incubation time (Figure 2.3b). Therefore, all further experiments were conducted with a 1.0 M/ml cell seeding density and were maintained in the CellRoll system overnight.

A macroscopic view of the cell-seeded silicone tubing is shown in Figure 2.3c. The cell distribution and viability along the length of the silicone tubing was determined by Live/Dead staining. The cells were nearly all viable, with only a few dead cells found per field. While the cell distribution along the length was initially non-uniform, a confluent monolayer of cells developed after one week (Figure 2.3d,e)

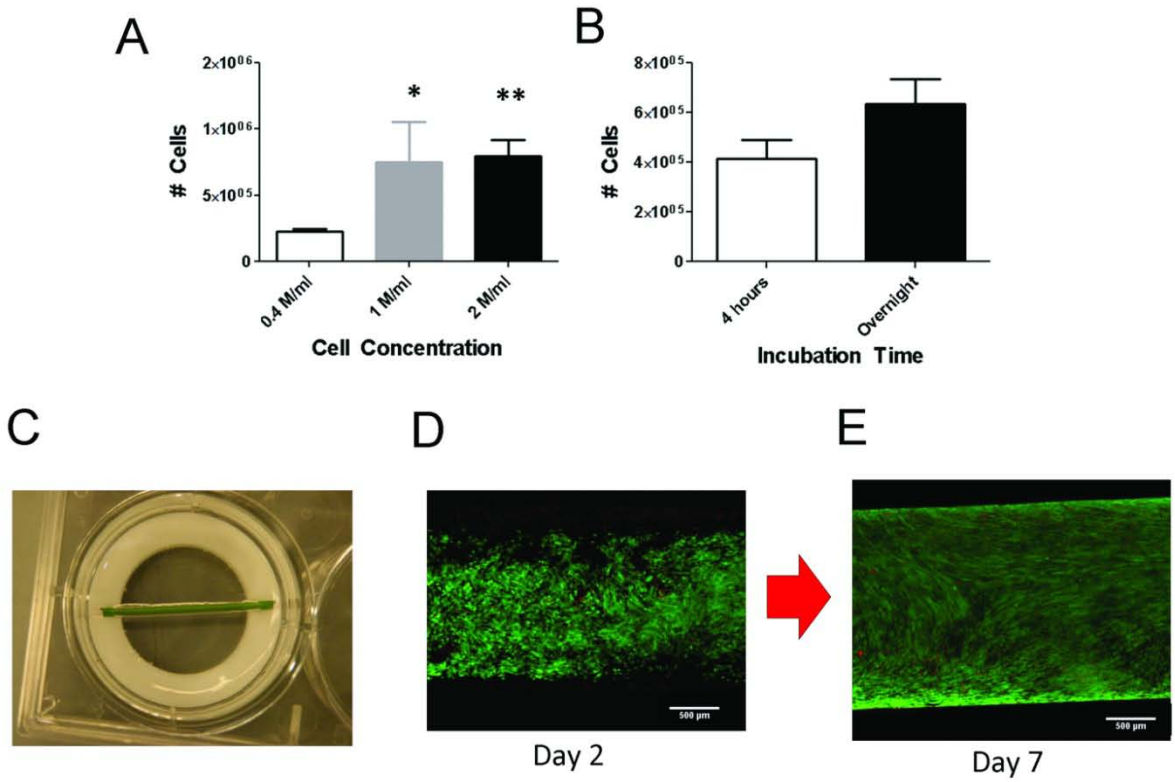

Figure 2.3: Influence of A) seeding density and B) incubation time on the number of cells adhered to the silicone tubing. With the exception of (A), all incubation times were overnight. C) Macroscopic view of cell-seeded silicone tubing. Live/Dead staining of silicone tubing D) immediately after seeding and E) one week after seeding. Scale bar = 500 µm. * indicates $p<0.05$ compared to 0.4 M/ml, ** indicates $p<0.01$ compared to 0.4 M/ml.

Influence of Cyclic Stretch on Unconstrained Tissue

After 4 weeks of static culture, samples were mounted into the cyclic distension bioreactor, without any axial constraint on the tissue. One group of samples was cyclically stretched at 5% circumferential strain at a frequency of 0.5 Hz. The control group was mounted in the bioreactor, but was not stretched. After 3 weeks of stretching, the samples were harvested for analysis.

Macroscopic Appearance

Stretched samples compacted extensively to a final length of 2.6±0.5 mm from an initial length of 20 mm, whereas the static samples compacted to a final length of 9.1±2.1 mm. The stretched samples were also thicker (160±12 μm) than the static samples (79±6 μm). When analyzed under polarized light, the stretched samples were highly aligned in the circumferential direction, as indicated by the red segments of the polarimetric alignment image in Figure 2.4a. Red dashed lines in Figure 2.4a indicate the boundary of the tissue, with the remainder of the area being composed of the silicone tubing. Note that there was no detectable alignment in areas with silicone tubing alone. In comparison, the static samples showed no detectable alignment (Figure 2.4b).

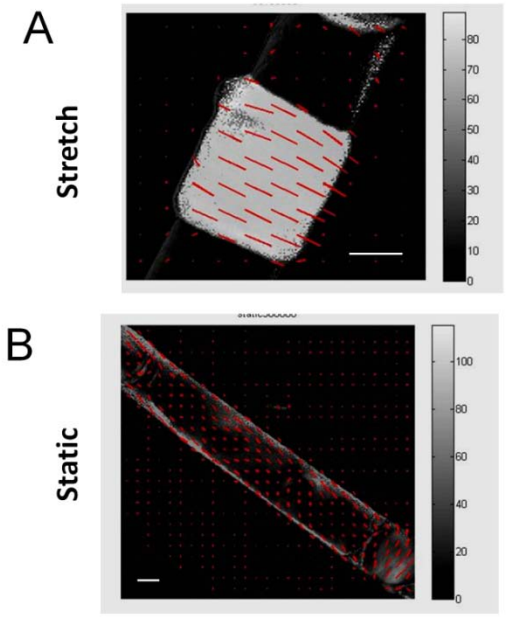

Figure 2.4: Polarized light image of A) stretched and B) static tissue after 3 weeks of bioreactor culture. Red segments indicate the local average direction and strength of alignment (retardation), with the gray level mapped to the retardation at each pixel. Scale bar = 1 mm.

Histology

H&E staining of sections show that cells were uniformly dispersed throughout the tissue in both the stretched and static samples, with the stretched samples being thicker (Figure 2.5a,d) as noted above. Lillie's Trichrome staining revealed the tissue was primarily composed of collagen that was distributed uniformly throughout the tissue (Figure 2.5b,e). Larger collagen fibrils appeared birefrigent under polarized light after staining with picrosirius red. (Figure 2.5c,f).

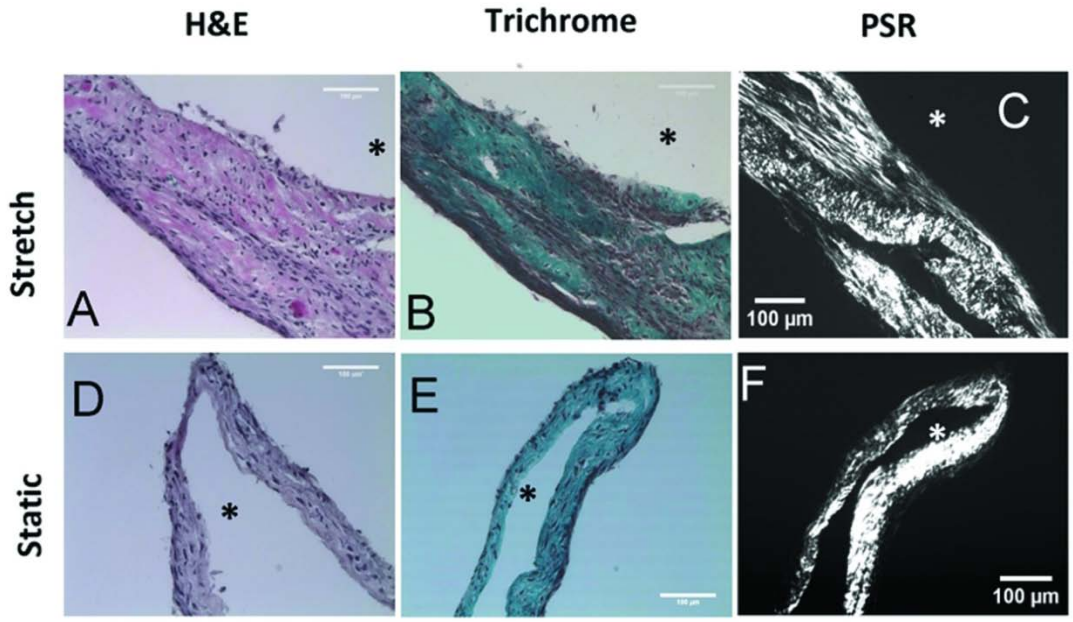

Figure 2.5: H&E, Lillie's Trichrome, and Picosirius red stained sections of unconstrained tissue, stretched (A-C) and static (D-F). Scale bar = 100 µm. * indicates position of the lumen of the tubular cell sheet.

Mechanical Properties

Stretched samples had a higher circumferential membrane stiffness (1068±222 N/m vs 399±58 N/m) and maximum tension (101.4±21.3 N/m vs 42.4±7.8 N/m) than static samples (Figure 2.6a,b). However, the intrinsic properties, the modulus (6.7±1.5

MPa stretch, 5.0±1.0 MPa static) and UTS (642±141 kPa stretch vs 537±83 kPa static), did not show statistical differences between stretched and static samples (Figure 2.6c,d). These results indicate that the collagen network in cyclically stretched tissue was maintained as it compacted, but cyclic stretch at the 5% strain used did not improve intrinsic mechanical properties.

Biochemical Properties

There was no statistical difference in cellularity between stretched and static samples (210±73 M/ml stretch vs. 270±60 M/ml static) (Figure 2.6e). The collagen content as a percentage of total protein was lower in static samples (10.0±0.2% stretch vs. 13.0±0.3% static (Figure 2.6f)). However, there was no difference in collagen concentration (Figure 2.6g) or in the collagen produced per cell (Figure 2.6h) between the stretched and static samples, indicating that there was no intrinsic difference in a cell's ability to produce collagen.

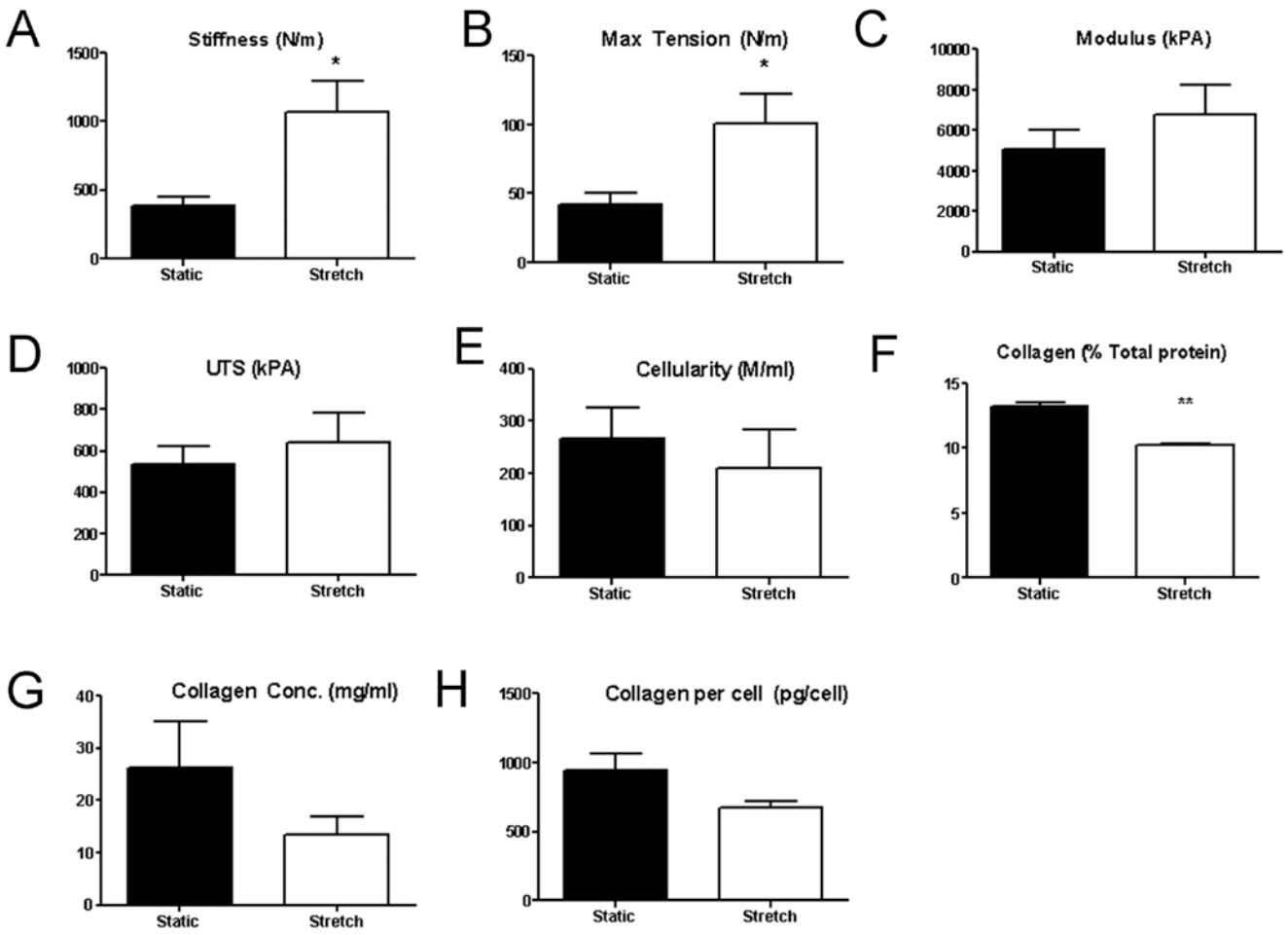

Figure 2.6: Plots of physical properties of unconstrained tissue: A) stiffness, B) maximum tension, C) modulus, D) UTS. Plots of biochemical properties of unconstrained tissue: E) cellularity, F) collagen (% total protein), G) collagen concentration (mg/ml), and h) collagen per cell * indicates $p<0.05$, ** indicates $p<0.01$.

Influence of Cyclic Stretch on Constrained Tissue

After 4 weeks of static culture, samples were mounted into the cyclic stretch bioreactor, and the tissue was constrained from compacting axially (shortening) by tying a suture onto each end. After 3 weeks of stretching at 5% circumferential strain at a frequency of 0.5 Hz, the samples were harvested for analysis.

In studies where the tissue was devitalized with sodium azide treatment, tissues were mounted in the bioreactor in a sodium azide solution for one week prior to the start

of stretching. One group of samples was then stretched at 5% circumferential strain at a frequency of 0.5 Hz. The control group was also mounted in the bioreactor and treated with the sodium azide solution for one week, but was not stretched.

Histology

H&E staining of sections show that cells were uniformly dispersed throughout the tissue in both the stretched and static samples (Figure 2.7a,c). Unlike the unconstrained tissue, axial constraints prevented the tissue from shortening, and the resulting thicknesses were similar. Lillie's Trichrome staining again revealed the tissue was primarily composed of collagen distributed uniformly throughout the tissue (Figure 2.7b,d). There were no obvious differences in picrosirius red staining (data not shown).

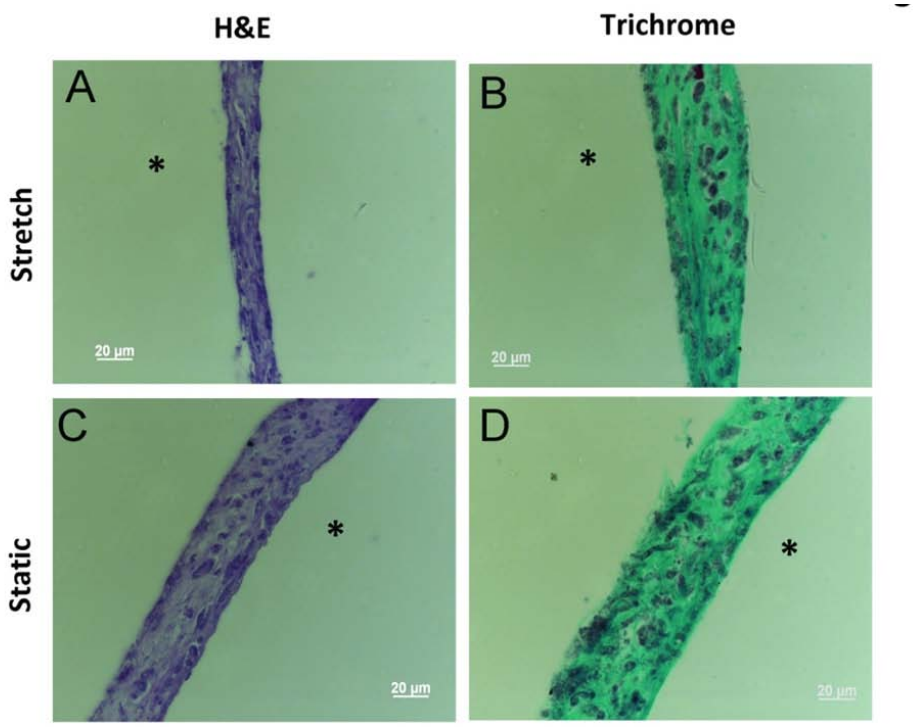

Figure 2.7: H&E and Lillie's Trichrome stained sections of constrained tissue, stretched (A,B) and static (C,D). Scale bar = 20 µm. * indicates position of the lumen of the tubular cell sheet.

Cellular and Extracellular Matrix Alignment

Stretched and static samples were immunostained for Type I Collagen and F-actin, and the alignment directions for each were determined by 2D FFT. When static tissue was prevented from shortening via axial constraint, samples displayed alignment, but when multiple samples were analyzed, there appeared to be no preferred alignment direction (Figure 2.8a,c,g). This is in contrast to samples that were never mounted in the bioreactor (premount), which showed different local alignment directions within the same sample. However, when the tissue was axially-constrained and stretched, only axial alignment was observed (Figure 2.8b,d,g). The Kolmogorov-Smirnov test demonstrated that the sampling of angles in stretched tissue is statistically different from a uniform distribution ($p=0.0018$). The results demonstrate that axial compaction is necessary to allow for circumferential cell and collagen alignment at this magnitude of cyclic stretch.

Next, the tissue was devitalized with a sodium azide treatment just prior to cyclic stretching, in order to determine the role of cytoskeletal tension in the development of the observed axial alignment of collagen with cyclic stretching. Figure 2.8e,f show representative collagen staining in azide-treated static and stretched tissue, respectively. Note that the F-actin staining in Figure 2.8e,f is punctate, indicating cytoskeletal disorganization. In contrast to results for the untreated tissue presented above, the Kolmogorov-Smirnov test demonstrated that the sampling of angles in stretched tissue that was azide treated was statistically indistinguishable from a uniform distribution ($p=0.08$, Figure 2.8f). Notwithstanding, the mean angles for stretched tissue and static controls were different, for reasons that are unclear.

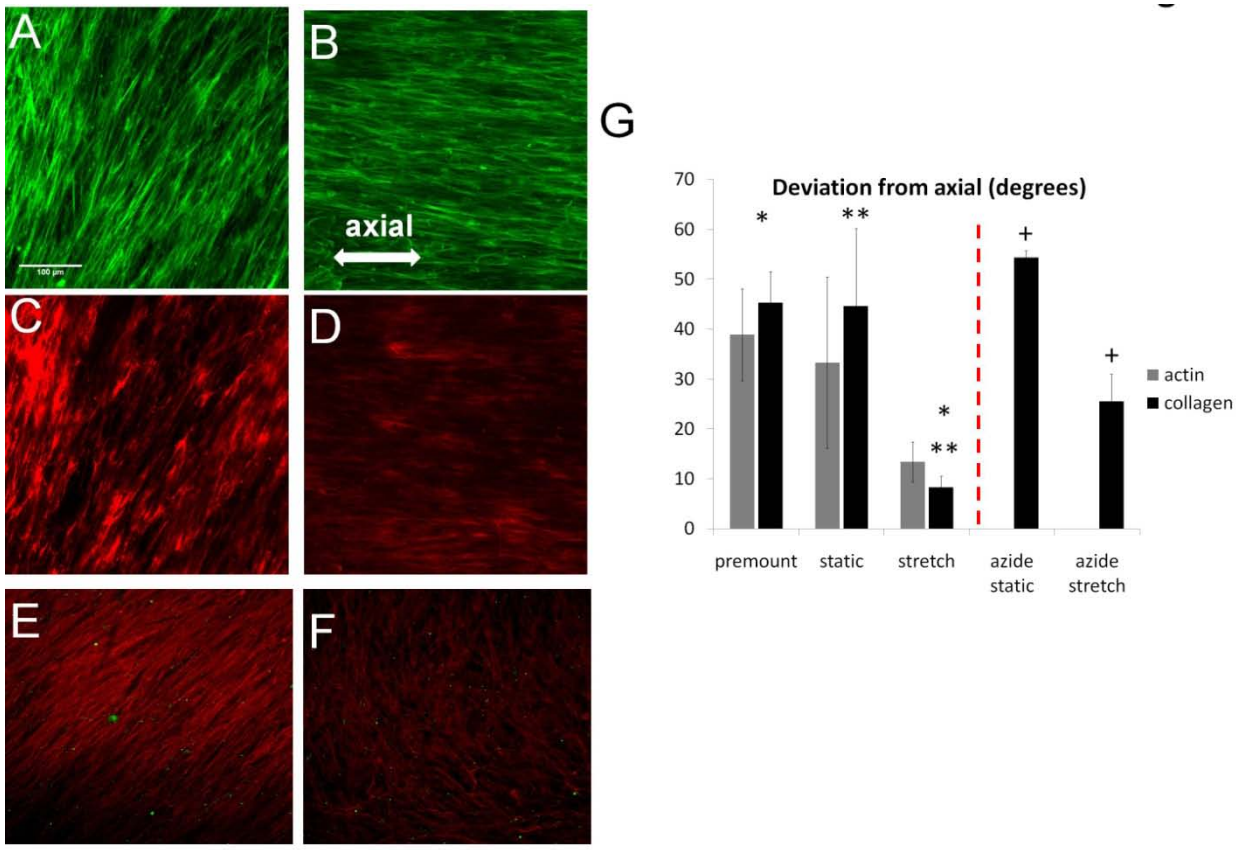

Figure 2.8: Representative images of F-actin alignment in constrained tissue, A) static and B) stretched. Representative images of type I collagen alignment in C) static and D) stretched. Representative images of type I collagen alignment of azide-treated in E) static and F) stretched. G) Quantification of tissue alignment with 2D FFT. Paired symbols indicate a statistical difference ($p<0.05$). Dashed line separates different experiments. Scale bar = 100 µm.

Discussion

In this work, a novel seeding method that allows for direct seeding of viable cells onto the outer surface of a distensible silicone tube was developed. While similar techniques have been used to seed porous biomaterials with high efficiency,[19,20] to our knowledge this is the first study demonstrating successful cell seeding onto the outer surface of a non-porous surface. Although the seeding efficiency is low (~15%), the

nHDF proliferated to form a confluent monolayer around the tube within 1 week and a robust, collagenous tissue with uniform cell distribution in 4 weeks.

After this period of static incubation, the silicone tubes with overlying cell sheets were mounted into the cyclic distension bioreactor and were stretched for 3 weeks (5% circumferential strain at 0.5 Hz), with or without axial constraints to tissue compaction. Tissue that was stretched, but not axially-constrained, shortened extensively, leading to an overall circumferential alignment of the tissue. The circumferential alignment of collagen did not improve intrinsic mechanical properties, consistent with a previous study of fibrin-based constructs with 5% cyclic stretch.[14] It is likely that the magnitude of stretch applied was not sufficient to increase collagen deposition and/or crosslinking in cell sheets. However, improvement in tensile properties with cyclic stretch can be achieved in tissue constructs with higher stretch magnitudes.[13,14,21–24] While the tissue compacted into a thicker structure, the collagen content as a percentage of total protein was slightly decreased due to mechanical stretching, which also may explain the lack of improvement in this study.

We also found that constraining the tissue axially to prevent shortening of the tissue during cyclic stretch prevented the development of circumferential alignment. To the contrary, the alignment of F-actin and collagen was found to be perpendicular to the stretch direction (i.e. axial). This suggests that without the ability to extensively compact the ECM axially (i.e. shorten the length of the tubular tissue), the cells aligned perpendicular to the stretch direction, a phenomenon known as strain avoidance. These results are similar to the response of fibroblasts on stretched membranes.[25]

When the influence of the cytoskeleton was removed by devitalizing the tissue with sodium azide, strong axial alignment of the collagen did not result with cyclic stretch. A similar result was recently reported by Foolen *et al.* when stretching collagen gel slabs containing entrapped cells. In this study, disruption of actin organization with a Rho associated protein kinase (ROCK) inhibitor diminished the strong alignment of collagen fibers seen in the untreated controls.[26] This suggests that, for the given experimental conditions, cytoskeletal tension influences collagen alignment. It also suggests the cells are directing the deposition and/or reorganization of collagen fibers, although it is not clear whether new collagen was being deposited in the direction of cell alignment or the cells were primarily reorganizing collagen existing prior to the stretching.

Several studies have shown that cells embedded in a matrix align with the direction of cyclic stretch. Gauvin *et al.* found that cell sheets maintained at 10% strain (static stretch) or cyclically stretched at 10% strain exhibited cell alignment in the stretch direction.[12] However, in this study the tissue compacted in the direction perpendicular to the stretching, making it difficult to determine if stretching or compaction led to cell alignment. Similarly, cyclic stretch induced alignment in the stretch direction has been reported by Seliktar *et al.* for cells entrapped in collagen gel subjected to 10% cyclic strain.[22,24] However, the collagen gel compacted perpendicular to the stretch direction during the experiment. Similar to a cell sheet, cell induced collagen gel compaction alone can directly cause alignment via a structural reorganization of the fiber network and subsequent cell alignment via contact guidance, so the true determinant of stretch induced alignment was confounded in these studies. In order to circumvent the confounding

factor of compaction, Syedain *et al.* used fully compacted, circumferentially-aligned fibrin-based tissue and subjected it to various circumferential stretching regimens. Increased circumferential alignment of collagen and cells was shown with 10% strain over a period of 5 weeks,[14] indicating that cells can align with the direction of cyclic stretching if they are pre-aligned via a contact guidance field existing in the tissue before stretching begins.

In our study, 5% circumferential cyclic stretch was insufficient to induce circumferential alignment of cells and collagen in a cell sheet, when the ends of the tissue were constrained. Instead, axial alignment of cells (based on F-actin) and collagen was observed. There are reports of cells at the surface of a 3D matrix aligning perpendicular to the stretch direction.[27,28] It is possible that because cell sheets are relatively thin, the cells behave more like cells at the surface of a thicker matrix, where the influence of contact guidance may be less pronounced.

Overall, this study indicates there is a coupling between internal, cell-generated tension associated with mechanical constraints on a tissue and external mechanical stretching, such that both factors need to be accounted for when determining the overall alignment of a tissue subjected to mechanical stretching. Future studies aim to determine the magnitude of mechanical stretching that is necessary to overcome the cell-generated tension, as well as how cell and collagen alignment vary as a function of tissue thickness.

References

1. Dong-Youn Lee, Jun-Mo Yang, Park K-H. A dermal equivalent developed from fibroblast culture alone: Effect of EGF and insulin. *Wound Repair & Regeneration*. 2007;15(6):936–939

2. L'heureux N, Paquet S, Labbe R, Germain L, Auger FA. A completely biological tissue-engineered human blood vessel. *FASEB J.* 1998;12(1):47–56.

3. Takahashi H, Nakayama M, Shimizu T, Yamato M, Okano T. Anisotropic cell sheets for constructing three-dimensional tissue with well-organized cell orientation. *Biomaterials*. 2011;32(34):8830–8838.

4. Isenberg BC, Backman DE, Kinahan ME, et al. Micropatterned cell sheets with defined cell and extracellular matrix orientation exhibit anisotropic mechanical properties. *Journal of Biomechanics*. 2012;45(5):756–761.

5. Williams C, Xie AW, Emani S, et al. A Comparison of Human Smooth Muscle and Mesenchymal Stem Cells as Potential Cell Sources for Tissue-Engineered Vascular Patches. *Tissue Engineering Part A.* 2012;18(9-10):986–998.

6. See EY-S, Toh SL, Goh JCH. Multilineage Potential of Bone-Marrow-Derived Mesenchymal Stem Cell Cell Sheets: Implications for Tissue Engineering. *Tissue Engineering Part A.* 2011;16(4):1421–1431.

7. Kumashiro Y, Yamato M, Okano T. Cell Attachment–Detachment Control on Temperature-Responsive Thin Surfaces for Novel Tissue Engineering. *Annals of Biomedical Engineering*. 2010;38(6):1977–1988.

8. Yang J, Yamato M, Shimizu T, et al. Reconstruction of functional tissues with cell sheet engineering. *Biomaterials*. 2007;28(34):5033–5043.

9. Humphrey JD. *Cardiovascular Solid Mechanics*. 2nd ed. New York, NY: Springer-Verlag; 2002.

10. Pietak A, McGregor A, Gauthier S, Oleschuk R, Waldman SD. Are micropatterned substrates for directed cell organization an effective method to create ordered 3D tissue constructs? *J Tissue Eng Regen Med*. 2008;2(7):450–453.

11. Grenier G, Rémy-Zolghadri M, Larouche D, et al. Tissue Reorganization in Response to Mechanical Load Increases Functionality. *Tissue Engineering*. 2005;11(1-2):90–100.

12. Gauvin R, Parenteau-Bareil R, Larouche D, et al. Dynamic mechanical stimulations induce anisotropy and improve the tensile properties of engineered tissues produced without exogenous scaffolding. *Acta Biomaterialia*. 2011;7(9):3294–3301.

13. Isenberg BC, Tranquillo RT. Long-Term Cyclic Distention Enhances the Mechanical Properties of Collagen-Based Media-Equivalents. *Annals of Biomedical Engineering*. 2003;31(8):937–949.

14. Syedain ZH, Weinberg JS, Tranquillo RT. Cyclic distension of fibrin-based tissue constructs: Evidence of adaptation during growth of engineered connective tissue. *Proceedings of the National Academy of Sciences*. 2008;105(18):6537–6542.

15. Stegemann H, Stalder K. Determination of hydroxyproline. *Clinica Chimica Acta*. 1967;18(2):267–273.

16. Kim Y-J, Sah RLY, Doong J-YH, Grodzinsky AJ. Fluorometric assay of DNA in cartilage explants using Hoechst 33258. *Analytical Biochemistry*. 1988;174(1):168–176.

17. Tower TT, Neidert MR, Tranquillo RT. Fiber Alignment Imaging During Mechanical Testing of Soft Tissues. *Annals of Biomedical Engineering*. 2002;30(10):1221–1233.

18. Ayres CE, Jha BS, Meredith H, et al. Measuring fiber alignment in electrospun scaffolds: a user's guide to the 2D fast Fourier transform approach. *Journal of Biomaterials Science, Polymer Edition*. May;19(5):603–621.

19. Nasseri BA, Pomerantseva I, Kaazempur-Mofrad MR, et al. Dynamic Rotational Seeding and Cell Culture System for Vascular Tube Formation. *Tissue Engineering*. 2003;9(2):291–299.

20. Soletti L, Nieponice A, Guan J, Stankus JJ, Wagner WR, Vorp DA. A seeding device for tissue engineered tubular structures. *Biomaterials*. 2006;27(28):4863–4870.

21. Schutte SC, Chen Z, Brockbank KGM, Nerem RM. Cyclic Strain Improves Strength and Function of a Collagen-Based Tissue-Engineered Vascular Media. *Tissue Engineering Part A*. 2010:

22. Seliktar D, Nerem RM, Galis ZS. Mechanical Strain-Stimulated Remodeling of Tissue-Engineered Blood Vessel Constructs. *Tissue Eng*. 2003;9(4):657–666.

23. Solan A [1], Dahl SLM, Niklason LE. Effects of Mechanical Stretch on Collagen and Cross-Linking in Engineered Blood Vessels. *Cell Transplantation*. 2009;18:915–921.

24. Seliktar D, Black R, Vito R, Nerem R. Dynamic Mechanical Conditioning of Collagen-Gel Blood Vessel Constructs Induces Remodeling In Vitro. *Annals of Biomedical Engineering*. 2000;28(4):351–362.

25. Boccafoschi F, Bosetti M, Gatti S, Cannas M. Dynamic Fibroblast Cultures. *Cell Adh Migr*. 2007;1(3):124–128.

26. Foolen J, Deshpande VS, Kanters FMW, Baaijens FPT. The influence of matrix integrity on stress-fiber remodeling in 3D. *Biomaterials*. 2012;33(30):7508–7518.

27. Balestrini J, Skorinko J, Hera A, Gaudette G, Billiar K. Applying controlled non-uniform deformation for in vitro studies of cell mechanobiology. *Biomechanics and Modeling in Mechanobiology*. 2010;9(3):329–344

28. Rubbens M, Driessen-Mol A, Boerboom R, et al. Quantification of the Temporal Evolution of Collagen Orientation in Mechanically Conditioned Engineered Cardiovascular Tissues. *Annals of Biomedical Engineering*. 2009;37(7):1263–1272.

Chapter 3: Influence of Extracellular Matrix Alignment on Mesenchymal Stem Cell Invasion into Decellularized Tissue

Introduction

Every year, more than 100,000 patients in the US need to have a dysfunctional valve replaced with a mechanical or bioprosthetic valve.[1] Although mechanical and bioprosthetic valves are the current gold standard for valve replacement surgeries, they both have advantages and disadvantages. Mechanical valves have a high durability, but require lifelong anticoagulation to prevent thromboembolism, whereas bioprosthetic valves do not require long term anticoagulation, but have less durability than mechanical valves. [2] In addition, both mechanical and bioprosthetic valves are acellular and do not repair, remodel, or grow with the patient. The ability of a prosthetic heart valve to grow is particularly important for pediatric patients, who may require several heart valve replacements.

Decellularized xenogeneic heart valves have been proposed as an alternative to glutaraldehyde-fixed or cryopreserved heart valves for valve replacements in aortic valve disease. Fixed heart valves often fail due to progressive tissue deterioration and /or calcification of the valve leaflets, where it is thought that the fixation process stabilizes calcifiable structures in the tissue.[3] Without viable cells to maintain homeostasis of the tissue, the calcification occurs unchecked until valve failure. Decellularized tissues aim to improve outcomes by removing these calcifiable structures and providing a biomaterial scaffold for host cell infiltration.

In vivo recellularization of decellularized native valve leaflets has proven difficult. For example, decellularized sheep pulmonary valves implanted in the

pulmonary position of juvenile sheep for 20 weeks showed limited recellularization.[4] A similar result was shown for decellularized pig aortic valves implanted in the aortic position of juvenile pigs for 6 months [5] and decellularized sheep valves implanted in the aortic position of juvenile sheep for 9 months. [6] In all of these cases, recellularization primarily occurred only in the valve root and leaflet nearest the commissures. Very little recellularization was seen near the leaflet free edge.

The limited *in vivo* recellularization of decellularized tissues motivates exploring means to improve recellularization. Several strategies have been proposed to improve the recellularization of decellularized tissues. The recellularization potential of decellularized porcine pulmonary valves was improved by conjugation of the CD133 antibody against endothelial progenitor cells (EPCs) in the decellularized tissue. The CD133 conjugated leaflets attracted more von Willebrand factor positive cells endothelial cells and alpha-smooth muscle actin (αSMA) positive cells than the unconjugated controls. However, significant recellularization was not seen until 3 months.[7] Syedain et. al. showed decellularized tissue-engineered leaflet analogs were capable of complete recellularization with human mesenchymal stem cells (hMSCs) in only 3 weeks of *in vitro* culture.[8] Similarly, Iop et. al. showed *in vitro* recellularization potential with MSCs seeded onto decellularized porcine and human pulmonary leaflets after 30 days. [9]

The variables that influence the *in vitro* recellularization potential of decellularized engineered matrices, such as decellularization protocol, cell culture conditions, and scaffold alignment, have yet to be fully explored. The goal of this work was to assess the influence of two soluble factors commonly used to promote tissue growth, insulin and ascorbic acid, and extracellular matrix alignment on the

recellularization of decellularized engineered tissues by hMSCs. From this point forward, the engineered tissues are referred to as "tissues" and the decellularized engineered tissues are referred to as "matrices".

Materials and Methods

Cell Culture

Neonatal Dermal Fibroblasts

Neonatal human dermal fibroblast (nHDF, Clonetics) were maintained in a 50/50 mixture of Dulbecco's Modification of Eagle's Medium and Ham's F12 cell culture medium (DMEM/F12, Cellgro) supplemented with 15% fetal bovine serum (FBS, Thermo-Fisher Scientific), 100 U/ml penicillin, and 100 μg/ml streptomycin. Cells were incubated at 37°C in 100% humidity and 5% CO2, passaged at ~90% confluency, and harvested for use at passage 9.

Mesenchymal Stem Cells

Human mesenchymal stem cells (hMSC, Lonza) from male donors aged 33 years old and 43 years old were maintained in mesenchymal stem cell growth media (MSCGM, Lonza). Cells were incubated at 37°C in 100% humidity and 5% CO2, passaged at ~80% confluency, and harvested for use at passage 6-7.

Phenotypic Marker Expression of hMSC

hMSCs were received from Lonza at passage 2. Prior to release from quality control, each lot of hMSCs was characterized by flow cytometry and were determined to be $CD105^+$, $CD29^+$, $CD44^+$, $CD14^-$, $CD34^-$, and $CD45^-$. Cells were also tested for *in vitro* differentiation capacity. When chemically induced, hMSCs were found to be

positive for the adipogenic lineage as indicated by neutral lipid uptake, chondrogenic lineage as indicated by collagen type II staining, and osteogenic lineage by calcium mineralization. Upon receipt from Lonza, hMSCs were expanded to passage 4 as described above and stored long-term in liquid nitrogen. Freezing media consisted of 70% mesenchymal stem cell basal medium (MSCBM), 10% DMSO, and 20% FBS.

In Vitro Differentiation of hMSC after Cryopreservation

In vitro differentiation assays were performed on hMSC p6. For adipogenic and osteogenic differentiation, differentiation media was added to the confluent monolayers of cells twice weekly for 3 weeks. For chondrogenic differentiation, differentiation media was added to micromass cell pellets three times weekly for 3 weeks. Micromass cell pellets were formed by centrifuging 250,000 hMSC p6 in a 5cc conical. See Table 3.1 for the composition of the differentiation media.

After 3 weeks of culture, samples were fixed in 4% paraformaldehyde for 10 min at 25°C, washed with PBS, and stained with Alizarin Red S (calcium mineralization, osteogenic differentiation), Oil Red O (neutral lipid uptake, adipogenic differentiation), and Alcian Blue (sulfated proteoglycans, chondrogenic differentiation).

Differentiation	Culture Type	Basal Media	Supplements
adipogenic	confluent monolayer	α-MEM + 10% FBS	1 µM dexamethasone, 5 µg/ml insulin, 60 µM indomethacin, 500 µM IBMX
chondrogenic	micromass cell pellets	D/F12 + 1% insulin, transferrin, selenium	100 nM dexamethasone, 200 µM ascorbate-2-phosphate, 10 ng/ml transforming growth factor β1 (TGF-β1), 1 mg/ml bovine serum albumin (BSA),
osteogenic	confluent monolayer	α-MEM + 10% FBS	100 nM dexamethasone, 200 µM ascorbate-2-phosphate, 10 mM β-glycerophosphate

Table 3.1: Differentiation media composition

Aligned and Non-Aligned Construct Preparation and Culture

A nhDF-seeded fibrin gel was formed by adding thrombin (Sigma) and calcium chloride in 20 mM HEPES-buffered saline to a suspension of nhDF in fibrinogen (Sigma). All components were kept on ice before mixing. The final component concentrations of the cell suspension were as follows: 4 mg/mL fibrinogen, 1.1 U/mL thrombin, 5.0 mM Ca^{2+}, and 1 million cells/mL. Cell suspensions were mixed and poured in a six-well tissue culture plastic plate. In each well, a mold was placed, which consisted of a C-shape (aligned) or O-shaped (non-aligned) 312-stainless (Mc Master Inc.) wire attached to a polyethylene mesh to create an attachment for the fibrin gel (Figure 3.1a) . The six-well plate was pretreated with 5% Pluronic F-127 (Sigma) solution for 1 hour prior to pouring the gel.

After injecting 5 mL of the fibrin-forming cell suspension into the mold cavity, the molds were placed in a humidified incubator and maintained at 37°C, 5% CO_2 for 20 min to allow for gelation. Subsequently, 5 mL of DMEM supplemented with 10% FBS, 100 U/mL penicillin, 100 µg/mL streptomycin, 2 µg/mL insulin, 50 µg/mL ascorbic acid (supplemented DMEM) was added. One day after casting, the molds were detached from the well and 8 molds were transferred to a larger jar with 100 mL of supplemented DMEM and incubated on an orbital shaker for 5 weeks (Figure 3.1b). 70% of the media was changed three times a week.

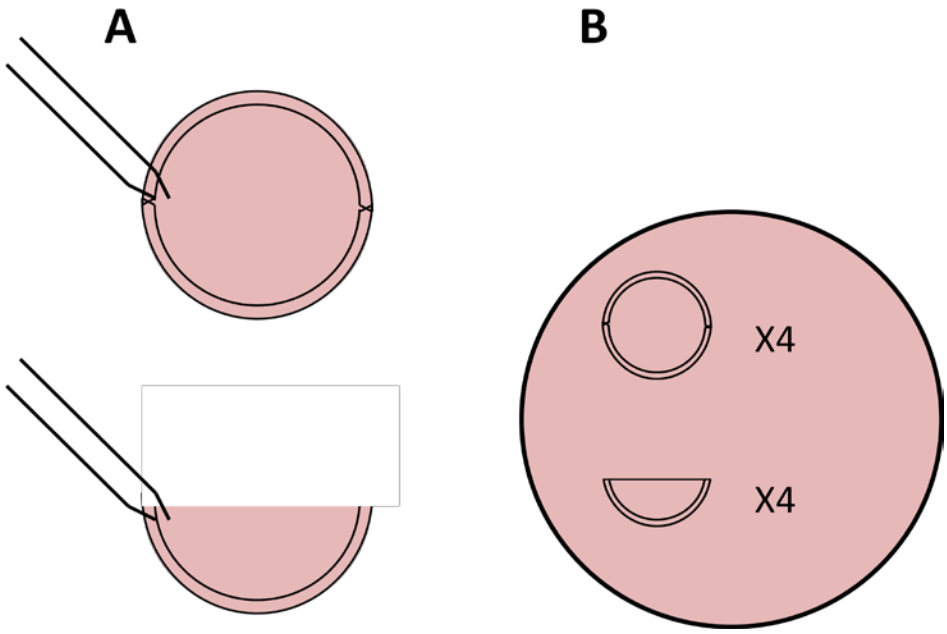

Figure 3.1: Schematic of construct preparation (A) a solution of fibrinogen, thrombin, and nHDF is pipetted into a 5% Pluronics-coated 35mm well containing a C-shaped mold (solid line) or O-shaped mold (dashed line). After overnight culture in the 6-well plate, (B) constructs are removed from the well and placed into a larger jar with 100 ml DMEM + 10% FBS + 50 µg/ml AA + 2 µg/ml insulin, where they are cultured for 5 weeks.

Decellularization

After 5 weeks of culture, constructs were rinsed in phosphate-buffered saline (PBS) and incubated on a shaker for 4 hrs or 24 hrs with 1% sodium dodecyl sulfate (SDS; Sigma). For the 4 hr SDS treatment protocol, the SDS solution was changed hourly. For the 24 hr SDS treatment, the SDS solution was changed at 30 min, 1 hr, and 4 hrs. The matrices were then rinsed in PBS and incubated with 1% Triton X-100 (Sigma) for 30 min. The matrices were extensively washed with PBS for 48 h and incubated in deoxyribonuclease enzyme (Sigma) in the DMEM supplemented with 10% FBS for 4 hrs.

hMSC Seeding onto Decellularized Matrices

Decellularized matrices were transferred to a 6-well plate and incubated in DMEM containing 10% FBS (DMEMC) for 4 hrs prior to being seeded with 100 µl of 1 M/ml hMSC p6 solution for non-aligned constructs and 50 µl of 1 M/ml hMSC p6 solution for aligned constructs (~0.5 area of non-aligned). After 3 hours of incubation at 37C, 5% CO_2, 5 ml of MSCGM, DMEM + 10% serum (DMEM – supp) , or DMEM + 10% FBS + 50 µg/ml AA and 2 µg/ml insulin (DMEM + supp) was added to each well. Complete media changes occurred 3 times weekly until harvest at 3 weeks.

Polarized Light Imaging

Polarized light imaging was conducted as previously described.[10] Briefly, a fiber source (Technispec), focusing lens (Edmund Scientific) and computer-controlled rotation (Mill-Shaf Technologies) of a linear polarizer sheet (Edmund Scientific) provided wide-field illumination of a sample with linearly polarized light of variable transmission axes. Images were acquired in transmission mode at each of 20 rotation angles of the linear

polarizer over the range of 0-180 degrees with a CCD device camera (Hitachi) and an effective circular analyzer made from a linear polarizer and a quarter-wave sheet (Oriel). Acquisition and image processing were done in Labview (National Instrument) and Matlab (MathWorks), respectively.

Uniaxial Mechanical Testing

Strips cut from each matrix were tested for tensile properties in both the circumferential and radial directions. The thickness of each strip was measured using a 50 g-force probe attached to a displacement transducer. Strips were placed in compressive grips, attached to the actuator arm and load cell of an Instron MicroBionix (Instron Systems), and straightened with an applied load of 0.005 N. This position was used as the reference length of the strip. After six cycles of 0%–10% strain conditioning at 2 mm/min, strips were stretched to failure at the same rate. True strain was calculated based on the natural log of the tissue length divided by the reference length. The stress was calculated as force divided by the initial cross-sectional area. The tangent modulus (E) was determined as the slope of the linear region of the stress–strain curve before failure. The peak stress was defined as ultimate tensile strength (UTS).

Collagen and Cell Quantification

Collagen content was quantified using a hydroxyproline assay previously described, assuming 7.46 mg of collagen per 1 mg of hydroxyproline.[11] The sample volume was calculated using the measured length, width, and thickness of the strips. The cell content was quantified with a modified Hoechst assay for DNA assuming 7.7 pg of DNA per cell.[12] Cell concentrations were calculated as the number of cells per unit volume using the measured dimensions of the strip.

Histology

Samples were fixed for 3 hrs in 4% paraformaldehyde at 4°C, infiltrated with a solution of 30% sucrose and 5% DMSO at 4C, frozen in OCT (Tissue-Tek) via slurry of pre-chilled isopentane in liquid N_2, and sectioned into 9 µm cross-sections. All sections were cross sections, cut perpendicular to the direction of compaction for the aligned matrices. Samples were stained as follows:

Lillie's Trichrome

After bringing slides to room temperature and rinsing for 5 min in PBS, slides were fixed for 20 min in formalin and rinsed in distilled water for 5 min. Slides were incubated with Bouin's solution (Sigma) for 1 hr at 56°C and rinsed in tap water for 5 min. Slides were then stained with Weigert's hematoxylin (Sigma) for 5 min and rinsed with distilled water for 5 min. Next, slides were stained with Beibrich Scarlet (Sigma) for 5 min and rinsed with distilled water for 5 min. Slides were then stained in phosphomolybdic acid/phosphotungstic acid solution (Sigma) for 5 min and immediately transferred to 2.5% Fast Green solution for 5 min. Finally, slides were dipped in 1% acetic acid for 1 min and dehydrated as described above for H&E. Slides were imaged with a color CCD camera.

Picosirius Red

After bringing slides to room temperature and rinsing for 5 min in PBS, slides were fixed for 30 min in formalin and rinsed in distilled water for 5 min. Slides were stained with 1% Sirius Red in picric acid (Sigma) for 1 hr, washed in 0.5% acetic acid for 10 min and dehydrated as described above for H&E. Slides were imaged with a color CCD camera with the sample placed between crossed polarizers.

Alizarin Red

After bringing slides to room temperature and rinsing for 5 min in PBS, slides were stained with 40 mM Alizarin Red S (pH 4.2, Sigma) for 3 min. Slides were then dehydrated in acetone for 15 sec and a 50:50 mix of acetone and xylene for 15 sec. Slides were cleared in xylene and coverslipped with Permount. Slides were imaged with a color CCD camera. A section of calcified artery was used as a positive control.

Oil Red O

After bringing slides to room temperature and rinsing for 5 min in PBS, slides were fixed for 15 min in formalin and rinsed in distilled water for 5 min. Slides were dipped in 60% isopropyl alcohol, stained with 0.3% Oil Red O (Sigma), and dipped again in 60% isopropyl alcohol. Slides were counterstained with Mayer's hematoxylin for 1 min and rinsed for 5 min in warm tap water. Slides were coverslipped with aqueous mounting medium (Dako). Slides were imaged with a color CCD camera. A section of ovine heart tissue with significant fatty deposits was used as a positive control.

Alcian Blue

After bringing slides to room temperature and rinsing for 5 min in PBS, slides were dipped in 0.1N HCl, stained with 1% Alcian Blue (pH 1.0) for 30 minutes, and dipped again in 0.1N HCl. Slides were then counterstained with 1% Nuclear Fast Red (Sigma) for 5 min and rinsed with distilled water for 5 min. Slides were dehydrated as described above for H&E. Slides were imaged with a color CCD camera. A section of human annulus fibrosa was used as a positive control

Immunostaining

Sections were stained for αSMA (1:200, Sigma A5228), collagen type I (1:200, Novus NB600-408), fibronectin (1:500, Abcam ab6584), and calponin (1:200, Abcam ab110128). All samples were blocked with 5% normal donkey serum for 2 hr before incubation in the primary antibody overnight. Samples were then stained with a Cy3 fluorescent-labeled secondary antibody (Jackson Immuno lab) at 1:200 dilution and nuclear Hoechst stain (1:1000).

Gelatin Zymography and Western Blotting

Gelatin zymography gels were made by polymerizing a 7.5% SDS-PAGE gel with 800 µg/ml gelatin. Conditioned medium with sample buffer was added to each well of the SDS-PAGE gel. The gel was run in a Biorad Mini-Protean cassette for 75 min at 0.03A. The gel was released and washed 3 x 5 min in double distilled water (ddH_20), incubated 2 times in 2.5% Triton-X for 15 min, and washed 3 x 5 min in ddH_20. The gel was incubated in incubation buffer overnight at 37°C. The incubation buffer consisted of 50 mM Tris HCl ph 8, 5 mM $CaCl_2$, and 1 nM $ZnCl_2$. After incubation, the gel was washed for 5 min in ddH_20, stained with 2.5% Coomassie Brilliant Blue for 30 min, and destained.

Western blotting was used to determine the expression of αSMA and calponin in cell monolayers. Cell pellets were flash-frozen in liquid N_2 at harvest. For each sample, 20 µg of total protein was boiled in a reducing sample buffer and separated by SDS–polyacrylamide gel electrophoresis. The proteins were transferred to nitrocellulose (Whatman) using a wet transfer buffer (10% methanol, 2.2 g/L CAPS, pH 11). The blot was incubated in a blocking solution (5% dry milk and 0.1% Tween-20 in PBS) for 1 h

and then incubated with a primary antibody overnight at 4°C (mouse monoclonal αSMA; Sigma, at 1:1500; rabbit polyclonal calponin antibody; Abcam, at 1:1000). The blot was then probed with horseradish peroxidase-conjugated secondary anti-IgG (Jackson Immuno Lab) at a dilution of 1:1000 and developed using enhanced chemiluminescence.

Quantification of Cell Invasion

Cell invasion was determined from DAPI-stained sections by a custom-made MATLAB ® script. Briefly, the user defines the surface of the tissue section by selecting a series of representative points on the tissue surface. The MATLAB ® program then determines the location of the centroid of each cell nucleus relative to the tissue surface, as well as the dimensions of the major and minor axes of the nucleus. The program outputs histograms of the location and aspect ratio of the invaded cells for comparison.

Cell Tracking

hMSC passage 7 were seeded at a density of 500 / sq. cm and cultured in DMEM + 10% FBS + 100 U/mL penicillin, 100 µg/mL streptomycin . After allowing the cells to adhere overnight, 20 mM HEPES and supplements were added to the medium and the cells were cultured for 12 hours on a temperature controlled microscope (Zeiss) . hMSC were cultured without additional supplements or in the presence of 50 µg/ml ascorbic acid, 2 µg/ml insulin, or 50 µg/ml ascorbic acid and 2 µg/ml insulin. Images of 12 field of views (~20 cells) were captured every 10 minutes for the duration of the experiment. The extent of migration was quantified by mean-squared displacement (MSD) over the time period divided by the estimated cell diameter . Cell diameter was estimated as the diameter of a circle of equivalent area to the area measured by selection in ImageJ.

Statistics

For all experiments, n=3 or higher sample number was used, unless otherwise indicated. Statistical significance of differences between groups was determined using Student's t-test for two treatments and one-way ANOVA for more than two treatments with the Tukey's post hoc test in GraphPad Prism® software for Windows. Error bars in plots represent the standard error of the mean (SEM). Any reference to a difference in the Results and Discussion sections implies statistical significance at the level $p< 0.05$, unless otherwise indicated.

Results

Verification of MSC Phenotype

hMSCs were expanded upon receipt from Lonza and cryopreserved at passage 4. After expansion to passage 6, the ability to achieve tri-lineage differentiation was tested. hMSCs retained their ability to differentiate into osteocytes as indicated by an Alizarin Red stain for mineral deposits (Figure 3.2a), adipocytes as indicated by Oil Red O stain for neutral lipid uptake (Figure 3.2b), and chondrocytes as indicated by Alcian Blue stain for sulfated proteoglycans (Figure 3.2c), when cultured for 3 weeks in the appropriate differentiation conditions. The expression of α-smooth muscle actin (αSMA) in subconfluent and confluent cultures was also tested. hMSCs express αSMA when subconfluent, but organized fibers were not seen (Figure 3.2d) . However, when hMSCs reached confluence, αSMA fibers were seen (Figure 3.2e).

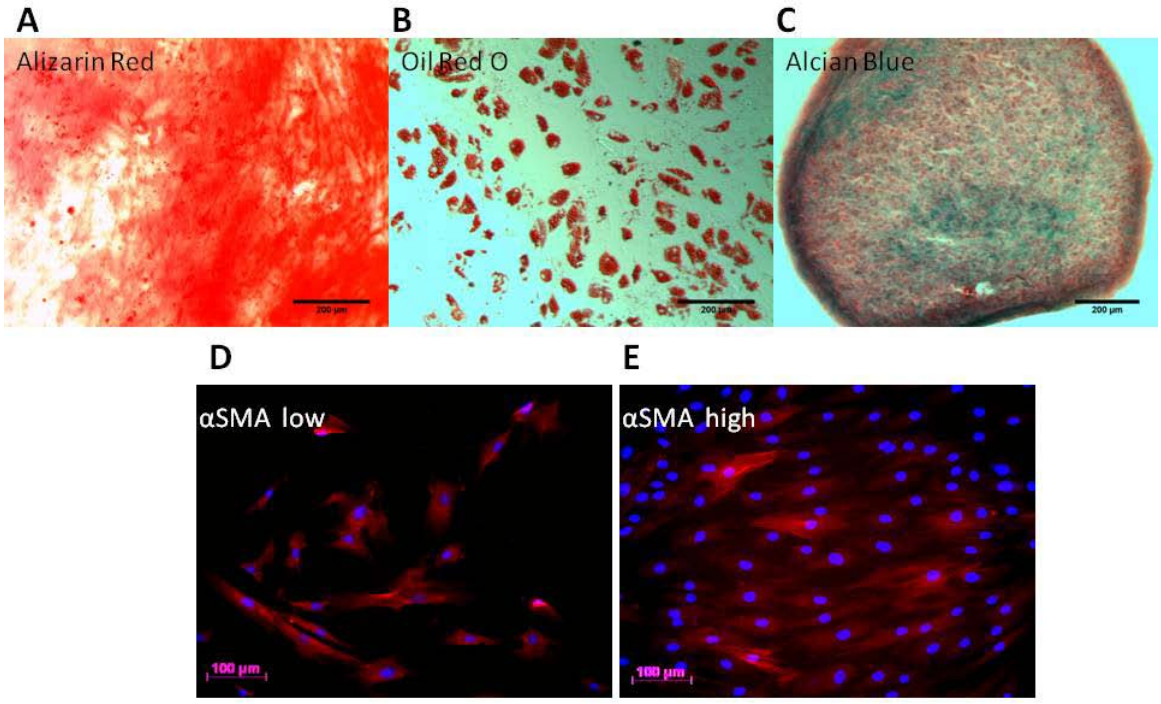

Figure 3.2: After 3 weeks of culture in the appropriate differentiation conditions, hMSCs were able to differentiate into (A) osteocytes, as indicated by Alizarin Red stain for mineral deposits, (B) adipocytes as indicated by Oil Red O stain for neutral lipid uptake, and (C) chondrocytes as indicated by Alcian Blue stain for sulfated proteoglycans. hMSCs stained positive for αSMA when subconfluent (D), but distinct αSMA fibers were only seen in confluent cultures (E). Images are representative of n ≥ 3 replicates

Verification of Matrix Alignment

In order to verify the alignment of aligned (C-shaped) and non -aligned (O-shaped) matrices, two approaches were taken. First, polarized light imaging was used to determine the macroscopic alignment of the samples. When imaged under polarized light, aligned matrices (Figure 3.3A) showed alignment perpendicular to the direction of compaction (from one edge of the "C" to the other), as indicated by the direction and magnitude of the red arrows in Figure 3.3B. In comparison, non-aligned samples (Figure 3.3C) did not show any preferred direction of alignment (Figure 3.3D). No obvious

differences in the expected alignment were seen between fresh and decellularized matrices (data not shown).

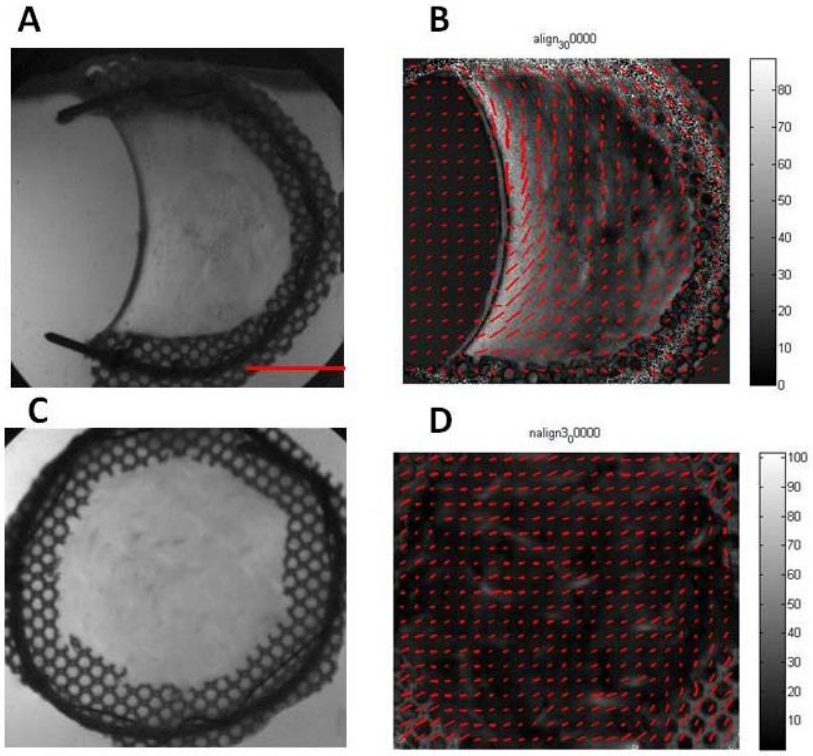

Figure 3.3: Macroscopic view of decellularized aligned (A) and non-aligned (C) matrices. Polarized light imaging shows that aligned matrices (B) exhibit alignment along the direction of compaction and that non-aligned constructs (D) exhibit no preferred alignment direction. Red arrows indicate magnitude and direction of alignment. Scale bar = 1 cm. Images representative of n = 6 samples.

Second, strips of fresh or 4 hr decellularized matrix that were cut in orthogonal directions underwent uniaxial mechanical testing in order to determine the ultimate tensile strength (UTS) and Young's modulus of the matrix in each direction. Anisotropy in the mechanical properties of the matrices was determined by defining the "UTS ratio" and "modulus ratio", where these ratios are defined as the value in the circumferential

direction divided by the value in the radial direction. The circumferential direction was arbitrarily defined in non aligned samples.

In freshly harvested matrices, the UTS ratio of aligned matrices was 2.20 ± 0.63 (n=5), whereas the UTS ratio of non-aligned matrices was 1.02 ± 0.14 (n=6). After decellularization for 4 hrs, the UTS ratio of aligned matrices was 3.00 ± 0.48 (n=6), whereas the UTS ratio of non-aligned matriceswas 1.48 ± 0.24 (n=6) (Figure 3.4a). The UTS ratio in decellularized aligned matrices was higher when compared to non-aligned matrices, however the difference was not significant in freshly harvested matrices ($p=0.065$). In addition, the UTS ratio of fresh and decellularized non-aligned matrices was not statistically different from the 1.00, which is the expected UTS ratio for non-aligned matrices. There was no difference in the UTS ratio between fresh and decellularized matrices.

In freshly harvested matrices, the modulus ratio of aligned matrices was 4.35 ± 1.11 (n=6), whereas the modulus ratio of non-aligned matrices was 1.04 ± 0.32 (n=6). After decellularization for 4 hrs, the modulus ratio of aligned matriceswas 4.25 ± 0.86 (n=6), whereas the UTS ratio of non-aligned matrices was 1.61 ± 0.29 (n=6) (Figure 3.4b). The modulus ratio in aligned matrices was higher when compared to non-aligned matrices in both fresh and decellularized tissue. In addition the modulus ratio of non-aligned matrices was not statistically different from the 1.00, which is the expected modulus ratio for non-aligned matrices. There was no difference in the modulus ratio between fresh and decellularized matrices.

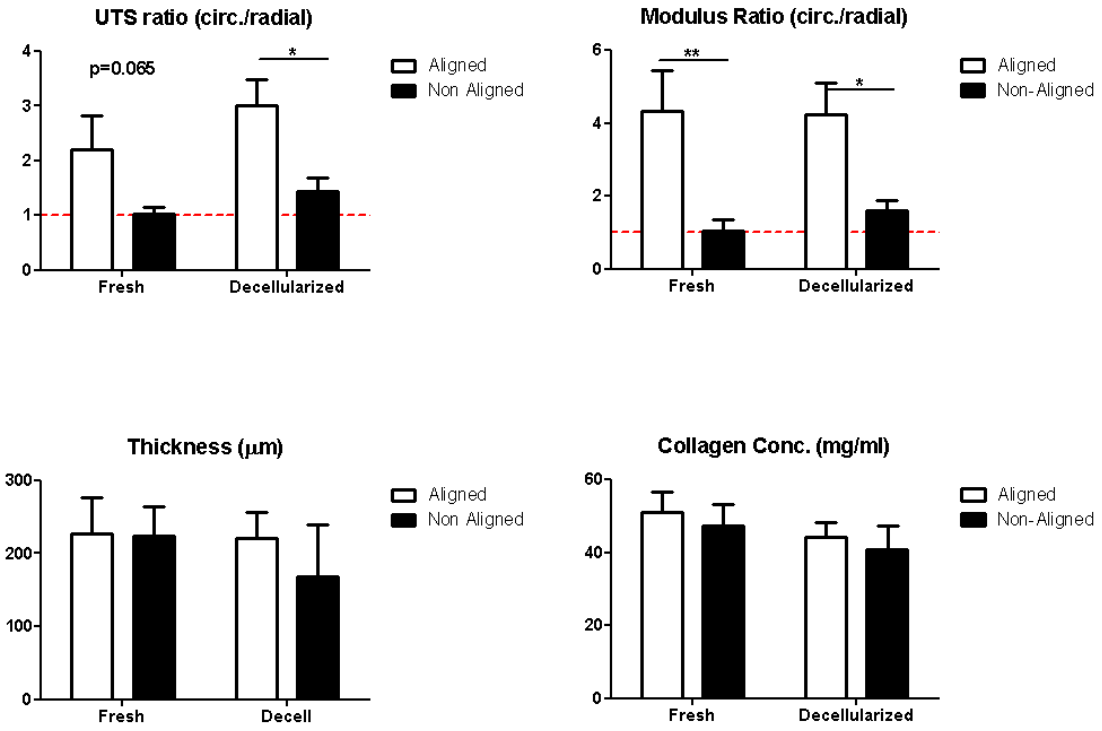

Figure 3.4: Properties of aligned and non-aligned tissues and matrices. (A) UTS ratio (B) Modulus ratio (C) Thickness (D) Collagen content. * indicates p<0.05 and ** indicates p<0.01.

Finally, there were no differences in thickness (Figure 3.4c) and collagen content (Figure 3.4d) between any of the groups. The measured thicknesses are as follows: aligned tissues = 228 ±21 μm, (n=12) non-aligned tissues = 222 ± 15 μm (n=12), aligned matrices = 225 ± 16 μm (n=12), non-aligned matrices = 168 ± 29 μm (n=12). The measured collagen contents are as follows: aligned tissues = 51 ±5 mg/ml (n=6), non-aligned tissues = 47 ± 6 mg/ml (n=7), aligned matrices = 44 ± 4 mg/ml (n=6), non-aligned matrices = 40 ± 7 (n=6).

Due to poor hMSC invasion into matrices that had been decellularized for 4 hrs (data not shown), the decellularization time was increased to an overnight incubation. The mechanical properties of aligned matrices that were decellularized for 4 hrs were not

different from previous studies with aligned matrices that were decellularized for 24 hrs (see Table 3.2), so mechanical testing was not repeated on overnight decellularized tissue.

	Circ. UTS (MPa)	Radial UTS (MPa)	UTS Ratio	Circ. Modulus (MPa)	Radial Modulus (MPa)	Modulus Ratio
4 hr decell	1.6 ± 0.2	0.6 ± 0.1	3.0 ± 0.5	3.8 ± 1.0	0.9± 0.1	4.3 ± 0.9
24 hr decell	2.2 ± 1.1	0.3 ± 0.1	2.8 ± 0.3	7.4 ± 3.5	0.7 ± 0.3	5.0 ± 1.6

Table 3.2 Influence of decellularization time on construct mechanical properties (aligned only)

Histology

Lillie's Trichrome staining showed that freshly harvested aligned and non-aligned matrices were composed primarily of collagen (blue-green) with a homogeneous distribution of cells throughout the matrix (black) (Figure 3.5a.b)., except at the outer surfaces of both aligned (Figure 3.5a) and non-aligned matrices (Figure 3.5b). After 4 hr decellularization, all cell nuclei were removed in both aligned (Figure 3.5c) and non-aligned matrices (Figure 3.5d), and only collagen remained.

Picosirius red staining of cross-sectionsshowed organized collagen fibrils in freshly harvested (Figure 3.5e,f) and decellularized (Figure 3.5g,h) matrices. Both aligned (Figure 3.5e,g) and non-aligned matrices (Figure 3.5f,h) showed birefringence, suggesting that non-aligned matrices were transversely isotropic rather than isotropic.

Acellular isotropic collagen gels did not show any birefringence when viewed under cross-polarized light (data not shown).

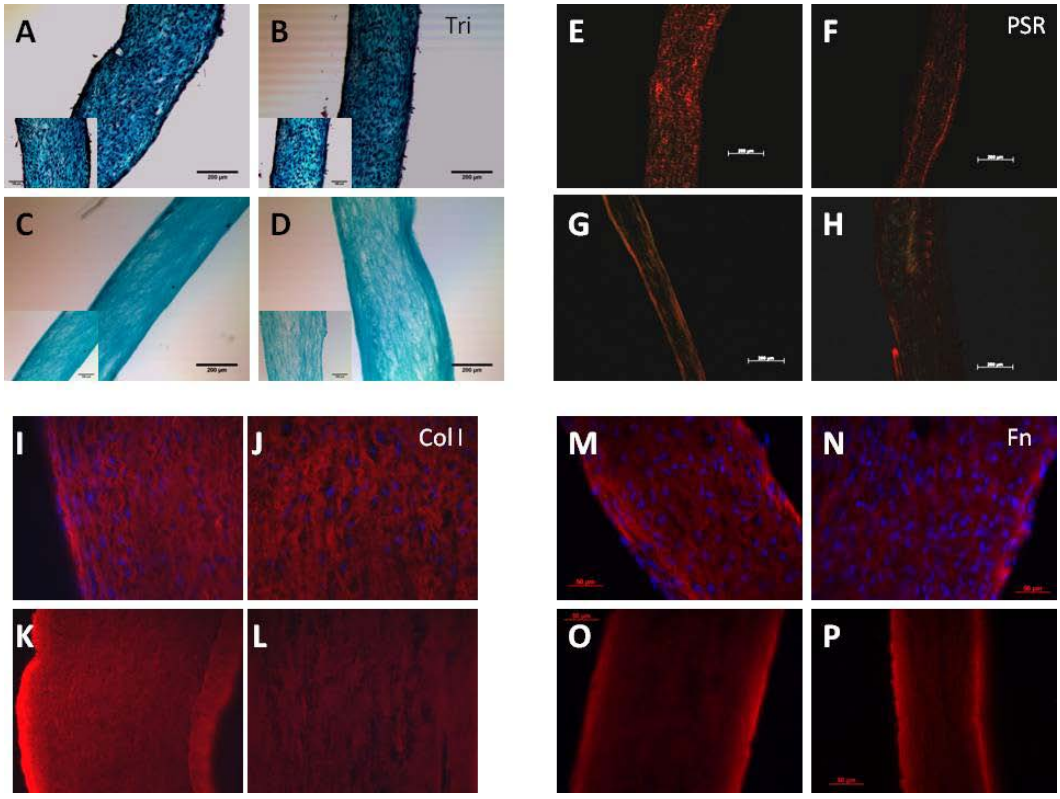

Figure 3.5: Histological evaluation of aligned and non-aligned matrices. Lillie's Trichrome stain of fresh aligned (A), fresh non-aligned (B), decellularized aligned (C), and decellularized non-aligned (D)matrices. Main panels were taken at 100x total magnification; insets were taken at 200x total magnification. Picosirius red stain of fresh aligned (E), fresh non-aligned (F), decellularized aligned (G), and decellularized non-aligned (H) tissue. Images were taken at 100x total magnification. Collagen type I immunostain of fresh aligned (I), fresh non-aligned (J), decellularized aligned (K), and decellularized non-aligned (L) matrices. Fibronectin immunostain of fresh aligned (M), fresh non-aligned (N), decellularized aligned (O), and decellularized non-aligned (P) matrices. Images were taken at 400x total magnification. All samples are cross sections, cut perpendicular to the direction of compaction for the aligned matrices. Images representative of n > 3 samples.

Immunostaining showed that both collagen type I and fibronectin werepresent in freshly harvested aligned (Figure 3.5i,m) and non-aligned (Figure 3.5j,n) matrices. Furthermore, these proteins were retained after decellularization in both aligned (Figure

3.5k,o) and non-aligned matrices (Figure 3.5l,p). The staining pattern did not appear to change.

Mesenchymal Stem Cell Invasion and Alignment

hMSCs were seeded onto aligned and non-aligned matrices and cultured in 3 different culture conditions; MSC growth media (MSCGM), DMEMC + 10% FBS (DMEM – supp), DMEMC + 10% FBS + 50 µg/ml ascorbic acid + µg/ml insulin (DMEM + supp). After 1 week of culture, cells cultured in DMEM + supp began to display a "mottled" appearance (Figure 3.6a,d), which did not appear in cells cultured in DMEM - supp (Figures 3.6b,e) or MSCGM (Figure 3.6c,f). These areas grew progressively to the point where the entire tissue was transparent at 3 weeks (data not shown).

Initially, we suspected that this observation was correlated with increased gelatinase activity in the DMEM + supp group. MMP2 has been shown to degrade fibrillar collagens as well as degraded collagens *in vitro*.[13] However, after completing a gelatin zymogram on conditioned media from all groups, no obvious differences in the pro-MMP2 (68 kDa) and active-MMP2 (62 kDa) bands were seen. There was very little detectable MMP9 (92 kDa) (Figure 3.6g). Lanes 1-2 represent unconditioned DMEM-supp and MSCGM, respectively. Lanes 3-6 represent DMEM + supp conditioned media, lanes 7-10 represent DMEM – supp conditioned media, and lanes 11-14 represent MSCGM conditioned media.

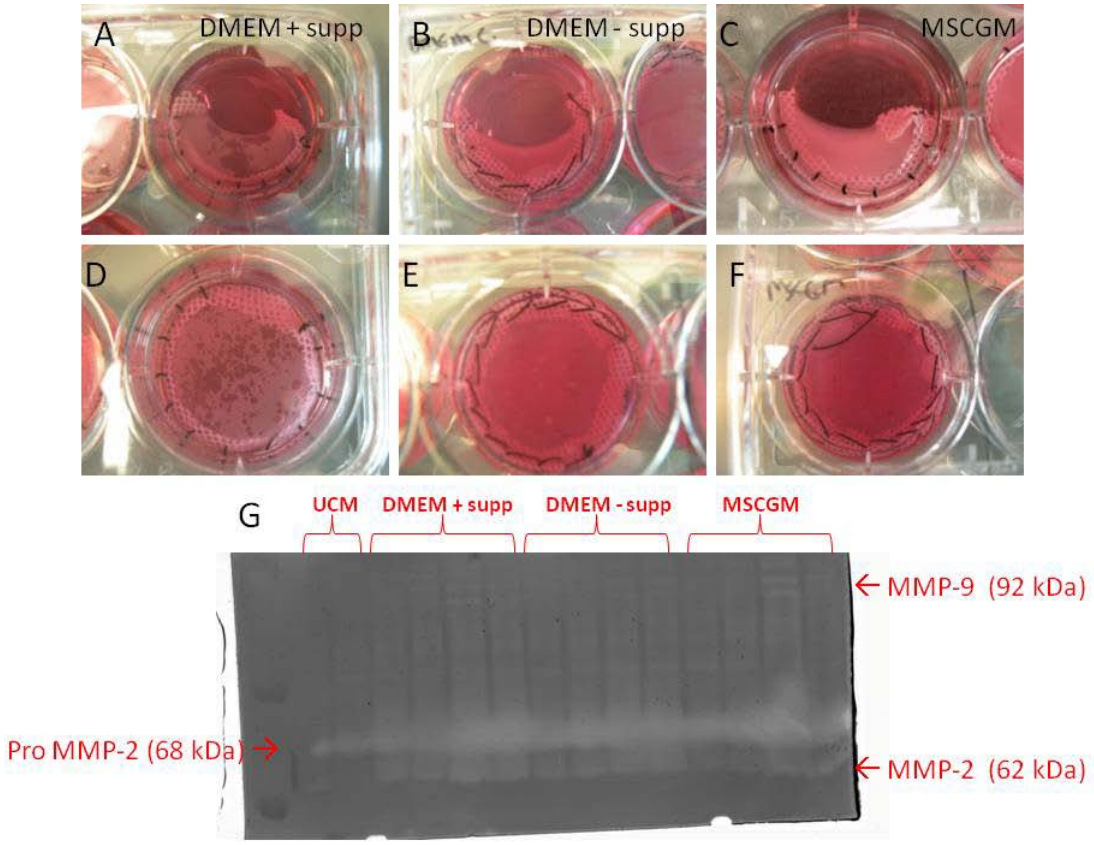

Figure 3.6: Macroscopic appearance of hMSCs reseeded, aligned (A-C) and non-aligned (D-F) matrices after 1 week of culture. Matrices cultured in DMEM + supp (A,D) displayed a "mottled" appearance, whereas matrices cultured in DMEM – supp (B,E) and MSCGM (C,F) did not. (G) Conditioned media from DMEM + supp (lanes 3-6), DMEM – supp (lanes 7-10) and MSCGM (lanes 11-14) showed no obvious difference in MMP2 activity. UCM = unconditioned media (lanes 1,2).

After 3 weeks of culture in the different media conditions, aligned and non-aligned matrices were harvested, sectioned, and stained with DAPI. The centroid and aspect ratio of the invaded cells was analyzed with a custom MATLAB algorithm. Aspect ratio is defined as the length of the minor axis divided by the length of the major axis. (A circular nuclei would have a circularity of 1 and a line would have a circularity of ∞). There were significantly more invaded cells seen in aligned (Figures 3.7a, 3.8a) and non-aligned (Figure 3.7d, 3.8d) matrices that were cultured in DMEM + supp. In

comparison there was minimal invasion in aligned (Figures 3.7b, 3.8b) and non-aligned (Figures 3.7e, 3.8e) tissues that were cultured in DMEM – supp, although the seeded surface had a confluent monolayer of cells. Minimal invasion was also seen in aligned (Figures 3.7c, 3.8c) and non-aligned (Figures 3.7f, 3.8f) matrices that were cultured in MSCGM. Again, the seeded surface had a confluent monolayer of cells.

The average number of cells in each section and the average number of cells that had invaded at least half the matrix thickness were calculated. Aligned and non-aligned matrices that were cultured in DMEM + supp had significantly more cells per section (Figure 3.9a) and cells that had invaded half the thickness of the matrix (Figure 3.9b) than all other groups. Aligned and non-aligned matrices that were cultured in DMEM + supp were not different from each other.

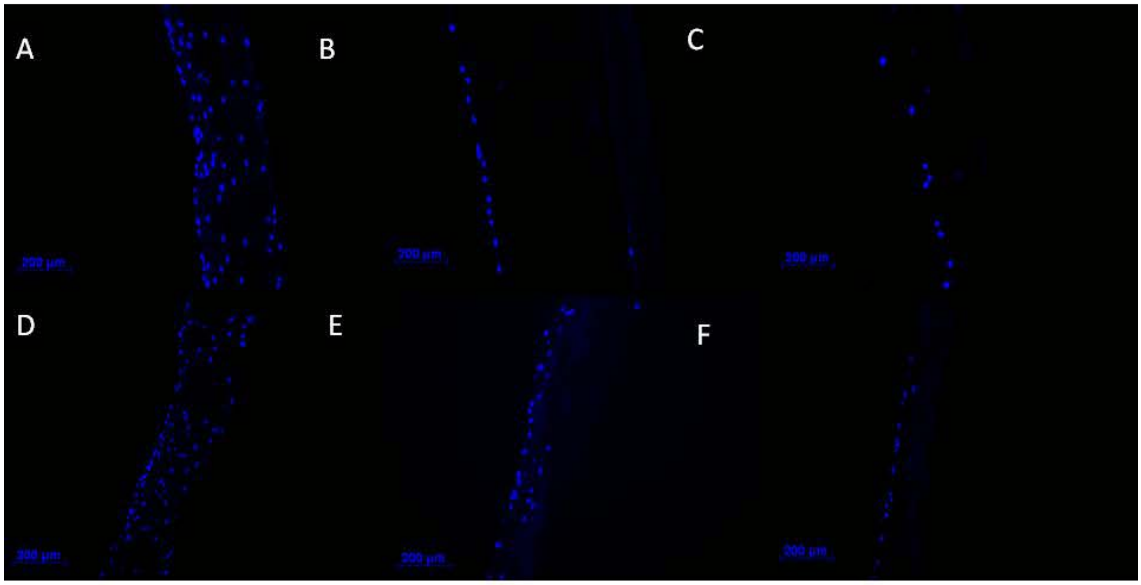

Figure 3.7: DAPI-stained sections of 3 week recellularized matrices. (A) aligned matrices cultured in DMEM + supp, (B) aligned matrices cultured in DMEM – supp, (C) aligned matrices cultured in MSCGM, (D) non-aligned matrices cultured in DMEM + supp, (E) non-aligned matrices cultured in DMEM – supp, (F) non-aligned matrices cultured in MSCGM. Images representative of n > 3 samples

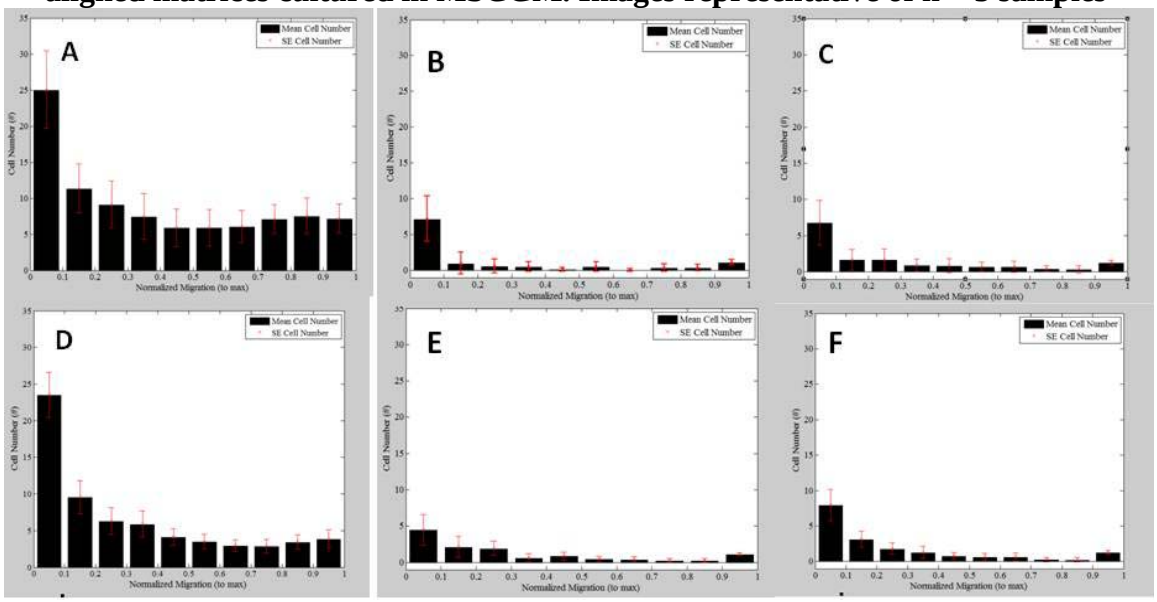

Figure 3.8: Histogram of cell invasion with number of cells plotted on the ordinate and normalized invasion depth plotted on the abscissa (A) aligned matrices cultured in DMEM + supp, (B) aligned matrices cultured in DMEM – supp, (C) aligned matrices cultured in MSCGM, (D) non-aligned matrices cultured in DMEM + supp, (E) non-aligned matrices cultured in DMEM – supp, (F) non-aligned matrices cultured in MSCGM

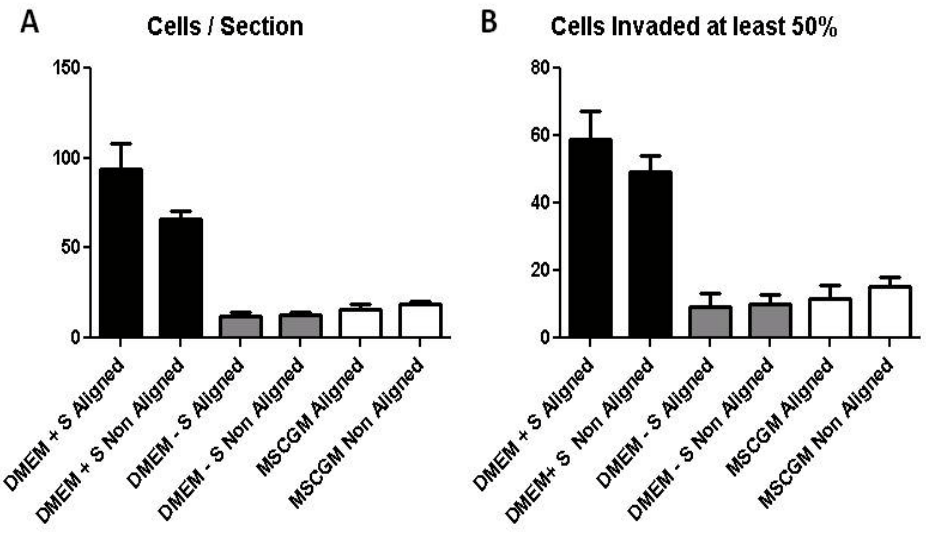

Figure 3.9: (A) number of cells per cross section (B) number of cells that invaded at least half the matrix thickness. S=supplement

The aspect ratio of the invaded cell nuclei was also compared in aligned and non-aligned samples. The aspect ratio was evaluated from cross-sections, cut perpendicular to the direction of compaction for the aligned matrix. Since the DMEM + supp group was the only group to show significant cell invasion, analysis was restricted to aligned and non-aligned samples from this group. As shown in Figure 3.10, aligned samples had a lower aspect ratio than non-aligned samples, suggesting that the cells that invaded aligned matrices were more aligned in the direction of matrix alignment. The distributions in Figure 3.10a and 3.10b were found to be statistically different from each other by the Kolmogorov-Smirnov test (Figure 3.10c, $p<0.01$).

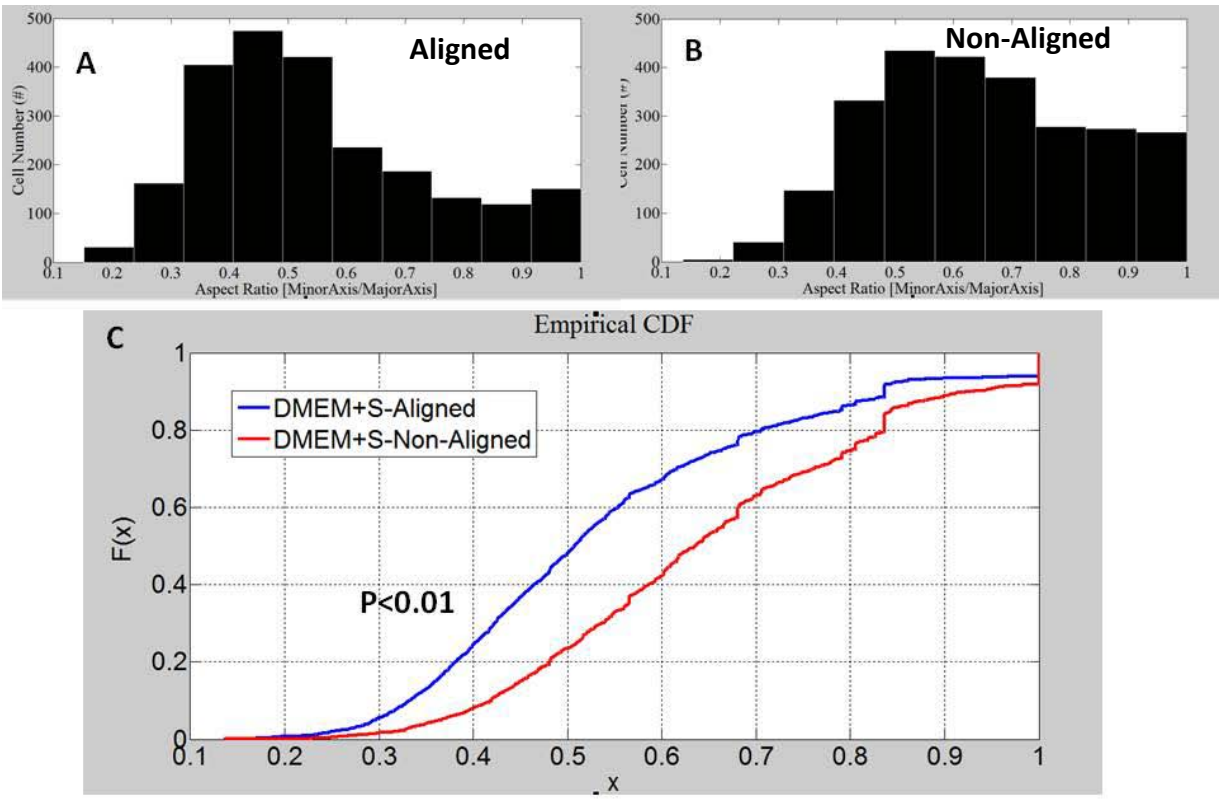

Figure 3.10 (A) histogram of circularity for aligned DMEM + supp group (B) histogram of circularity for non-aligned DMEM + supp group (C) comparison of the cumulative distribution functions of each group shows that the alignment distributions are significantly different from each other (p<0.01)

Differentiation of Invaded Cells

After 3 weeks of culture in the different media conditions, aligned and non-aligned matrices were harvested, sectioned, and stained for differentiation markers. The differentiation markers analyzed were as follows: Oil Red O - stains neutral lipid uptake, an indicator of adipogenic differentiation. Alizarin Red S - stains calcium deposits, an indicator of osteogenic differentiation. Alcian Blue - stains sulfated proteoglycans, an indicator of chondrogenic differentiation. αSMA and calponin are indicators of myofibroblast/smooth muscle cell differentiation. There were no differences seen between aligned and non-aligned matrices, so aligned matrices are shown for simplicity.

There was no indication of neutral lipid uptake in aligned matrices cultured in DMEM + supp (Figure 3.11b), DMEM – supp (Figure 3.11c) or MSCGM (Figure 3.11d) when compared to positive controls (Figure 3.11a). There was also no indication of calcium deposition in aligned matrices cultured in DMEM + supp (Figure 3.11f), DMEM – supp (Figure 3.11g) or MSCGM (Figure 3.11h) when compared to positive controls (Figure 3.11e). There was no indication of proteoglycan synthesis in aligned matrices cultured in DMEM – supp (Figure 3.11k) or MSCGM (Figure 3.11l) when compared to positive controls (Figure 3.11i). However, there appeared to be higher staining inmatrices cultured in DMEM + supp (Figure 3.11j). Finally, cells that had invaded allmatrices expressed αSMA (Figures 3.11n-p), but cellular calponin staining was not above background.

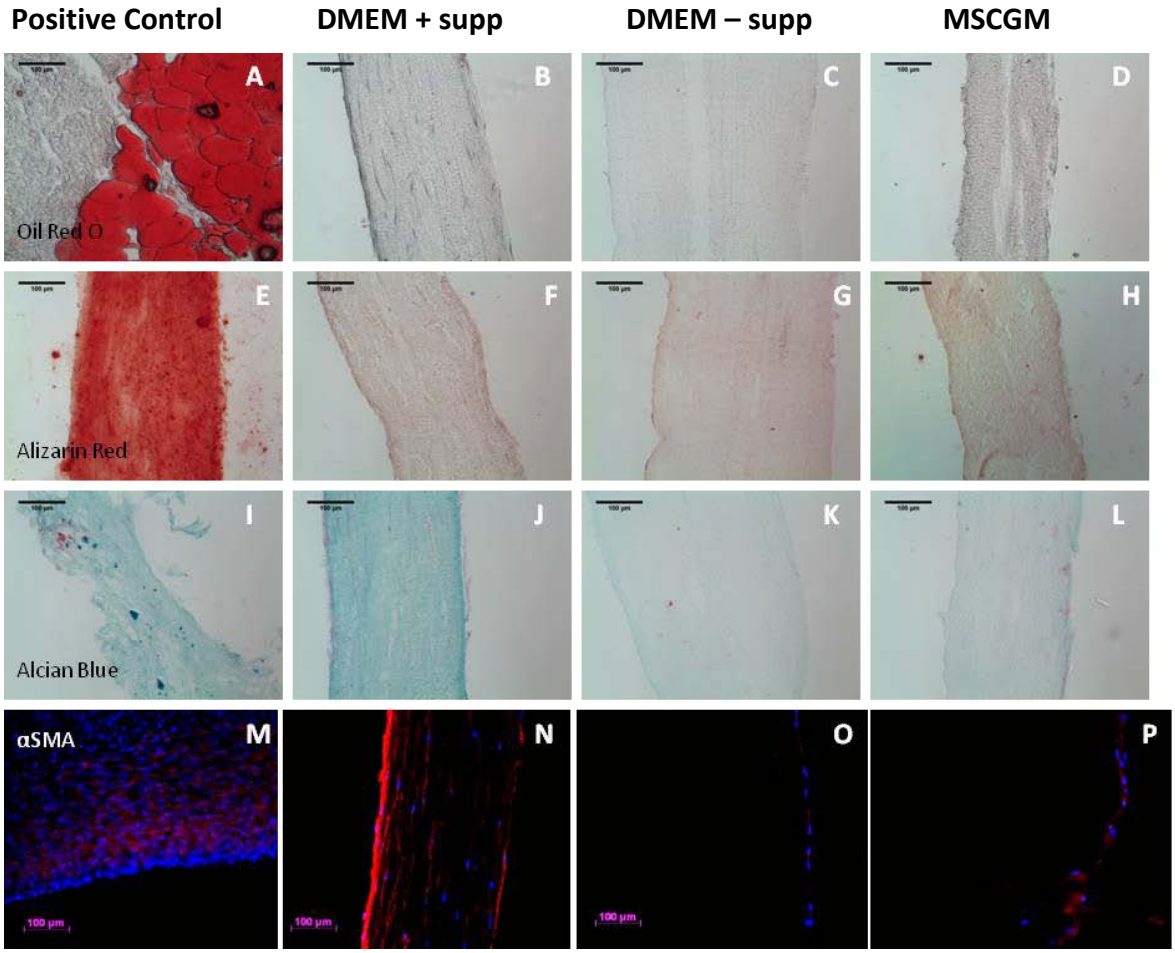

Figure 3.11: Differentiation of Invaded Cells. (A-D) Oil Red O, (E-H) Alizarin Red, (I-L) Alcian Blue, (M-P) αSMA. Groups are labeled above the corresponding column. Images are representative of n > 3 samples.

Proliferation and Migration in 2D

In order to decouple the effects of ascorbic acid and insulin on hMSCs in culture, cells were cultured in unsupplemented medium, medium containing 50 µg/ml ascorbic acid, medium containing 2 µg/ml insulin, or medium containing both 50 µg/ml ascorbic acid and 2 µg/ml insulin. After 2.5 weeks, supplementation with ascorbic acid or the combination of ascorbic acid and insulin led to approximately a 3-fold increase in cell number, whereas supplementation of insulin alone did not lead to an increase in cell number (Figure 3.12a). In addition, cells cultured in ascorbic acid or the combination of ascorbic acid and insulin showed an increase in both αSMA and calponin expression via

western blot (Figure3.12b,c). hMSCs did not show a statistically significant increase in migration over a 12 hour period when cultured in these supplements, although more cells migrated more than one cell diameter when cultured in ascorbic acid, insulin, or the combination of ascorbic acid and insulin than in unsupplemented conditions. (Table 3.3).

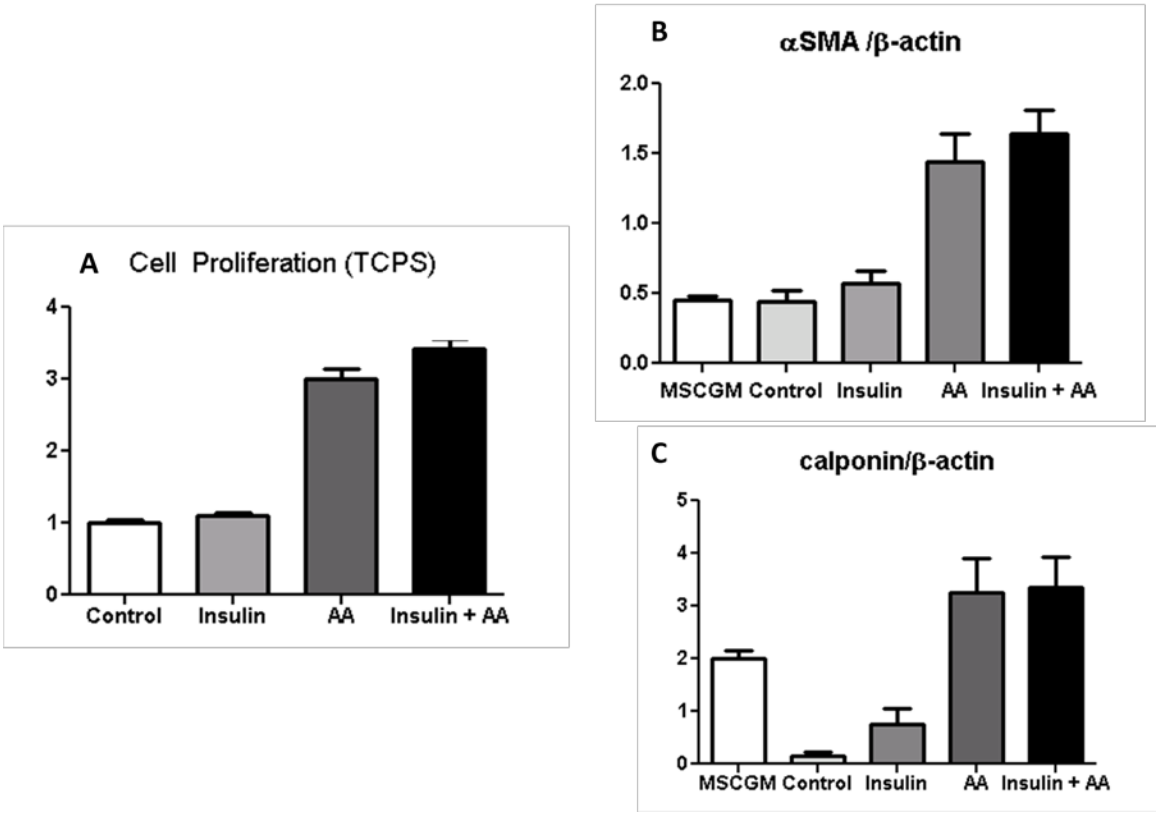

Figure 3.12: Influence of ascorbic acid and insulin on hMSC proliferation and differentiation. (A) proliferation after 2.5 weeks of culture (B) αSMA expression after 2.5 weeks of culture, (C) calponin expression after 2.5 weeks of culture. Non-overlapping error bars are statistically different from each other $p<0.05$.

	MSD/est. cell diameter			
	Mean ± SEM	N	# cells >0.50	# cells >1.00
Control	0.141 ± 0.056	19	2	0
Insulin	0.401 ± 0.160	22	5	4
Ascorbic Acid	0.605 ± 0.208	20	7	4
Insulin + Ascorbic Acid	0.530 ± 0.215	18	5	2

Table 3.3: Comparison of hMSC Migration

Discussion

The use of decellularized tissue in development of tissue-engineered heart valves has been proposed as an alternative to chemically-fixed xenogeneic valves. Decellularized tissues aim to reduce the calcification and degradation associated with chemically-fixed valves by removing calcifiable structures and providing a biomaterial scaffold that supports host cell infiltration. However, to date, recellularization of decellularized native tissues has proven difficult. Previous work in our lab has shown that *in vitro* recellularization of decellularized engineered matrices is possible within 3 weeks of culture, but this study did not fully explore the variables that influence hMSCs invasion into these matrices.[8] The goal of this work was to investigate the influence of ECM alignment and the soluble factors insulin and ascorbic acid on the recellularization of decellularized engineered tissues by hMSCs.

By specifying the geometry and associated mechanical constraints to fibroblast-mediated fibrin gel contraction using circular and C-shaped molds, the creation of aligned and non-aligned tissues was possible. The matrix alignment (or lack of alignment) was confirmed both prior to and following decellularization via polarized light imaging, immunohistochemistry for collagen I, and mechanical anisotropy. The mechanical

anisotropy did not appear to be influenced by exposure of the tissues to decellularization detergents, consistent with results shown for decellularized rat ventricles and porcine thoracic aorta.[15,16] Evaluation of histological sections showed that decellularization effectively removed cell nuclei, but preserved the extracellular matrix proteins collagen type I and fibronectin, which are important for hMSC adhesion.[17,18] Preservation of collagens and fibronectin after decellularization of tissues has been previously reported in the literature.[19] Interestingly, birefringence was seen in cross sections of non-aligned samples. This suggests that the matrix is not isotropic, but rather is transversely isotropic (i.e. random organization in the x-y plane, but different properties normal to the x-y plane). This is not entirely surprising, since although non-aligned matrices are prevented from compacting laterally, they were still able to compact the thickness of the gel, inducing alignment of ECM in the plane normal to the thickness direction.[20] Immunohistochemical staining for collagen I was consistent with transverse isotropy of non-aligned samples and uni-directional alignment of aligned samples.

hMSCs were seeded onto the decellularized aligned and non-aligned matrices and cultured in different media for 3 weeks for assessment of cell invasion. In matrices cultured with complete medium supplemented insulin and ascorbic acid, the matrix displayed translucent “patches” that appeared after one week of culture. These patches grew with extended culture until the entire matrix appeared translucent. There were no qualitative differences in MMP-2 potential in medium from these samples, suggesting that the effect was not due to secreted MMP-2. These patches could correlate with regions of increased cell proliferation and invasion, but no matrices were harvested at earlier time points to definitively answer this question. By 3 weeks, the invasion appeared

homogeneous so any heterogeneous invasion associated with patches was not evident then. Another possibility is that culture in the presence of ascorbic acid led to a local depolymerization of cell-produced hyaluronic acid, [21–23] which could potentially change the optical properties of the matrix. Further investigation is required to determine the quantity and molecular weight distribution of hyaluronic acid within the decellularized tissue before and after recellularization.

Very little invasion was seen in aligned and non-aligned matrices that were cultured in cell culture medium without insulin and ascorbic acid (DMEM–supp and MSCGM). Both aligned and non-aligned matrices that were cultured with insulin and ascorbic acid showed an increase in cellularity and in the number of cells invaded at least half the thickness of the matrix, but the invasion of aligned and non-aligned matrices by these metrics was not different from each other.

Insulin-like growth factors have been shown to increase MSC migration *in vitro*. Culture of rat MSCs in the presence of insulin-like growth factor 1 (IGF-1) increased the expression of the chemokine receptor CXCR4 and increased the migration of rat MSCs towards stromal-derived factor 1 (SDF-1), but did not increase rat MSC proliferation.[24] Human MSCs have also been shown to migrate in response to IGF-1.[25] Since insulin, IGF-1, and IGF-2 are all capable of binding to both the insulin receptor (IR) and insulin growth factor receptor 1 (IGF-1R), [26] it is possible that insulin increases the motility of hMSCs through a similar mechanism as IGF-1. Ascorbic acid has been shown to increase hMSC proliferation *in vitro* (Figure 3.12a and [27–29]). Although an increase in cell motility due to insulin and/or ascorbic acid was not shown, enhanced proliferation due to ascorbic acid is consistent with our results.

Nuclei of cells that invaded aligned matrices appeared more elongated (aspect ratio <1) when compared to cells that had invaded non-aligned matrices. Furthermore, cells were primarily aligned with the direction of matrix alignment based on nuclear orientation, suggesting that they were aligned with the matrix fibers via contact guidance.[30,31] The fact that there were more circular nuclei seen in non-aligned matrices and few nuclei oriented in the (z-direction of the thickness of these matrices, supports our inference from the polarized light microscopy and collagen I immunohistochemistry that the non-aligned matrices were transversely isotropic. We also infer that cells invading both aligned and non-aligned matrices migrated preferentially within the plane, and that cell speed and directional persistence in the thickness direction were similar for both the aligned and non-aligned matrices, which explains why there were no obvious differences in the invasion profiles between aligned and non-aligned samples.

Several other studies have explored the influence of ECM or synthetic fiber alignment on *in vitro* cell proliferation and invasion. Smooth muscle cells derived from hair follicle stem cells (HF-SMCs) seeded onto decellularized small intestinal submucosa (SIS) for 2 weeks were only found to invade into SIS when 10% static strain was applied.[32] 10% static strain induced alignment of the ECM fibers in the SIS. Cells that were seeded onto unstrained tissue were round and non-proliferative, whereas cells that were seeded onto strained tissue were proliferative and elongated in the direction of strain. Similarly, Kurpinski *et al.* showed that aligned poly-l-lactide (PLLA) scaffolds supported greater invasion of bovine aortic endothelial cells (BAECs) after 1 week of *in vitro* culture.[33] In both of these studies, the porosity of the aligned and non-aligned samples did not appear qualitatively different, although quantification was not performed.

These data suggest that fiber alignment influences the invasion of these cell types. It is possible that modification of the alignment of these scaffolds created an environment more suitable for surface penetration and migration within the matrix, for example, by changing the porosity of the matrix. These differences may not have been as pronounced in our matrices.

Finally, our results suggest that contact with decellularized matrices does not induce spontaneous differentiation towards an adipogenic or osteogenic phenotype, independent of culture conditions. However, invaded cells cultured in the presence of insulin and ascorbic acid appeared to stain more intensely for Alcian Blue, suggesting that this condition stimulated production of sulfated GAGs. The invaded cells also stained positive for α smooth muscle actin (αSMA) and negative for calponin, indicating a myofibroblast phenotype. Although the invading cells did not express calponin, it was upregulated by the presence of ascorbic acid in cultured cells . These data suggest that there are differences in hMSC differentiation when cultured in 2D versus 3D, consistent with prior studies.[34,35]

The presence of sulfated GAGs is commonly used as an indicator of chondrogenic differentiation, however it is not a definitive indicator, since sulfated GAGs are also present in the artery. [36] MSCs grown as cell sheets for 2-3 weeks were also stained positively for Alcian Blue when stimulated with transforming growth factor – β1 (TGF-β1) and ascorbic acid.[37] These hMSC cell sheets also expressed αSMA, calponin, and SM22α, and produced significant amounts of collagen and elastin. This result was confirmed, as extended culture of hMSCs in the presence of ascorbic acid increased protein expression for αSMA and calponin. Since the culture supplements to induce

smooth muscle differentiation and chondrogenic differentiation are similar, soluble factors alone may not suffice to determine hMSC differentiation towards these phenotypes.[38] Furthermore, Park et. al. found that there was an interaction between substrate stiffness and TGF-β1 signaling, where hMSCs cultured on soft substrates in the presence of TGF-β1 led to a decrease in αSMA and calponin expression and an increase in collagen II expression.[39] Taken together, these data suggest that although the invaded hMSCs may not be fully-differentiated towards a mature phenotype, it is unlikely that they will be further differentiated towards a chondrocyte phenotype, due to the high stiffness environment to which the cells are exposed, and their pronounced αSMA expression.

Fiber alignment has been shown to have an influence on the differentiation of stem cells in 3D systems. Human tendon stem/progenitor cells, which are phenotypically similar to hMSCs, increase tendon-related gene expression when cultured on aligned PLLA scaffolds, as opposed to an increase in osteocyte-related gene expression when cultured on isotropic PLLA scaffolds.[40] This result occurred even when cultured in osteogenic culture conditions, suggesting that fiber alignment suppresses osteogenic differentiation. hMSCs were shown to increase expression of cardiac myocyte-related genes when cultured on aligned polycaprolactone (PCL) scaffolds, when compared to isotropic PCL scaffolds.[41] Similarly, protein expression of cardiac myosin heavy chain (MHC) was upregulated in hMSCS that were cultured on micropatterned PLGA scaffolds.[42] However, differentiation differences were not evident in our aligned *vs.* non-aligned matrices.

In summary, these studies show that the soluble factors insulin and ascorbic acid promote the invasion of hMSCs into decellularized engineered tissues. We speculate that this is primarily due to an increase in motility of hMSCs when exposed to insulin and ascorbic acid, which is amplified due to proliferation stimulated by ascorbic acid. Furthermore, hMSC invasion into aligned and non-aligned matrices was not different, although there was a difference in cell orientation between aligned and non-aligned matrices based on nuclear aspect ratio measurements. Finally, we show that, regardless of culture medium or matrix alignment, hMSCs appear to be differentiating toward a myofibroblast or SMC-like phenotype. Further work could elucidate the mechanisms of insulin- and ascorbic acid-induced hMSC invasion and differentiation.

References

1. Vesely I. Heart Valve Tissue Engineering. *Circ Res*. 2005;97(8):743–755.

2. Mendelson K, Schoen FJ. Heart Valve Tissue Engineering: Concepts, Approaches, Progress, and Challenges. *Ann Biomed Eng*. 2006;34(12):1799–1819.

3. Schoen FJ, Levy RJ. Calcification of Tissue Heart Valve Substitutes: Progress Toward Understanding and Prevention. *Ann Thorac Surg*. 2005;79(3):1072–1080.

4. Quinn RW, Hilbert SL, Bert AA, et al. Performance and Morphology of Decellularized Pulmonary Valves Implanted in Juvenile Sheep. *Ann Thorac Surg*. 2011;92(1):131–137.

5. Honge JL, Funder J, Hansen E, Dohmen PM, Konertz W, Hasenkam JM. Recellularization of aortic valves in pigs. *Eur J Cardiothorac Surg*. 2011;39(6):829–834..

6. Baraki H, Tudorache I, Braun M, et al. Orthotopic replacement of the aortic valve with decellularized allograft in a sheep model. *Biomaterials*. 2009;30(31):6240–6246.

7. Jordan JE, Williams JK, Lee S-J, Raghavan D, Atala A, Yoo JJ. Bioengineered self-seeding heart valves. *J Thorac Cardiovasc Surg*. 2012;143(1):201–208.

8. Syedain ZH, Bradee AR, Kren S, Taylor DA, Tranquillo RT. Decellularized Tissue-Engineered Heart Valve Leaflets with Recellularization Potential. *Tissue Eng Part A*. 2013;19(5-6):759–769.

9. Iop L, Renier V, Naso F, et al. The influence of heart valve leaflet matrix characteristics on the interaction between human mesenchymal stem cells and decellularized scaffolds. *Biomaterials*. 2009;30(25):4104–4116..

10. Tower TT, Neidert MR, Tranquillo RT. Fiber Alignment Imaging During Mechanical Testing of Soft Tissues. *Ann Biomed Eng*. 2002;30(10):1221–1233.

11. Stegemann H, Stalder K. Determination of hydroxyproline. *Clin Chim Acta*. 1967;18(2):267–273.

12. Kim Y-J, Sah RLY, Doong J-YH, Grodzinsky AJ. Fluorometric assay of DNA in cartilage explants using Hoechst 33258. *Anal Biochem*. 1988;174(1):168–176.

13. Carson FL, Hladik C. *Histotechnology: A Self-Instructional Text*. 3rd Edition. American Society for Clinical Pathology; 2009.

14. Aimes RT, Quigley JP. Matrix Metalloproteinase-2 Is an Interstitial Collagenase Inhibitor-Free Enzyme Catalyzes the Cleavage of Collagen Fibrils and Soluble Native Type I Collagen Generating the Specific ¾- and ¼-Length Fragments. *J Biol Chem*. 1995;270(11):5872–5876.

15. Witzenburg C, Raghupathy R, Kren SM, Taylor DA, Barocas VH. Mechanical changes in the rat right ventricle with decellularization. *Spec Issue Cardiovasc Solid Mech*. 2012;45(5):842–849..

16. Zou Y, Zhang Y. Mechanical Evaluation of Decellularized Porcine Thoracic Aorta. *J Surg Res*. 2012;175(2):359–368.

17. Semon J, Nagy L, Llamas C, Tucker HA, Lee R, Prockop D. Integrin expression and integrin-mediated adhesion in vitro of human multipotent stromal cells (MSCs) to endothelial cells from various blood vessels. *Cell Tissue Res*. 2010;341(1):147–158.

18. Goessler UR, Bugert P, Bieback K, et al. Integrin expression in stem cells from bone marrow and adipose tissue during chondrogenic differentiation. *Int J Mol Med*. 2008;21(3):271.

19. Ott HC, Matthiesen TS, Goh S-K, et al. Perfusion-decellularized matrix: using nature's platform to engineer a bioartificial heart. *Nat Med*. 2008;14(2):213–221.

20. Barocas VH, Tranquillo RT. An anisotropic biphasic theory of tissue-equivalent mechanics: the interplay among cell traction, fibrillar network deformation, fibril alignment, and cell contact guidance. *J Biomech Eng*. 1997;119(2):137–145.

21. Fink RM, Lengfelder E. Hyaluronic acid degradation by ascorbic acid and influence of iron. *Free Radic Res Commun*. 1987;3(1-5):85–92.

22. Motohashi N, Mori I. The effect of synovial fluid proteins in the degradation of hyaluronic acid induced by ascorbic acid. *J Inorg Biochem*. 1985;24(1):69–74.

23. Edward M, Oliver RF. Changes in the synthesis, distribution and sulphation of glycosaminoglycans of cultured human skin fibroblasts upon ascorbate feeding. *J Cell Sci*. 1983;64:245–254.

24. Li Y, Yu X, Lin S, Li X, Zhang S, Song Y-H. Insulin-like growth factor 1 enhances the migratory capacity of mesenchymal stem cells. *Biochem Biophys Res Commun*. 2007;356(3):780–784.

25. Ponte AL, Marais E, Gallay N, et al. The In Vitro Migration Capacity of Human Bone Marrow Mesenchymal Stem Cells: Comparison of Chemokine and Growth Factor Chemotactic Activities. *Stem Cells*. 2007;25(7):1737–1745.

26. Ward CW, Lawrence MC. Ligand-induced activation of the insulin receptor: a multi-step process involving structural changes in both the ligand and the receptor. *BioEssays*. 2009;31(4):422–434.

27. Gharibi B, Hughes FJ. Effects of medium supplements on proliferation, differentiation potential, and in vitro expansion of mesenchymal stem cells. *Stem Cells Transl Med*. 2012;1(11):771–782.

28. Potdar PD, D'souza SB. Ascorbic acid induces in vitro proliferation of human subcutaneous adipose tissue derived mesenchymal stem cells with upregulation of embryonic stem cell pluripotency markers Oct4 and SOX 2. *Hum Cell*. 2010;23(4):152–155.

29. Choi K-M, Seo Y-K, Yoon H-H, et al. Effect of ascorbic acid on bone marrow-derived mesenchymal stem cell proliferation and differentiation. *J Biosci Bioeng*. 2008;105(6):586–594.

30. Guido S, Tranquillo RT. A methodology for the systematic and quantitative study of cell contact guidance in oriented collagen gels. Correlation of fibroblast orientation and gel birefringence. *J Cell Sci*. 1993;105(2):317–331.

31. Tranquillo RT, Girton TS, Bromberek BA, Triebes TG, Mooradian DL. Magnetically orientated tissue-equivalent tubes: application to a circumferentially orientated media-equivalent. *Biomaterials*. 1996;17(3):349–357.

32. Peng H-F, Liu JY, Andreadis ST, Swartz DD. Hair Follicle-Derived Smooth Muscle Cells and Small Intestinal Submucosa for Engineering Mechanically Robust and Vasoreactive Vascular Media. *Tissue Eng Part A*. 2011:17(7-8): 981-990.

33. Kurpinski KT, Stephenson JT, Janairo RRR, Lee H, Li S. The effect of fiber alignment and heparin coating on cell infiltration into nanofibrous PLLA scaffolds. *Biomaterials*. 2010;31(13):3536–3542.

34. Tseng P-C, Young T-H, Wang T-M, Peng H-W, Hou S-M, Yen M-L. Spontaneous osteogenesis of MSCs cultured on 3D microcarriers through alteration of cytoskeletal tension. *Biomaterials*. 2012;33(2):556–564.

35. Breyner NM, Hell RCR, Carvalho LRP, et al. Effect of a Three-Dimensional Chitosan Porous Scaffold on the Differentiation of Mesenchymal Stem Cells into Chondrocytes. *Cells Tissues Organs*. 2010;191(2):119–128.

36. Kawamura K, Chu CR, Sobajima S, et al. Adenoviral-mediated transfer of TGF-β1 but not IGF-1 induces chondrogenic differentiation of human mesenchymal stem cells in pellet cultures. *Exp Hematol*. 2005;33(8):865–872.

37. Williams C, Xie AW, Emani S, et al. A Comparison of Human Smooth Muscle and Mesenchymal Stem Cells as Potential Cell Sources for Tissue-Engineered Vascular Patches. *Tissue Eng Part A*. 2012;18(9-10):986–998

38. Vater C, Kasten P, Stiehler M. Culture media for the differentiation of mesenchymal stromal cells. *Acta Biomater*. 2011;7(2):463–477.

39. Park JS, Chu JS, Tsou AD, et al. The effect of matrix stiffness on the differentiation of mesenchymal stem cells in response to TGF-[beta]. *Biomaterials*. 2011;32(16):3921–3930.

40. Yin Z, Chen X, Chen JL, et al. The regulation of tendon stem cell differentiation by the alignment of nanofibers. *Biomaterials*. 2010;31(8):2163–2175.

41. Wang Z, Teo EY, Chong MSK, et al. Biomimetic Three-Dimensional Anisotropic Geometries by Uniaxial Stretch of Poly(ε-Caprolactone) Films for Mesenchymal Stem Cell Proliferation, Alignment, and Myogenic Differentiation. *Tissue Eng Part C Methods*. 2013: 19(7):538-549.

42. Tay CY, Yu H, Pal M, et al. Micropatterned matrix directs differentiation of human mesenchymal stem cells towards myocardial lineage. *Exp Cell Res*. 2010;316(7):1159–1168.

Chapter 4: Conclusions and Future Directions

Tubular Cell Sheet Investigations

Summary of Results

In Chapter 2, methods were described to create tubular fibroblast-derived cell sheets and to explore the influence of mechanical cyclic stretch on these tissues. The original goal of this project was to create tubular cell sheets via direct cell seeding, as opposed to cell sheets that were created via rolling of planar cell sheets. Creating cell sheets via rolling takes a significant amount of culture time (~10 weeks) to allow for fusion of the cell sheet layers.[1,2] It was hypothesized that thick tubular cell sheets could be grown directly on a tubular mandrel, bypassing the need for cell layer fusion.

Despite attempts to improve collagen production and organization by modifying the culture conditions (Figures 2.2 and 2.3) and applying 5% cyclic stretch (Figures 2.4 thru 2.6), tissue that was thick enough to be act as a tissue replacement was unable to be grown. While cyclically stretching the tubular cell sheets promoted the axial compaction of the cell sheet, leading to a circumferential orientation of cells and ECM, this organization did not lead to any improvement to the intrinsic mechanical properties. This is likely due to the fact that the cells were not stimulated to produce additional collagen. It is possible that higher magnitudes of cyclic stretch or longer culture periods could improve mechanical properties by promoting collagen synthesis, but it is unlikely that the potential benefit would offset the detriment of having a thin tissue that compacts uncontrollable when stretched.

The bioreactor used to explore the influence of cyclic stretch on cell sheet mechanical properties was also found useful in exploring the effects of mechanical

constraints on cell and collagen alignment (Figure 2.7 and 2.8). It was found that when prevented from compacting axially, both cells and collagen showed axial alignment. The effect could be partially removed by killing the cells with sodium azide. The work completed suggests that there is a coupling between internal, cell-generated tension associated with mechanical constraints on a tissue and external mechanical stretching, such that both factors need to be accounted for when predicting the overall alignment of a tissue subjected to mechanical stretching.

Future Work

The thickness of non-compacted 2 mm diameter tubular cell sheets was approximately 50 μm. In comparison, our group has been able to engineer 2 mm tubular tissues with thicknesses of 300-400 μm using our fibrin-based system.[3] These tissues are significantly easier to handle, manipulate, and have near-native mechanical properties when cultured in bioreactors that allow for both cyclic distension and enhanced nutrient delivery via transmural flow (termed PFS system). If cell sheets could be grown to similar thicknesses as fibrin-based grafts, such that they would be able to be mounted in the PFS system, the approach may be more useful for tissue engineering purposes.

There are several approaches that could be taken to enhance the thickness of tubular cell sheets. 1) Cell sheets could be grown on a permeable substrate to allow culture media access from both sides. 2) The cyclic stretch bioreactor could be redesigned to allow for higher magnitudes of cyclic stretch and incremental cyclic stretch.

Ahlfors and Billiar were able to create cell sheets that were 100-400 μm thick, depending on the composition of the culture medium.[4] These tissues were cultured on porous transwell inserts and cell culture medium was able to access both the top and bottom surface of the tissues. While the greatest improvements in thickness and mechanical properties of cell sheets was attributed to the use of chemically defined medium, the tissues that were cultured in media containing 10% FBS were still approximately twice as thick as what we were able to obtain culturing tissues on non-porous surfaces. It is possible that this strategy could be used to increase the thickness of tubular cell sheets, by growing the cells on a hollow porous tube and flowing tissue culture medium through the lumen of the tube. Unfortunately, it has been difficult to find a porous material that has the extensibility to be compatible with the cyclic stretch bioreactor and allow for direct culture of cells.

Furthermore, the benefits of cyclic stretch on collagen synthesis and mechanical properties are most apparent when the magnitude of stretch is incremented from 5% to 15% over 5 weeks.[5] When redesigning the bioreactor to accommodate 2 mm silicone tubing, we were only able to reliably reach stretch magnitudes of 5% for 3 weeks, without air leaking into the system. Since the system had to be assembled manually under aseptic conditions, the only reliable securing method was with sterile sutures. It is possible that if the dimensions of the system were scaled up to accommodate larger tubing (>4 mm), stronger securing methods such as cable ties or clamps could be used to allow for higher stretch magnitudes, enabling incremental cyclic stretch studies. The ability to increase the strain magnitude would also prove useful in further exploring the

influence of mechanical constraints and mechanical stretch on overall cell and ECM alignment.

Recellularization Investigations

Summary of Results

In Chapter 3, methods were described to create aligned and non-aligned decellularized tissues for use in recellularization studies. The tissue alignment (or lack of alignment) was confirmed both prior and following decellularization via polarized light imaging and mechanical anisotropy (Figures 3.4 & Figures 3.5). Furthermore, the mechanical anisotropy did not appear to be influenced by exposure of tissue to decellularization detergent (Table 3.2). Histology suggest that the extracellular matrix of the tissue was largely unchanged by decellularization, but birefringence in picosirius red staining suggests that the tissue was not isotropic, but rather transversely isotropic (i.e. random organization in the x-y plane, but different properties normal to the x-y plane) (Figure 3.5). This is not entirely surprising, since although non-aligned tissues are prevented from compacting laterally, they are still able to compact the thickness of the gel, providing some alignment through the thickness.

hMSCs were seeded onto the tissues, and after 3 weeks of culture, tissue was harvested and the extent of invasion was evaluated (Figure 3.7, Figure 3.8, Figure 3.9). Very little invasion or proliferation was seen in aligned and non-aligned tissues that were cultured in cell culture media without insulin and ascorbic acid (DMEM–supp and MSCGM). Both aligned and non-aligned tissues that were cultured with insulin and ascorbic acid showed an increase in cellularity and in the number of cells invaded at least

half the thickness of the tissue, but aligned and non-aligned tissues were not different from each other.

Cells that invaded into aligned tissue were more likely to have a lower nuclear circularity when compared to non-aligned tissues (Figure 3.10). The fact that there were more circular cells seen in non-aligned tissues and no cells oriented towards the thickness of the tissue, support our inference that the tissue was transversely isotropic. We speculate that cells that invaded both aligned and non-aligned scaffold migrated preferentially within the plane, which would explain why there were no obvious differences in invasion between aligned and non-aligned samples.

Finally, our results also suggest that contact with decellularized tissue does not induce spontaneous differentiation towards an adipogenic or osteogenic phenotype, independent of culture conditions (Figure 3.11). However, invaded cells cultured in the presence of insulin and ascorbic acid appeared to stain more intensely for Alcian Blue, suggesting that this condition stimulated production of proteoglycans. The invaded cells also stained positive for the smooth muscle marker, α smooth muscle actin (αSMA). These data suggest that the invaded cells are being pushed towards a smooth muscle phenotype.

Overall, these studies show that the soluble factors insulin and ascorbic acid are necessary for the invasion of hMSCs into decellularized engineered tissues. We speculate that this is due to an increase in migration proliferation of hMSCs when exposed to these factors. Furthermore, in-plane ECM alignment did not influence hMSCs invasion into decellularized engineered tissues, although it did influence cell

alignment distribution. Finally, we show that, regardless of culture conditions or ECM alignment, hMSCs appear to be differentiating towards a smooth muscle phenotype.

Future Work

Additional studies should be performed to determine the degree of recellularization that is necessary to maintain tissue-engineered heart valve homeostasis *in vivo.* Current studies show a cellularity of less than 50% of the initial tissue cellularity after 3 weeks. This degree of recellularization may be acceptable provided that hMSCs have the ability to synthesize matrix to maintain the tissue *in vivo,* and/or the ability to attract host cells that are able to maintain the tissue. Although further work would be needed to determine which mechanism is more important, previous work suggests that hMSCs do not remain in the tissue beyond the first week.[6]

Regardless of the mechanism of homeostasis, *in vitro* and *in vivo* experimentation would be necessary to determine the appropriate degree of recellularization that would ensure long term homeostasis of the tissue *in vivo*. *In vitro* studies should focus on: 1) developing and understanding techniques that improve the degree of *in vitro* recellularization and 2) developing a bioreactor to recellularized whole valves.

Improving Degree of In Vitro Recellularization

Previous studies have shown that supplementation of cell culture media with insulin and ascorbic acid is essential for invasion of hMSCs into decellularized engineered tissue. It is currently unclear which of these supplements influences hMSCs invasion, and what the mechanisms of action are. As a first step to understanding the mechanisms, the influence of these supplements on cell proliferation and motility are

currently being explored. Prelimary work suggest that ascorbic acid increases cell migration and proliferation (Figure 3.12 and Table 3.3). Once more is understood about the mechanisms of action, further optimization can be done to potentially improve recellularization.

Preliminary studies have also shown that the length of time the tissue is exposed to SDS detergents during decellularization can also impact recellularization potential. The collagen density of the tissue after decellularization does not change, even with extended exposure to detergents. Not surprisingly, the mechanical properties also do not appear to be significantly altered after decellularization. It is possible that the organization and structure of the collagen fibrils are changing in a way that affects recellularization potential, but not mechanical properties. More work should be done to explore the impact of decellularization on the ultra-structure of the tissue and how this relates to recellularization potential and interacts with culture conditions, if at all.

Recellularization of Whole Valves – Bioreactors with Chemotaxis

Methods should be developed to recellularize whole tissue-engineered valves. I believe the most practical approach is to seed cells directly onto the inside of the valve, including direct seeding onto the valve root and leaflets. Even distribution of cells around the circumference of the valve can be ensured with manual or automatic rotation of the valve about its longitudinal axis.

After a period of static incubation, the valve could potentially be mounted into a bioreactor that allows periodic flow through the inside of the valve (Figure 4.1a). Since the culture medium in the inner and outer compartments of the valve bioreactor is

segregated, it is possible to apply a chemical gradient across the wall of the valve and explore the influence of an insulin and/or ascorbic acid gradient on the magnitude and speed of recellularization.

Preliminary work has shown that it is possible to maintain a serum gradient across the wall of tissue for up to 2 days without cells (Figure 4.1b). Unfortunately, there was no benefit of a serum gradient on the motility of hMSCs in a transwell assay (Figure 4.1c). More work would be needed to validate the stability of an insulin/ascorbic acid gradient and the benefits of an insulin gradient in the presence of serum containing medium (which presumably also contains some amount of insulin that may influence the magnitude of the gradient).

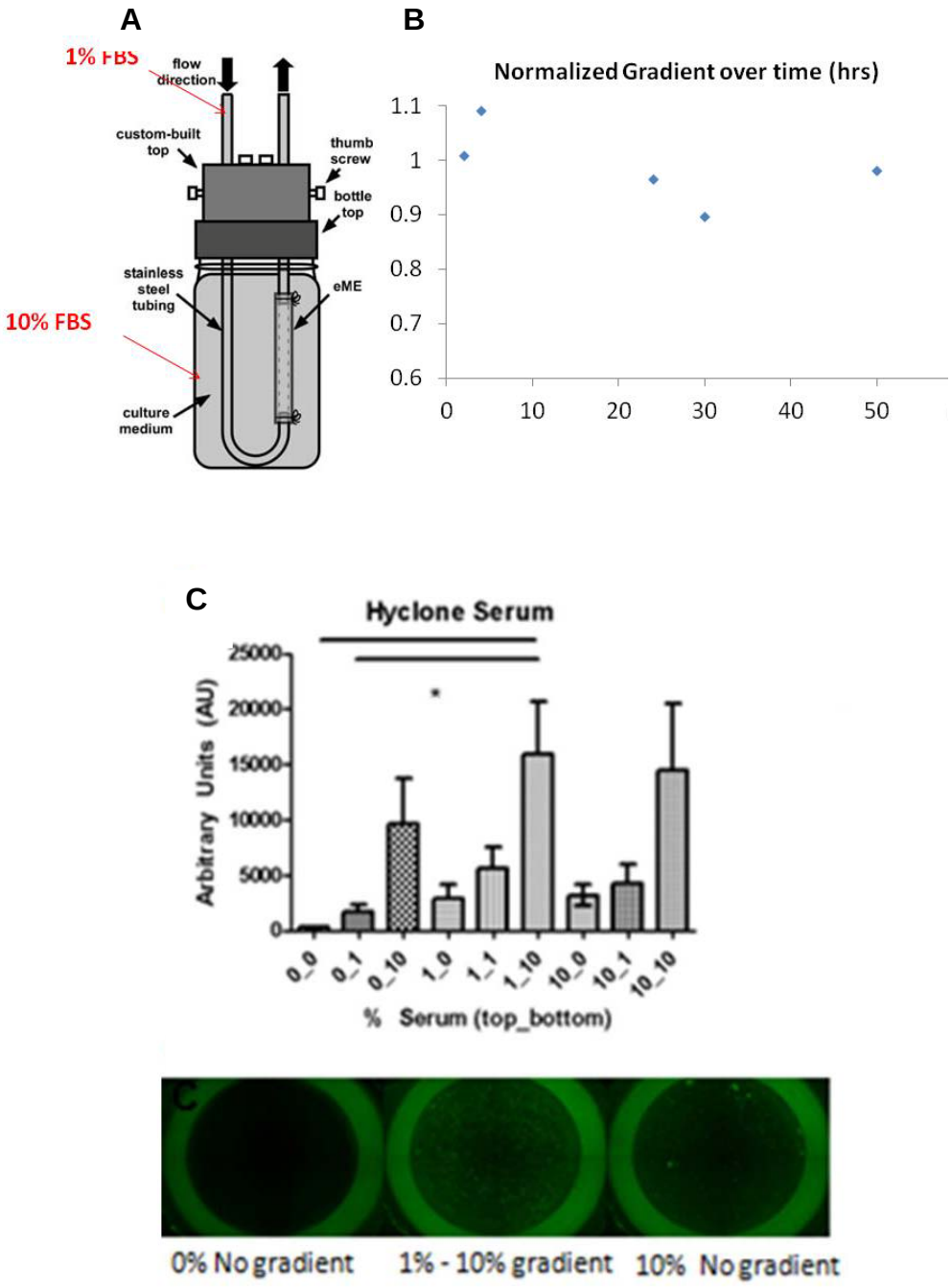

Figure 4.1: (A) Schematic of proposed bioreactor for recellularizing whole valves. (B) Preliminary data confirming maintenance of initial gradient over 2 days, without cells (C) Quantification of cell migration in a 96-well transwell assay.

Once the *in vitro* work has been completed, the work should be validated in long-term animal studies (ovine). Decellularized and recellularized tissue-engineered heart valves implanted in the pulmonary or aortic position should be compared to sham controls in terms of physiological performance, calcification, and degree of recellularization. Although technically more difficult, it would also be interesting to monitor the localization and fate of the transplanted cells.

References

1. L'heureux N, Paquet S, Labbe R, Germain L, Auger FA. A completely biological tissue-engineered human blood vessel. *FASEB J.* 1998;12(1):47–56.

2. L'Heureux N, Dusserre N, Konig G, et al. Human tissue-engineered blood vessels for adult arterial revascularization. *Nat Med*. 2006;12(3):361–365.

3. Syedain ZH, Meier LA, Bjork JW, Lee A, Tranquillo RT. Implantable arterial grafts from human fibroblasts and fibrin using a multi-graft pulsed flow-stretch bioreactor with noninvasive strength monitoring. *Biomaterials*. 2011;32(3):714–722..

4. Ahlfors J-EW, Billiar KL. Biomechanical and biochemical characteristics of a human fibroblast-produced and remodeled matrix. *Biomaterials*. 2007;28(13):2183–2191..

5. Syedain ZH, Weinberg JS, Tranquillo RT. Cyclic distension of fibrin-based tissue constructs: Evidence of adaptation during growth of engineered connective tissue. *Proceedings of the National Academy of Sciences*. 2008;105(18):6537–6542.

6. Roh JD, Sawh-Martinez R, Brennan MP, et al. Tissue-engineered vascular grafts transform into mature blood vessels via an inflammation-mediated process of vascular remodeling. *Proc Natl Acad Sci U S A*. 2010;107(10):4669–4674.

Bibliography

Aaronson, Philip I. (Philip Irving). *The Cardiovascular System at a Glance*. 4th ed. Chichester, West Sussex ; Malden, MA: Wiley-Blackwell, 2013

Ahlfors, Jan-Eric W., and Kristen L. Billiar. "Biomechanical and Biochemical Characteristics of a Human Fibroblast-produced and Remodeled Matrix." *Biomaterials* 28.13 (2007): 2183–2191.

Aimes RT, Quigley JP. "Matrix Metalloproteinase-2 Is an Interstitial Collagenase Inhibitor-Free Enzyme Catalyzes the Cleavage of Collagen Fibrils and Soluble Native Type I Collagen Generating the Specific ¾- and ¼-Length Fragments" *J Biol Chem*. (1995): 270(11):5872–5876.

Alberts, Bruce et al. *Molecular Biology of the Cell*. 4th ed. New York, NY: Garland Science, 2002.

Alt, Eckhard et al. "Fibroblasts Share Mesenchymal Phenotypes with Stem Cells, but Lack Their Differentiation and Colony-forming Potential." *Biology of the Cell* 103 (2011): 197–208..

Ayres, Chantal E. et al. "Measuring Fiber Alignment in Electrospun Scaffolds: a User's Guide to the 2D Fast Fourier Transform Approach." *Journal of Biomaterials Science, Polymer Edition* 19.5 (May): 603–621.

Balestrini, Jenna et al. "Applying Controlled Non-uniform Deformation for in Vitro Studies of Cell Mechanobiology." *Biomechanics and Modeling in Mechanobiology* 9.3 (2010): 329–344.

Balguid, Angelique et al. "Hypoxia Induces Near-Native Mechanical Properties in Engineered Heart Valve Tissue." *Circulation* 119.2 (2009): 290–297.

Bank, Alan J. et al. “Contribution of Collagen, Elastin, and Smooth Muscle to In Vivo Human Brachial Artery Wall Stress and Elastic Modulus.” *Circulation* 94.12 (1996): 3263–3270.

Baraki, Hassina et al. “Orthotopic Replacement of the Aortic Valve with Decellularized Allograft in a Sheep Model.” *Biomaterials* 30.31 (2009): 6240–6246..

Barocas, V H, and R T Tranquillo. “An Anisotropic Biphasic Theory of Tissue-equivalent Mechanics: The Interplay Among Cell Traction, Fibrillar Network Deformation, Fibril Alignment, and Cell Contact Guidance.” *Journal of biomechanical engineering* 119.2 (1997): 137–145.

Baron, Frédéric et al. “Cotransplantation of Mesenchymal Stem Cells Might Prevent Death from Graft-versus-Host Disease (GVHD) Without Abrogating Graft-versus-Tumor Effects After HLA-Mismatched Allogeneic Transplantation Following Nonmyeloablative Conditioning.” *Biology of Blood and Marrow Transplantation* 16.6 (2010): 838–847.

Barrientos, Stephan et al. “Growth Factors and Cytokines in Wound Healing.” *Wound Repair and Regeneration* 16.5 (2008): 585–601. *Wiley Online Library*.

Bjork, Jason W., and Robert T. Tranquillo. “Transmural Flow Bioreactor for Vascular Tissue Engineering.” *Biotechnology and Bioengineering* 104.6 (2009): 1197–1206. *Wiley InterScience*.

Boccafoschi, F et al. “Dynamic Fibroblast Cultures.” *Cell Adhesion & Migration* 1.3 (2007): 124–128.

Bourget, Jean-Michel et al. “Human Fibroblast-derived ECM as a Scaffold for Vascular Tissue Engineering.” *Biomaterials* 33.36 (2012): 9205–9213.

Brennan, Matthew P. et al. “Tissue Engineered Vascular Grafts Demonstrate Evidence of Growth and Development When Implanted in a Juvenile Animal Model.” *Annals of surgery* 248.3 (2008): 370–377.

Breyner, Natália M. et al. “Effect of a Three-Dimensional Chitosan Porous Scaffold on the Differentiation of Mesenchymal Stem Cells into Chondrocytes.” *Cells Tissues Organs* 191.2 (2010): 119–128.

Butcher, Jonathan T et al. “Transcriptional Profiles of Valvular and Vascular Endothelial Cells Reveal Phenotypic Differences: Influence of Shear Stress.” *Arteriosclerosis, thrombosis, and vascular biology* 26.1 (2006): 69–77.

Butcher, Jonathan T. et al. “Unique Morphology and Focal Adhesion Development of Valvular Endothelial Cells in Static and Fluid Flow Environments.” *Arteriosclerosis, Thrombosis, and Vascular Biology* 24.8 (2004): 1429–1434.

Carson, Freida L., and Christa Hladik. *Histotechnology: A Self-Instructional Text*. 3rd Edition. American Society for Clinical Pathology, 2009.

Choi, Kyung-Min et al. “Effect of Ascorbic Acid on Bone Marrow-derived Mesenchymal Stem Cell Proliferation and Differentiation.” *Journal of Bioscience and Bioengineering* 105.6 (2008): 586–594.

Christie, Grant W., and Brian G. Barratt-Boyes. “Mechanical Properties of Porcine Pulmonary Valve Leaflets: How Do They Differ from Aortic Leaflets?” *The Annals of Thoracic Surgery* 60.suppl_2 (1995): S195.

Conte, Michael S. “The Ideal Small Arterial Substitute: a Search for the Holy Grail?” *FASEB J.* 12.1 (1998): 43–45.

Crapo, Peter M., and Yadong Wang. “Physiologic Compliance in Engineered Small-diameter Arterial Constructs Based on an Elastomeric Substrate.” *Biomaterials* 31.7 (2010): 1626–1635.

Dahl, Shannon et al. “Mechanical Properties and Compositions of Tissue Engineered and Native Arteries.” *Annals of Biomedical Engineering* 35.3 (2007): 348–355.

Dahl, Shannon L. M. et al. “Readily Available Tissue-Engineered Vascular Grafts.” *Science Translational Medicine* 3.68 (2011): 68ra9–68ra9.

Davidson, Jeffrey M. et al. “Ascorbate Differentially Regulates Elastin and Collagen Biosynthesis in Vascular Smooth Muscle Cells and Skin Fibroblasts by Pretranslational Mechanisms.” *Journal of Biological Chemistry* 272.1 (1997): 345–352.

De Clerck Y A, and Jones P A. “The Effect of Ascorbic Acid on the Nature and Production of Collagen and Elastin by Rat Smooth-muscle Cells.” 15 Jan. 1980.

Dickinson, Richard B., Stefano Guido, and Robert T. Tranquillo. “Biased Cell Migration of Fibroblasts Exhibiting Contact Guidance in Oriented Collagen Gels.” *Annals of Biomedical Engineering* 22.4 (1994): 342–356.

Dobrin, P. B. “Mechanical Properties of Arteries.” *Physiological Reviews* 58.2 (1978): 397–460.

Dominici, M et al. “Minimal Criteria for Defining Multipotent Mesenchymal Stromal Cells. The International Society for Cellular Therapy Position Statement.” *Cytotherapy* 8.4 (2006): 315–317.

Dong-Youn Lee, Jun-Mo Yang, and Kwan-Hyun Park. “A Dermal Equivalent Developed from Fibroblast Culture Alone: Effect of EGF and Insulin.” *Wound Repair & Regeneration* 15.6 (2007): 936–939.

Edward, M, and R F Oliver. “Changes in the Synthesis, Distribution and Sulphation of Glycosaminoglycans of Cultured Human Skin Fibroblasts Upon Ascorbate Feeding.” *Journal of Cell Science* 64 (1983): 245–254.

Emmert, Maximilian Y. et al. “Stem Cell–Based Transcatheter Aortic Valve Implantation: First Experiences in a Pre-Clinical Model.” *JACC: Cardiovascular Interventions* 5.8 (2012): 874–883.

Fink, R M, and E Lengfelder. “Hyaluronic Acid Degradation by Ascorbic Acid and Influence of Iron.” *Free Radical Research Communications* 3.1-5 (1987): 85–92.

Flanagan, Thomas C. et al. “The in Vitro Development of Autologous Fibrin-based Tissue-engineered Heart Valves Through Optimised Dynamic Conditioning.” *Biomaterials* 28.23 (2007): 3388–3397.

Foolen, Jasper et al. “The Influence of Matrix Integrity on Stress-fiber Remodeling in 3D.” *Biomaterials* 33.30 (2012): 7508–7518.

Freiberger, Harley et al. “Procollagen I Synthesis in Human Skin Fibroblasts: Effect of Culture Conditions on Biosynthesis.” *Journal of Investigative Dermatology* 75.5 (1980): 425–430.

Gauvin, Robert, Taby Ahsan, et al. “A Novel Single-Step Self-Assembly Approach for the Fabrication of Tissue-Engineered Vascular Constructs.” *Tissue Engineering Part A* 16.5 (2010): 1737–1747.

Gauvin, Robert, Rémi Parenteau-Bareil, et al. “Dynamic Mechanical Stimulations Induce Anisotropy and Improve the Tensile Properties of Engineered Tissues Produced Without Exogenous Scaffolding.” *Acta Biomaterialia* 7.9 (2011): 3294–3301.

Gauvin, Robert, Maxime D Guillemette, et al. “Mechanical Properties of Tissue-Engineered Vascular Constructs Produced Using Arterial or Venous Cells.” *Tissue Engineering Part A* (2011)

Gelse, K., E. Pöschl, and T. Aigner. “Collagens—structure, Function, and Biosynthesis.” *Advanced Drug Delivery Reviews* 55.12 (2003): 1531–1546.

Gharibi, Borzo, and Francis J Hughes. “Effects of Medium Supplements on Proliferation, Differentiation Potential, and in Vitro Expansion of Mesenchymal Stem Cells.” *Stem Cells Translational Medicine* 1.11 (2012): 771–782.

Girton, T. S. et al. “Mechanisms of Stiffening and Strengthening in Media-Equivalents Fabricated Using Glycation.” *Journal of Biomechanical Engineering* 122.3 (2000): 216–223.

Goessler, Ulrich Reinhart et al. “Integrin Expression in Stem Cells from Bone Marrow and Adipose Tissue During Chondrogenic Differentiation.” *International Journal of Molecular Medicine* 21.3 (2008): 271.

Gong, Zhaodi et al. “Influence of Culture Medium on Smooth Muscle Cell Differentiation from Human Bone Marrow–Derived Mesenchymal Stem Cells.” *Tissue Engineering Part A* 15.2 (2009): 319–330.

Gong, Zhaodi, and Laura E. Niklason. “Small-diameter Human Vessel Wall Engineered from Bone Marrow-derived Mesenchymal Stem Cells (hMSCs).” *FASEB J.* 22.6 (2008): 1635–1648.

Grassl, E. D., T. R. Oegema, and R. T. Tranquillo. “A Fibrin-based Arterial Media Equivalent.” *Journal of Biomedical Materials Research Part A* 66A.3 (2003): 550–561.

. “Fibrin as an Alternative Biopolymer to type-I Collagen for the Fabrication of a Media Equivalent.” *Journal of Biomedical Materials Research* 60.4 (2002): 607–612.

Grenier, Guillaume et al. “Tissue Reorganization in Response to Mechanical Load Increases Functionality.” *Tissue Engineering* 11.1-2 (2005): 90–100.

Grinnell, Frederick et al. “Collagen Processing, Crosslinking, and Fibril Bundle Assembly in Matrix Produced by Fibroblasts in Long-term Cultures Supplemented with Ascorbic Acid.” *Experimental Cell Research* 181.2 (1989): 483–491.

Grouf, Jaime Lynn et al. “Differential Effects of EGF and TGF-β1 on Fibroblast Activity in Fibrin-Based Tissue Equivalents.” *Tissue Engineering* 13.4 (2007): 799–807.

Gui, Liqiong, Akihito Muto, et al. “Development of Decellularized Human Umbilical Arteries as Small-Diameter Vascular Grafts.” *Tissue Engineering Part A* 15.9 (2011): 2665–2676.

Gui, Liqiong, Liping Zhao, et al. “Development of Novel Biodegradable Polymer Scaffolds for Vascular Tissue Engineering.” *Tissue Engineering Part A* 17.9-10 (2011): 1191–1200.

Guido, S., and R. T. Tranquillo. “A Methodology for the Systematic and Quantitative Study of Cell Contact Guidance in Oriented Collagen Gels. Correlation of Fibroblast Orientation and Gel Birefringence.” *Journal of Cell Science* 105.2 (1993): 317–331.

Hashi, Craig K. et al. “Antithrombogenic Property of Bone Marrow Mesenchymal Stem Cells in Nanofibrous Vascular Grafts.” *Proceedings of the National Academy of Sciences* 104.29 (2007): 11915 –11920.

Hoerstrup, Simon P. et al. “Tissue Engineering of Functional Trileaflet Heart Valves From Human Marrow Stromal Cells.” *Circulation* 106.12 suppl 1 (2002): I–143–I–150.

Hoganson, David M. et al. “The Retention of Extracellular Matrix Proteins and Angiogenic and Mitogenic Cytokines in a Decellularized Porcine Dermis.” *Biomaterials* 31.26 (2010): 6730–6737.

Honge, Jesper Langhoff et al. “Recellularization of Aortic Valves in Pigs.” *European Journal of Cardio-Thoracic Surgery* 39.6 (2011): 829–834.

Humphrey, Jay D. *Cardiovascular Solid Mechanics*. 2nd ed. New York, NY: Springer-Verlag, 2002.

Huynh, Tam et al. “Remodeling of an Acellular Collagen Graft into a Physiologically Responsive Neovessel.” *Nature Biotechnology* 17.11 (1999): 1083–1086.

Iop, Laura et al. “The Influence of Heart Valve Leaflet Matrix Characteristics on the Interaction Between Human Mesenchymal Stem Cells and Decellularized Scaffolds.” *Biomaterials* 30.25 (2009): 4104–4116.

Isenberg, Brett C. et al. “Micropatterned Cell Sheets with Defined Cell and Extracellular Matrix Orientation Exhibit Anisotropic Mechanical Properties.” *Journal of Biomechanics* 45.5 (2012): 756–761.

Isenberg, Brett C., and Robert T. Tranquillo. “Long-Term Cyclic Distention Enhances the Mechanical Properties of Collagen-Based Media-Equivalents.” *Annals of Biomedical Engineering* 31.8 (2003): 937–949.

Iwasaki, Kiyotaka et al. “Bioengineered Three-Layered Robust and Elastic Artery Using Hemodynamically-Equivalent Pulsatile Bioreactor.” *Circulation* 118.14_suppl_1 (2008): S52–57.

Janeczek Portalska, Karolina et al. “Endothelial Differentiation of Mesenchymal Stromal Cells.” *PLoS ONE* 7.10 (2012): n. pag.

Jordan, James E. et al. “Bioengineered Self-seeding Heart Valves.” *The Journal of Thoracic and Cardiovascular Surgery* 143.1 (2012): 201–208.

Kawamura, Koichiro et al. “Adenoviral-mediated Transfer of TGF-β1 but Not IGF-1 Induces Chondrogenic Differentiation of Human Mesenchymal Stem Cells in Pellet Cultures.” *Experimental Hematology* 33.8 (2005): 865–872.

Kim, Young-Jo et al. “Fluorometric Assay of DNA in Cartilage Explants Using Hoechst 33258.” *Analytical Biochemistry* 174.1 (1988): 168–176.

Koch, Sabine et al. “Fibrin-polylactide-based Tissue-engineered Vascular Graft in the Arterial Circulation.” *Biomaterials* 31.17 (2010): 4731–4739.

Konig, Gerhardt et al. “Mechanical Properties of Completely Autologous Human Tissue Engineered Blood Vessels Compared to Human Saphenous Vein and Mammary Artery.” *Biomaterials* 30.8 (2009): 1542–1550.

Kumashiro, Yoshikazu, Masayuki Yamato, and Teruo Okano. “Cell Attachment–Detachment Control on Temperature-Responsive Thin Surfaces for Novel Tissue Engineering.” *Annals of Biomedical Engineering* 38.6 (2010): 1977–1988.

Kurata, S., and R. Hata. “Epidermal Growth Factor Inhibits Transcription of Type I Collagen Genes and Production of Type I Collagen in Cultured Human Skin Fibroblasts in the Presence and Absence of L-ascorbic Acid 2-phosphate, a Long-acting Vitamin C Derivative.” *Journal of Biological Chemistry* 266.15 (1991): 9997–10003.

Kurata, Shun-Ichi, Haruki Senoo, and Ryu-Ichiro Hata. “Transcriptional Activation of Type I Collagen Genes by Ascorbic Acid 2-Phosphate in Human Skin Fibroblasts and Its Failure in Cells from a Patient with α2(I)-Chain-Defective Ehlers-Danlos Syndrome.” *Experimental Cell Research* 206.1 (1993): 63–71.

Kurpinski, Kyle et al. “Transforming Growth Factor-β and Notch Signaling Mediate Stem Cell Differentiation into Smooth Muscle Cells.” *STEM CELLS* 28.4 (2010): 734–742.

L’Heureux, N et al. “In Vitro Construction of a Human Blood Vessel from Cultured Vascular Cells: a Morphologic Study.” *Journal of Vascular Surgery: Official Publication, the Society for Vascular Surgery [and] International Society for Cardiovascular Surgery, North American Chapter* 17.3 (1993): 499–509.

L’heureux, Nicolas et al. “A Completely Biological Tissue-engineered Human Blood Vessel.” *FASEB J.* 12.1 (1998): 47–56

L’Heureux, Nicolas et al. “Human Tissue-engineered Blood Vessels for Adult Arterial Revascularization.” *Nat Med* 12.3 (2006): 361–365.

Langer, Robert, and Joseph P. Vacanti. “Tissue Engineering.” *Science* 260.5110 (1993): 920–926.

Lazarus, Hillard M. et al. “Cotransplantation of HLA-Identical Sibling Culture-Expanded Mesenchymal Stem Cells and Hematopoietic Stem Cells in Hematologic Malignancy Patients.” *Biology of Blood and Marrow Transplantation* 11.5 (2005): 389–398.

Le Blanc, K. et al. “Mesenchymal Stem Cells Inhibit and Stimulate Mixed Lymphocyte Cultures and Mitogenic Responses Independently of the Major Histocompatibility Complex.” *Scandinavian Journal of Immunology* 57.1 (2003): 11–20.

Le Blanc, Katarina et al. “Treatment of Severe Acute Graft-versus-host Disease with Third Party Haploidentical Mesenchymal Stem Cells.” *The Lancet* 363.9419 (2004): 1439–1441.

Lee, Chang H. et al. “CTGF Directs Fibroblast Differentiation from Human Mesenchymal Stem/stromal Cells and Defines Connective Tissue Healing in a Rodent Injury Model.” 120.9 (2010): 3340–3349.

Levene, C. I., and C. J. Bates. “Ascorbic Acid and Collagen Synthesis in Cultured Fibroblasts.” *Annals of the New York Academy of Sciences* 258.Second Conference on Vitamin C (1975): 288–306.

Li, Yangxin et al. “Insulin-like Growth Factor 1 Enhances the Migratory Capacity of Mesenchymal Stem Cells.” *Biochemical and Biophysical Research Communications* 356.3 (2007): 780–784.

Lloyd-Jones, Donald et al. “Heart Disease and Stroke Statistics—2010 Update.” *Circulation* 121.7 (2010): e46–e215.

Mendelson, Karen, and Frederick J. Schoen. “Heart Valve Tissue Engineering: Concepts, Approaches, Progress, and Challenges.” *Annals of Biomedical Engineering* 34.12 (2006): 1799–1819.

Mol, Anita et al. “Autologous Human Tissue-Engineered Heart Valves Prospects for Systemic Application.” *Circulation* 114.1 suppl (2006): I–152–I–158.

Motohashi, N, and I Mori. “The Effect of Synovial Fluid Proteins in the Degradation of Hyaluronic Acid Induced by Ascorbic Acid.” *Journal of Inorganic Biochemistry* 24.1 (1985): 69–74.

Nasseri, Boris A. et al. “Dynamic Rotational Seeding and Cell Culture System for Vascular Tube Formation.” *Tissue Engineering* 9.2 (2003): 291–299.

Nauta, A. J., and W. E. Fibbe. “Immunomodulatory Properties of Mesenchymal Stromal Cells.” *Blood* 110.10 (2007): 3499–3506.

Neidert, M. R. et al. “Enhanced Fibrin Remodeling in Vitro with TGF-[beta]1, Insulin and Plasmin for Improved Tissue-equivalents.” *Biomaterials* 23.17 (2002): 3717–3731.

Nicola, Massimo Di et al. “Human Bone Marrow Stromal Cells Suppress T-lymphocyte Proliferation Induced by Cellular or Nonspecific Mitogenic Stimuli.” *Blood* 99.10 (2002): 3838–3843.

Niklason, L. E. et al. “Functional Arteries Grown in Vitro.” *Science* 284.5413 (1999): 489–493.

Niklason, Laura E. et al. “Morphologic and Mechanical Characteristics of Engineered Bovine Arteries.” *Journal of Vascular Surgery* 33.3 (2001): 628–638.

O’Cearbhaill, Eoin D. et al. “Behavior of Human Mesenchymal Stem Cells in Fibrin-Based Vascular Tissue Engineering Constructs.” *Annals of Biomedical Engineering* 38.3 (2010): 649–657.

Ott, Harald C et al. “Perfusion-decellularized Matrix: Using Nature’s Platform to Engineer a Bioartificial Heart.” *Nat Med* 14.2 (2008): 213–221.

Owens, Gary K., Meena S. Kumar, and Brian R. Wamhoff. “Molecular Regulation of Vascular Smooth Muscle Cell Differentiation in Development and Disease.” *Physiol. Rev.* 84.3 (2004): 767–801.

Park, Jennifer S. et al. “The Effect of Matrix Stiffness on the Differentiation of Mesenchymal Stem Cells in Response to TGF-[beta].” *Biomaterials* 32.16 (2011): 3921–3930.

Peng, Hao-Fan et al. “Hair Follicle-Derived Smooth Muscle Cells and Small Intestinal Submucosa for Engineering Mechanically Robust and Vasoreactive Vascular Media.” *Tissue Engineering Part A* (2011): 110306231138043.

Pevsner-Fischer, Meirav, Sarit Levin, and Dov Zipori. “The Origins of Mesenchymal Stromal Cell Heterogeneity.” *Stem Cell Reviews and Reports* 7.3 (2011): 560–568.

Pietak, A et al. “Are Micropatterned Substrates for Directed Cell Organization an Effective Method to Create Ordered 3D Tissue Constructs?” *Journal of tissue engineering and regenerative medicine* 2.7 (2008): 450–453.

Pittenger, Mark F. et al. “Multilineage Potential of Adult Human Mesenchymal Stem Cells.” *Science* 284.5411 (1999): 143–147.

Ponte, Adriana López et al. “The In Vitro Migration Capacity of Human Bone Marrow Mesenchymal Stem Cells: Comparison of Chemokine and Growth Factor Chemotactic Activities.” *Stem Cells* 25.7 (2007): 1737–1745.

Potdar, Pravin D, and Stephanie B D’souza. “Ascorbic Acid Induces in Vitro Proliferation of Human Subcutaneous Adipose Tissue Derived Mesenchymal Stem Cells with Upregulation of Embryonic Stem Cell Pluripotency Markers Oct4 and SOX 2.” *Human Cell* 23.4 (2010): 152–155.

Quinn, Rachael W. et al. “Performance and Morphology of Decellularized Pulmonary Valves Implanted in Juvenile Sheep.” *The Annals of Thoracic Surgery* 92.1 (2011): 131–137.

Quint, Clay et al. “Decellularized Tissue-engineered Blood Vessel as an Arterial Conduit.” *Proceedings of the National Academy of Sciences* (2011): n. pag.

Ramaswamy, Sharan et al. “The Role of Organ Level Conditioning on the Promotion of Engineered Heart Valve Tissue Development In-Vitro Using Mesenchymal Stem Cells.” *Biomaterials* 31.6 (2010): 1114.

Robinson, Paul S. et al. “Functional Tissue-Engineered Valves from Cell-Remodeled Fibrin with Commissural Alignment of Cell-Produced Collagen.” *Tissue Engineering Part A* 14.1 (2008): 83–95.

Roh, Jason D. et al. “Tissue-engineered Vascular Grafts Transform into Mature Blood Vessels via an Inflammation-mediated Process of Vascular Remodeling.” *Proceedings of the National Academy of Sciences of the United States of America* 107.10 (2010): 4669–4674. *PubMed Central*. Web.

Roh, Jason D. et al. “Tissue-engineered Vascular Grafts Transform into Mature Blood Vessels via an Inflammation-mediated Process of Vascular Remodeling.” *Proceedings of the National Academy of Sciences of the United States of America* 107.10 (2010): 4669–4674.

Rubbens, Mirjam et al. “Quantification of the Temporal Evolution of Collagen Orientation in Mechanically Conditioned Engineered Cardiovascular Tissues.” *Annals of Biomedical Engineering* 37.7 (2009): 1263–1272.

Schaner, Patrick J et al. “Decellularized Vein as a Potential Scaffold for Vascular Tissue Engineering.” *Journal of Vascular Surgery* 40.1 (2004): 146–153.

Schoen, Frederick J., and Simon P. Hoerstrup. “Chapter II.6.10 - Heart Valve Tissue Engineering.” *Biomaterials Science (Third Edition)*. Ed. Buddy D. Ratner et al. Academic Press, 2013. 1246–1261.

Schoen, Frederick J., and Robert J. Levy. “Calcification of Tissue Heart Valve Substitutes: Progress Toward Understanding and Prevention.” *The Annals of Thoracic Surgery* 79.3 (2005): 1072–1080.

Schutte, Stacey C. et al. “Cyclic Strain Improves Strength and Function of a Collagen-Based Tissue-Engineered Vascular Media.” *Tissue Engineering Part A* (2010)

See, Eugene Yong-Shun, Siew Lok Toh, and James Cho Hong Goh. “Multilineage Potential of Bone-Marrow-Derived Mesenchymal Stem Cell Cell Sheets: Implications for Tissue Engineering.” *Tissue Engineering Part A* 16.4 (2011): 1421–1431.

Seliktar, Dror et al. “Dynamic Mechanical Conditioning of Collagen-Gel Blood Vessel Constructs Induces Remodeling In Vitro.” *Annals of Biomedical Engineering* 28.4 (2000): 351–362..

Seliktar, Dror, Robert M. Nerem, and Zorina S. Galis. “Mechanical Strain-Stimulated Remodeling of Tissue-Engineered Blood Vessel Constructs.” *Tissue Engineering* 9.4 (2003): 657–666.

Semon, Julie. et al. “Integrin Expression and Integrin-mediated Adhesion in Vitro of Human Multipotent Stromal Cells (MSCs) to Endothelial Cells from Various Blood Vessels.” *Cell and Tissue Research* 341.1 (2010): 147–158.

Solan, Amy, Shannon L. M. Dahl, and Laura E. Niklason. “Effects of Mechanical Stretch on Collagen and Cross-Linking in Engineered Blood Vessels.” *Cell Transplantation* 18 (2009): 915–921.

Soletti, Lorenzo et al. “A Seeding Device for Tissue Engineered Tubular Structures.” *Biomaterials* 27.28 (2006): 4863–4870.

Stegemann, Hermann, and Karlheinz Stalder. “Determination of Hydroxyproline.” *Clinica Chimica Acta* 18.2 (1967): 267–273..

Stegemann, Jan P., and Robert M. Nerem. “Altered Response of Vascular Smooth Muscle Cells to Exogenous Biochemical Stimulation in Two- and Three-dimensional Culture.” *Experimental Cell Research* 283.2 (2003): 146–155.

. Stegemann, Jan P., and Robert M. Nerem “Phenotype Modulation in Vascular Tissue Engineering Using Biochemical and Mechanical Stimulation.” *Annals of Biomedical Engineering* 31.4 (2003): 391–402.

Stella, John A., Jun Liao, and Michael S. Sacks. “Time-dependent Biaxial Mechanical Behavior of the Aortic Heart Valve Leaflet.” *Journal of Biomechanics* 40.14 (2007): 3169–3177.

Subramony, Siddarth D. et al. “The Guidance of Stem Cell Differentiation by Substrate Alignment and Mechanical Stimulation.” *Biomaterials* 34.8 (2013): 1942–1953.

Swartz, Daniel D., James A. Russell, and Stelios T. Andreadis. “Engineering of Fibrin-based Functional and Implantable Small-diameter Blood Vessels.” *Am J Physiol Heart Circ Physiol* 288.3 (2005): H1451–1460.

Syedain, Zeeshan et al. “Implantation of a Tissue-engineered Heart Valve from Human Fibroblasts Exhibiting Short Term Function in the Sheep Pulmonary Artery.” *Cardiovascular Engineering and Technology* 2.2 (2011): 101–112.

Syedain, Zeeshan H., Allison R. Bradee, et al. “Decellularized Tissue-Engineered Heart Valve Leaflets with Recellularization Potential.” *Tissue Engineering Part A* 19.5-6 (2013): 759–769.

Syedain, Zeeshan H., Lee A. Meier, et al. “Implantable Arterial Grafts from Human Fibroblasts and Fibrin Using a Multi-graft Pulsed Flow-stretch Bioreactor with Noninvasive Strength Monitoring.” *Biomaterials* 32.3 (2011): 714–722.

Syedain, Zeeshan H., and Robert T. Tranquillo. “Controlled Cyclic Stretch Bioreactor for Tissue-Engineered Heart Valves.” *Biomaterials* 30.25 (2009): 4078–4084.

- “TGF-Î²1 Diminishes Collagen Production During Long-term Cyclic Stretching of Engineered Connective Tissue: Implication of Decreased ERK Signaling.” *Journal of Biomechanics* 44.5 (2011): 848–855.

Syedain, Zeeshan H., Justin S. Weinberg, and Robert T. Tranquillo. “Cyclic Distension of Fibrin-based Tissue Constructs: Evidence of Adaptation During Growth of Engineered Connective Tissue.” *Proceedings of the National Academy of Sciences* 105.18 (2008): 6537–6542.

Takahashi, Hironobu et al. “Anisotropic Cell Sheets for Constructing Three-dimensional Tissue with Well-organized Cell Orientation.” *Biomaterials* 32.34 (2011): 8830–8838.

Tay, Chor Yong et al. “Micropatterned Matrix Directs Differentiation of Human Mesenchymal Stem Cells Towards Myocardial Lineage.” *Experimental Cell Research* 316.7 (2010): 1159–1168.

Tower, Theodore T., Michael R. Neidert, and Robert T. Tranquillo. “Fiber Alignment Imaging During Mechanical Testing of Soft Tissues.” *Annals of Biomedical Engineering* 30.10 (2002): 1221–1233.

Tranquillo, R.T. et al. “Magnetically Orientated Tissue-equivalent Tubes: Application to a Circumferentially Orientated Media-equivalent.” *Biomaterials* 17.3 (1996): 349–357. *ScienceDirect*. Web. 8 May 2013.

Tschoeke, Beate, Thomas C. Flanagan, Anne Cornelissen, et al. “Development of a Composite Degradable/Nondegradable Tissue-engineered Vascular Graft.” *Artificial Organs* 32.10 (2008): 800–809.

Tschoeke, Beate, Thomas C. Flanagan, Sabine Koch, et al. “Tissue-Engineered Small-Caliber Vascular Graft Based on a Novel Biodegradable Composite Fibrin-Polylactide Scaffold.” *Tissue Engineering Part A* 15.8 (2009): 1909–1918.

Tse, William T et al. “Suppression of Allogeneic T-cell Proliferation by Human Marrow Stromal Cells: Implications in Transplantation.” *Transplantation* 75.3 (2003): 389–397.

Tseng, Pei-Chi et al. “Spontaneous Osteogenesis of MSCs Cultured on 3D Microcarriers through Alteration of Cytoskeletal Tension.” *Biomaterials* 33.2 (2012): 556–564.

Tudorache, Igor et al. “Orthotopic Replacement of Aortic Heart Valves with Tissue Engineered Grafts.” *Tissue Engineering Part A* (2013): 130314140332008.

Van Hinsbergh, Victor W.M. “The Endothelium: Vascular Control of Haemostasis.” *European Journal of Obstetrics & Gynecology and Reproductive Biology* 95.2 (2001): 198–201.

Vater, Corina, Philip Kasten, and Maik Stiehler. “Culture Media for the Differentiation of Mesenchymal Stromal Cells.” *Acta Biomaterialia* 7.2 (2011): 463–477.

Vesely, Ivan. “Heart Valve Tissue Engineering.” *Circulation Research* 97.8 (2005): 743–755.

Von Maltzahn, W W, R G Warriyar, and W F Keitzer. “Experimental Measurements of Elastic Properties of Media and Adventitia of Bovine Carotid Arteries.” *Journal of biomechanics* 17.11 (1984): 839–847.

Wagenseil, Jessica E., and Robert P. Mecham. “New Insights into Elastic Fiber Assembly.” *Birth Defects Research Part C: Embryo Today: Reviews* 81.4 (2007): 229–240.

Wang, Zu-yong et al. “Biomimetic Three-Dimensional Anisotropic Geometries by Uniaxial Stretch of Poly(ε-Caprolactone) Films for Mesenchymal Stem Cell Proliferation, Alignment, and Myogenic Differentiation.” *Tissue Engineering Part C: Methods* (2013):

Ward, Colin W., and Michael C. Lawrence. “Ligand-induced Activation of the Insulin Receptor: a Multi-step Process Involving Structural Changes in Both the Ligand and the Receptor.” *BioEssays* 31.4 (2009): 422–434.

Weber, Benedikt et al. “Injectable Living Marrow Stromal Cell-based Autologous Tissue Engineered Heart Valves: First Experiences with a One-step Intervention in Primates.” *European Heart Journal* 32.22 (2011): 2830–2840.

Weinberg, CB, and E Bell. “A Blood Vessel Model Constructed from Collagen and Cultured Vascular Cells.” *Science* 231.4736 (1986): 397–400.

Williams, Chrysanthi, and Timothy M. Wick. “Perfusion Bioreactor for Small Diameter Tissue-Engineered Arteries.” *Tissue Engineering* 10.5-6 (2004): 930–941.

Williams, Corin et al. “A Comparison of Human Smooth Muscle and Mesenchymal Stem Cells as Potential Cell Sources for Tissue-Engineered Vascular Patches.” *Tissue Engineering Part A* 18.9-10 (2012): 986–998.

Witzenburg, Colleen et al. “Mechanical Changes in the Rat Right Ventricle with Decellularization.” *Special Issue on Cardiovascular Solid Mechanics* 45.5 (2012): 842–849.

Wu, Wei, Robert A. Allen, and Yadong Wang. “Fast Degrading Elastomer Enables Rapid Remodeling of a Cell-free Synthetic Graft into a Neo-artery.” *Nature medicine* 18.7 (2012): 1148–1153.

Wystrychowski, Wojciech et al. “Case Study: First Implantation of a Frozen, Devitalized Tissue-engineered Vascular Graft for Urgent Hemodialysis Access.” *The journal of vascular access* 12.1 (2011): 67–70.

Yang, Joseph et al. “Reconstruction of Functional Tissues with Cell Sheet Engineering.” *Biomaterials* 28.34 (2007): 5033–5043. *ScienceDirect*.

Yao, Lan et al. “Fibrin-Based Tissue-Engineered Blood Vessels: Differential Effects of Biomaterial and Culture Parameters on Mechanical Strength and Vascular Reactivity.” *Tissue Engineering* 11.7-8 (2005): 991–1003.

Yazdani, Saami K. et al. “Smooth Muscle Cell Seeding of Decellularized Scaffolds: The Importance of Bioreactor Preconditioning to Development of a More Native Architecture for Tissue-Engineered Blood Vessels.” *Tissue Engineering Part A* 15.4 (2009): 827–840.

Yin, Zi et al. “The Regulation of Tendon Stem Cell Differentiation by the Alignment of Nanofibers.” *Biomaterials* 31.8 (2010): 2163–2175.

Zhao, Yilin et al. “The Development of a Tissue-engineered Artery Using Decellularized Scaffold and Autologous Ovine Mesenchymal Stem Cells.” *Biomaterials* 31.2 (2010): 296–307.

Zou, Yu, and Yanhang Zhang. “Mechanical Evaluation of Decellularized Porcine Thoracic Aorta.” *Journal of Surgical Research* 175.2 (2012): 359–368.

Appendix A: Influence of SDS Exposure on Mechanical Properties

Purpose

When developing a protocol for decellularizing native or engineered tissue, the goal is to maximize DNA and antigen removal without adversely impacting mechanical properties. The purpose of this experiment was to determine the influence of increased exposure to 1% sodium dodecyl sulfate (SDS) on DNA removal and mechanical properties in engineered tissue. We hypothesized that increased exposure to SDS would remove more DNA without significantly impacting mechanical properties and collagen content.

Materials and Methods

Media equivalents (MEs) were created by adding thrombin and calcium chloride in 20 mM HEPES-buffered saline to a suspension of nhDF p9 in fibrinogen. The final component concentrations of the cell suspension were as follows: 4 mg/mL fibrinogen, 1.1 U/mL thrombin, 5.0 mM Ca^{2+}, and 1 million cells/mL. Cell suspensions were mixed and injected into a tubular mold. The mold had a cylindrical glass mandrel pretreated with 5% Pluronics F-127 solution for 1 hr and a concentric glass casing. The outer diameter of the mandrel was 4 mm, the width of the tubular cavity was 3.5 mm, and the length of the mold was 80 mm.

After injection of the cell/fibrinogen suspension, the molds were placed vertically in a humidified incubator and maintained at 37C, 5% CO2 for 15 min to allow for gelation. Subsequently, the casing was removed, and the grafts were placed horizontally in culture medium comprised of DMEM supplemented with 10% FBS, 100 U/ml

penicillin, 100 µg/ml streptomycin, 2 µg/ml insulin, and 50 µg/ml ascorbic acid. MEs were cultured at 37C, 5% CO2 for 5 weeks on an orbital shaker. 70% of the media was changed 3 times per week.

MEs were then rinsed in phosphate-buffered saline (PBS) and incubated on a shaker for 4 hrs or 8 hrs with 1% sodium dodecyl sulfate (SDS; Sigma). The samples were then rinsed in PBS and incubated with 1% Triton X-100 (Sigma) for 30 min. The MEs were extensively washed with PBS for 24 h and incubated in deoxyribonuclease enzyme in DMEM supplemented with 10% FBS for 4 h.

After the decellularization was complete, freshly harvested (n=4), 4 hour decellularized (n=4), and 8 hours decellularized (n=4) MEs were cut into samples for histological evaluation, evaluation of mechanical properties, and quantification of collagen content and DNA content. For more details on these methods, see Chapter 2.

Results

Freshly harvested tissue had an UTS of 405 ± 121 kPa and a modulus of 2.01 ± 0.48 MPa. After 4 hours of SDS exposure, tissue had UTS of 391 ± 70 kPa and a modulus of 2.25 ± 0.17 MPa. After 8 hours of SDS exposure, tissue had a UTS of 176 ± 28 kPA and a modulus of 1.80 ± 0.3. Although there appears to be a decrease in UTS upon 8 hours of SDS exposure, this difference was not statistically significant (Figure A.1a). There were no differences in modulus (Figure A.1b).

Freshly harvested tissue had a collagen content of 16.5 ± 1.3 mg/ml. After a 4 hours and 8 hours of SDS exposure, collagen contents were 16.7 ± 2.9 mg/ml and 9.7 ± 0.2 mg/ml respectively. Although there appears to be a decrease in collagen

concentration after 8 hours of decellularization, this difference was not statistically significant (Figure A.1c).

Freshly harvested tissue of equivalent size contained 6704 ± 2232 ng of DNA. After a 4 hours and 8 hours of SDS exposure, 78 ± 38 ng DNA and 51 ± 6 ng DNA remained, respectively. Both 4 hour and 8 hour decellularization resulted in a significant reduction in DNA, but they were not different from each other (Figure A.1d). When normalized to fresh tissue, 1.1 ± 0.7% of DNA remained after 4 hours of SDS exposure and 0.8± 0.3% of DNA remained after 8 hours of SDS exposure.

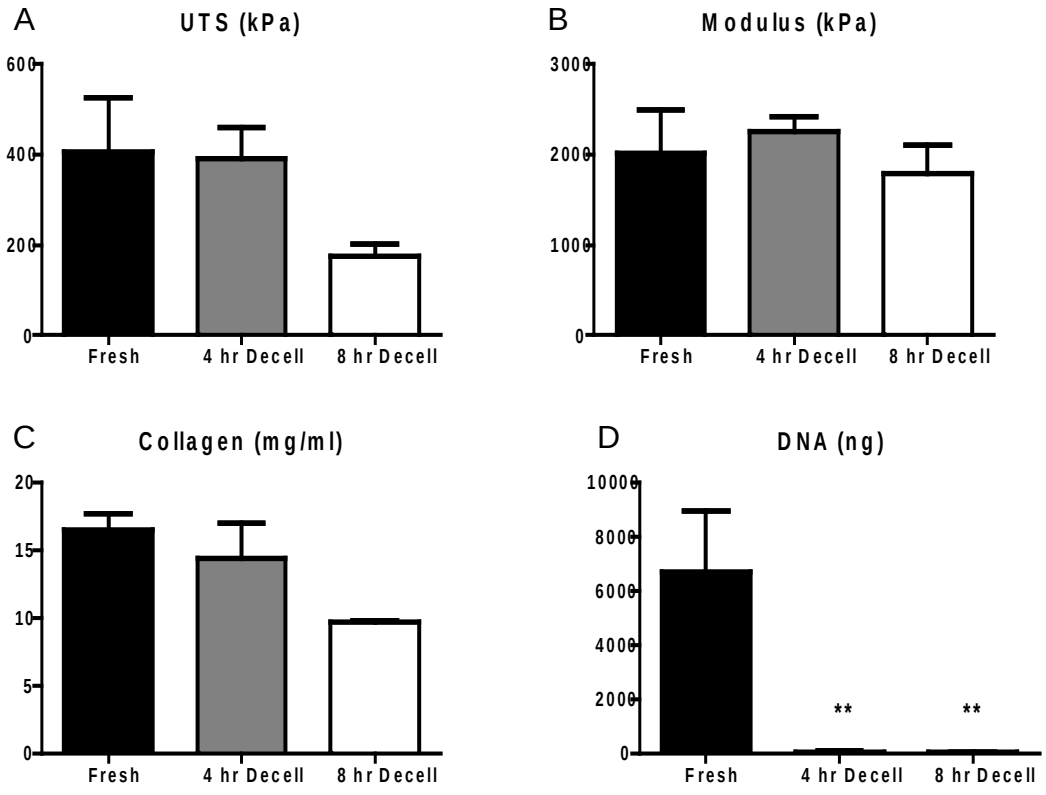

Figure A.1 Mechanical and biochemical properties of fresh and decellularized tissue (A) UTS, (B) modulus, (C) collagen concentration, and (D) DNA content. ** indicates p<0.01 when compared to Fresh.

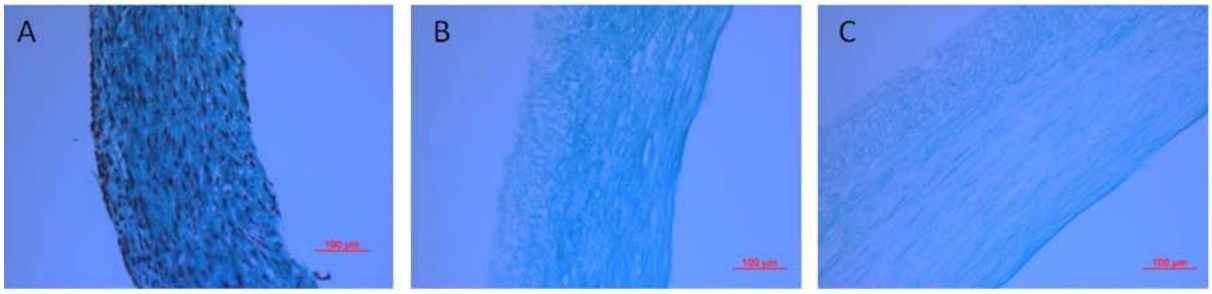

Figure A.2 Lillie's Trichrome of (A) fresh, (B) 4 hour decellularized, and (C) 8 hour decellularized tissue.

Lillie's Trichrome staining showed that freshly tissues were composed primarily of collagen (blue-green) with a homogeneous distribution of cells throughout the tissue (black) (Figure A.2a). No nuclei were present in 4 hour (Figure A.2b) or 8 hour (Figure A.2c) decellularized tissue. Collagen staining appeared less intense with larger aligned pores in 8 hour decellularized tissue.

Discussion

These data suggest that 4 hours of SDS exposure time is sufficient to remove ~99% of the DNA content of an engineered tissue. However more work needs to be completed to determine whether removal of DNA and other cellular antigens will translate into a lack of host immune response when implanted. In order to determine this, there is ongoing work in our lab to determine whether T-cell proliferation occurs *in vitro* in response to contact with decellularized tissue.

While 8 hour SDS exposure showed no statistical differences in UTS, modulus or collagen content, there appeared to be a decreasing trend in UTS and collagen content as SDS exposure increased. It is likely that this decrease in UTS is linked to the decreased collagen content, but it is unclear that this was in response to the increased exposure to

SDS or sample to sample variation. Previous data in our lab suggest support the conclusion that there is no change in UTS and modulus upon decellularization (see Figure 3.4 and Table 3.2), but care should be taken in determining the optimal decellularization protocol.

Ideally, the need to maintain the appropriate mechanical properties needs to be balanced with the desire to have tissue porosity amenable to recellularization. Lillie's Trichrome staining showed a more "open" tissue structure when comparing 4 hour SDS exposure time to 8 hour SDS exposure, but light level histology is insufficient to conclude that the tissue density / porosity was changed. Environmental SEM would need to be conducted to confirm that the porosity has not changed

Appendix B: MATLAB Code for Cell Invasion Analysis

Before running the SCIA Program

Several steps have to be completed before executing the SCIA program. The SCIA MATLAB® script calls several functions that need to be located within the computers appropriate MATALB® directory/path, in order to function (Figure B.1). All these functions have been added in a compressed folder with the SCIA program.

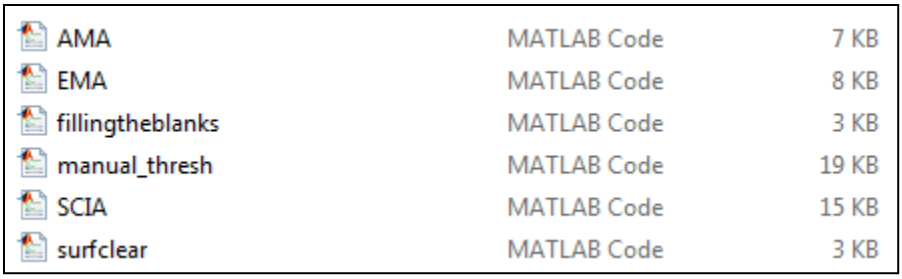

Figure B.1: SCIA Program and Sub-functions

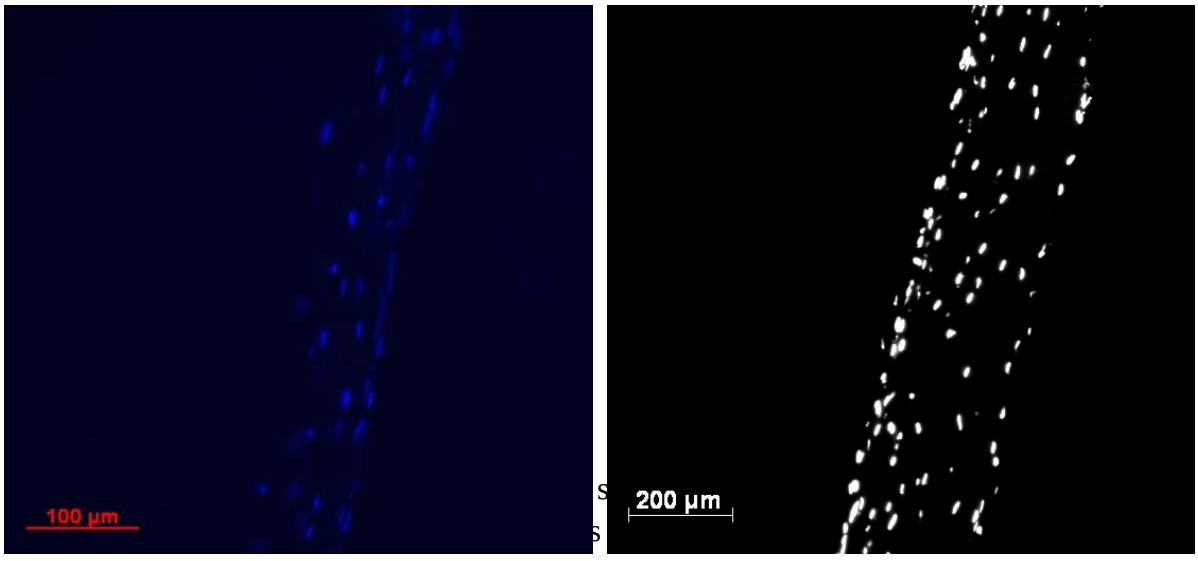

Figure B.2: Input(s) - Arbitrary of view from a sample's section (A) DAPI stain RGB image (B) Black and white image

Input(s) and Interface

The following directions will guide the user through the implementation of SCIA and its sub-functions. **All manual steps are numbered, while automated steps are only referenced and explained.**

Locating and Importing the Image(s)

1. The execution of the program immediately triggers the Analysis Type question dialog. To speed-up the process of analysis, the program has been tailored so that, both, single and multiple image analysis can be performed.
2. After selecting the type, the program will allow for the user to locate the image(s) to be analyzed (Figure B.3).

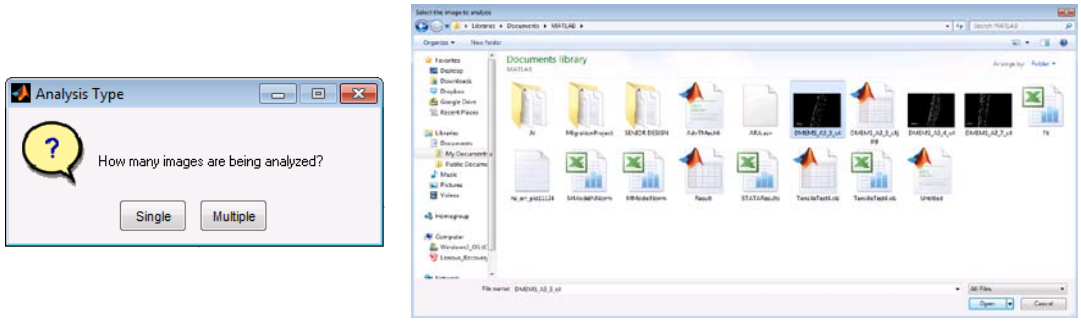

Figure B.3: Analysis Type (A) Browsing for Image(s) (B)

Pixel Scaling

1. The first processing step, executed by the program, consists in treating the scale-bar. The program shows the selected image and requests that the user crops the region of the scale-bar (Figure B.4).

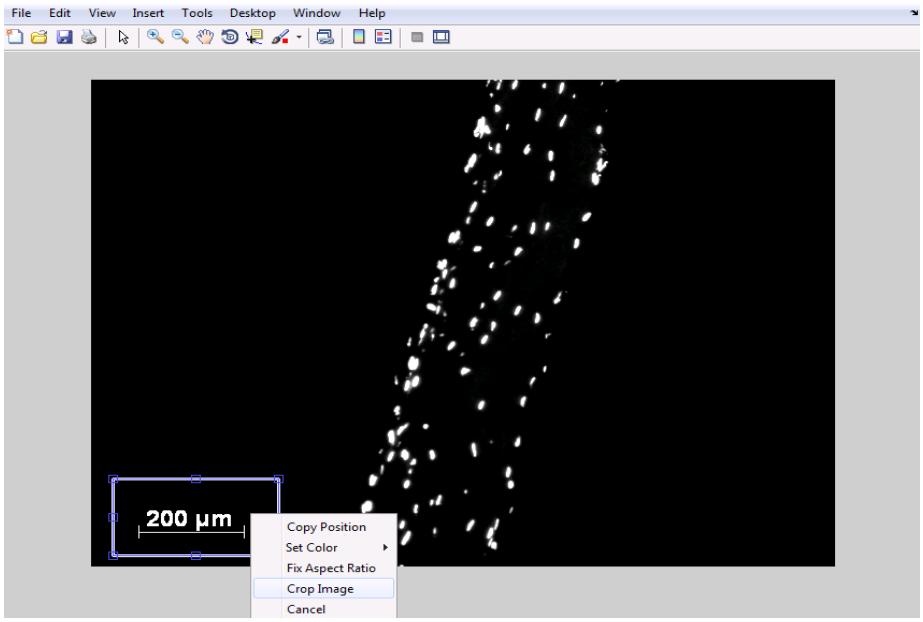

Figure B.4: Treating the Scale-bar

In addition to removing the scale-bar, the cropping window can be resized to eliminate additional noise.

Once defined, a right-click over the cropping window will allow the user to click on the “Crop Image” option and complete the task.

2. The following request should be considered essential towards increasing the speed of the analysis. If the user has selected the first image in a series, or the only image being to be analyzed, the user must extract the conversion ratio [unit/pixel] by selecting “Scalebar.” Otherwise, the user may choose “User Input.” (Figure B.5)

   a. Scale-bar
   Selecting this option will trigger an image containing the cropped scale-bar. Using the “Measure Distance” tool on the window, draw a line parallel to the scale-bar. Make sure both lines are equal in magnitude. Right-click over the line and select “Export to Workspace.” An additional window will open, just select “ok.” A following window will request the magnitude of the scale-bar in the measuring units, and the specific units. (Figure B.6)

   b. User Input
   This option will display a window requesting the magnitude of the conversion ratio and the units of such. (Figure B.6)

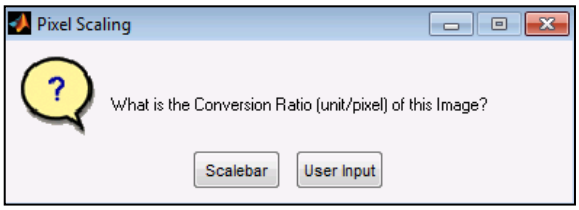

Figure B.5: Method to determine the Conversion Ratio

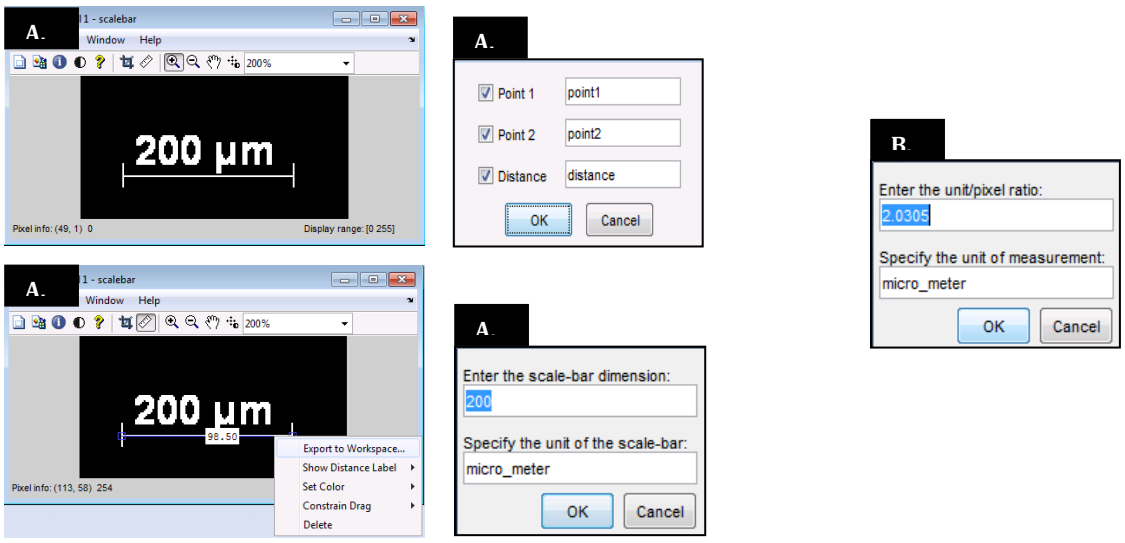

Figure B.6: Scalebar option (A.1-4) User Input (B.1)

Surface Delimiting

Delimiting the surface takes place following the calculation of the conversion ratio. The program shows the image of the slide and requests for the user to select “vortices” to mark the surface of the slide. These “vortices” are created using “Data Tips.” Multiple “Data Tips” can be placed along the surface by holding the Alt key, while left-clicking on the image (Figure B.7).

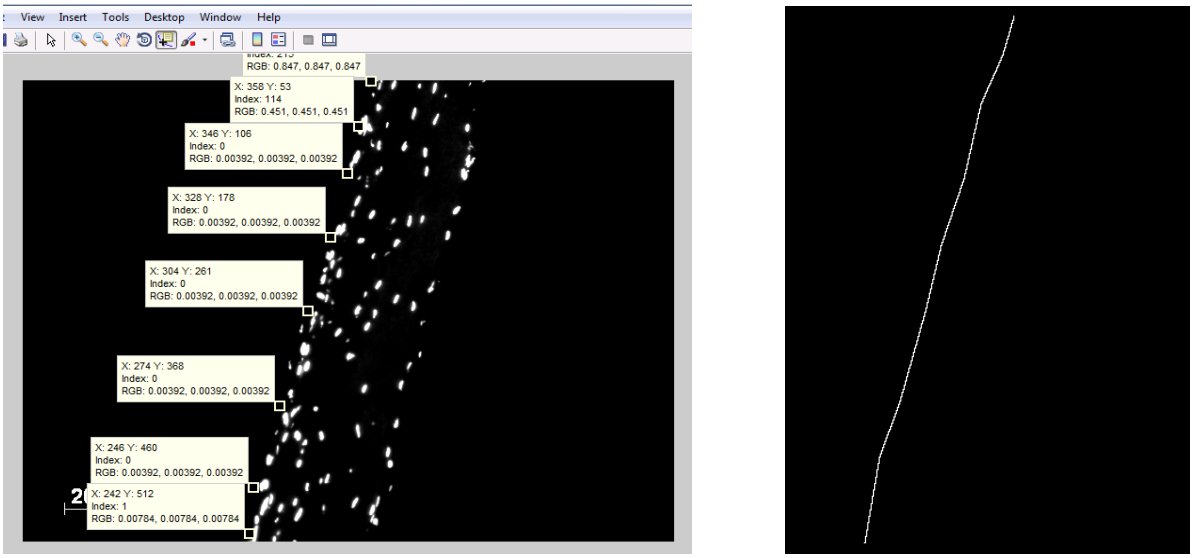

Figure B.7: Delimiting the Surface with Data Tips (A) Marked surface after processing through fillingtheblanks.m (B)

After covering the surface, the users must right-click on any cursor and select the “export” option on the drop-down menu. The user must leave the default variable names as shown in the windows.

Marking the Surface

The function fillingintheblanks.m has been designed to draw or fill the pixels between the specified “vortices” or “Data Tips” in the previous image. The output can be seen in

Errors may arise when treating migration occurring mostly in the “y” axis/direction. However, the image may be also be rotated by the user if the program does not seem to capture the surface correctly.

Generating Binary Image

Manual thresholding has to be implemented by the program to create a binary image. Since binary images are necessary for object detection, erosion, dilation, and characterization (determination of physical properties), all input images need to be converted. Image thresholding can be achieved through a handful of automated MATLAB® functions or a quick filter. However, because of the intensity difference between images, the manual_thresh.m script has been chosen for the task. Note that this function was made by a third-party and, therefore, little consulting can be provided about the GUI.

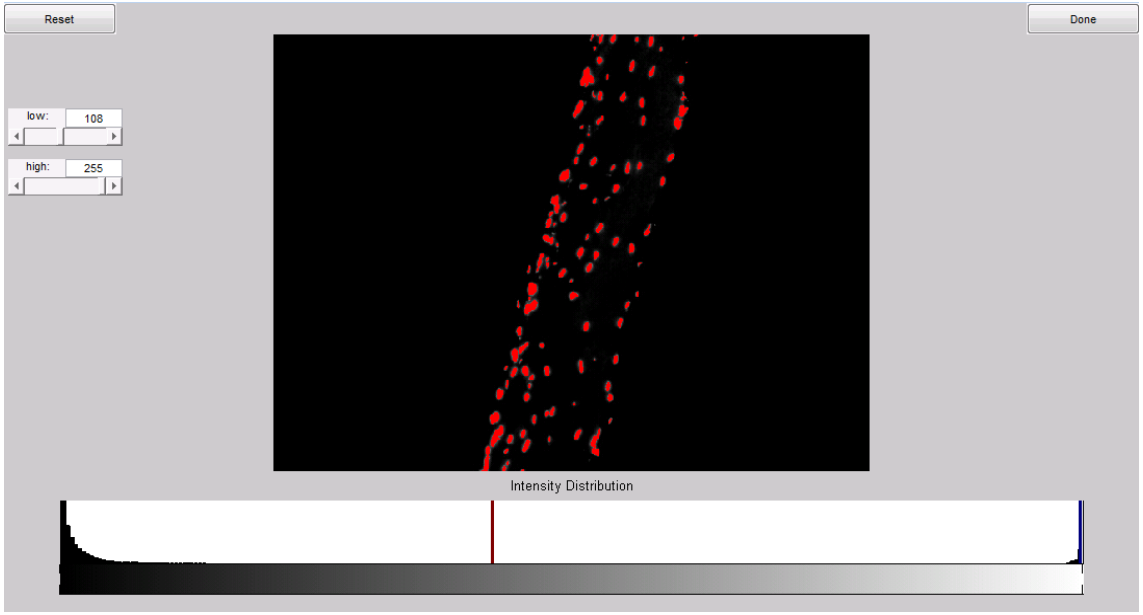

Figure B.8: Manual Tresholding

The manual thresholding GUI (Figure B.8) displays the image to be converted, the intensity histogram, and the “low” and “high” limits or boundaries to sweep through the histogram. In simple terms, the desired object must be marked or filled in red by the user. To fill these objects, the user must sweep through the histogram, using both the “low” and “high” boundaries, to contain as many objects as possible. The boundaries exclude any object with intensity different to those found between the boundaries. Once the user is satisfied with the boundary parameters, clicking “Done” (top right corner) will export the information to the main program.

The next step in the SCIA program consists in eliminating the noise before migration analysis. The function surfclear.m has been designed to accomplish this task. The function takes the image and eliminates any noise above the marked surface.

Once the noise has been reduced, the binary image is processed by either of two functions built towards counting and characterizing objects within the image. EMA or AMA processing are two distinct methods that may be chosen by the user.

Erosion-based Method of Analysis (EMA)

EMA has been developed to separate cell/object clusters that may be skewing the overall characterization data (object number, average area, centroid location, etc.). The true objective of EMA is to preserve the location of each individual cell/object, given that the most important variable of interest is migration. EMA may also be affected by the selected thresholding parameters. Furthermore, the processing time makes EMA a much slower function than its counterpart.

Area-based Method of Analysis (AMA)

AMA has been developed for counting speed. AMA compares the areas of each object in the image with an average area. If a cluster has an area "n" times greater than the average, it is said that "n" objects are contained within such cluster. AMA saves computing time by eliminating the image processing. However, the lack of processing renders inaccuracy when selecting the centroids of each object.

Regardless of the method of analysis, the SCIA retrieves the following parameters:

- Number: The number of the object.
- Area: The area, in pixels, of the labeled object.
- Centroid: The coordinate [x, y] of the labeled object's centroid.
- Eccentricity: A [0-1] ratio representing the accentuation of the object's elliptical shape. 0 represents a very circular object, while 1 represents a more elliptical object.
- Orientation: Angle between the labeled object's major axis of alignment and the horizontal axis.
- Major and Minor Axis of alignment: The magnitude of the perpendicular lines that describe width and length of the object.

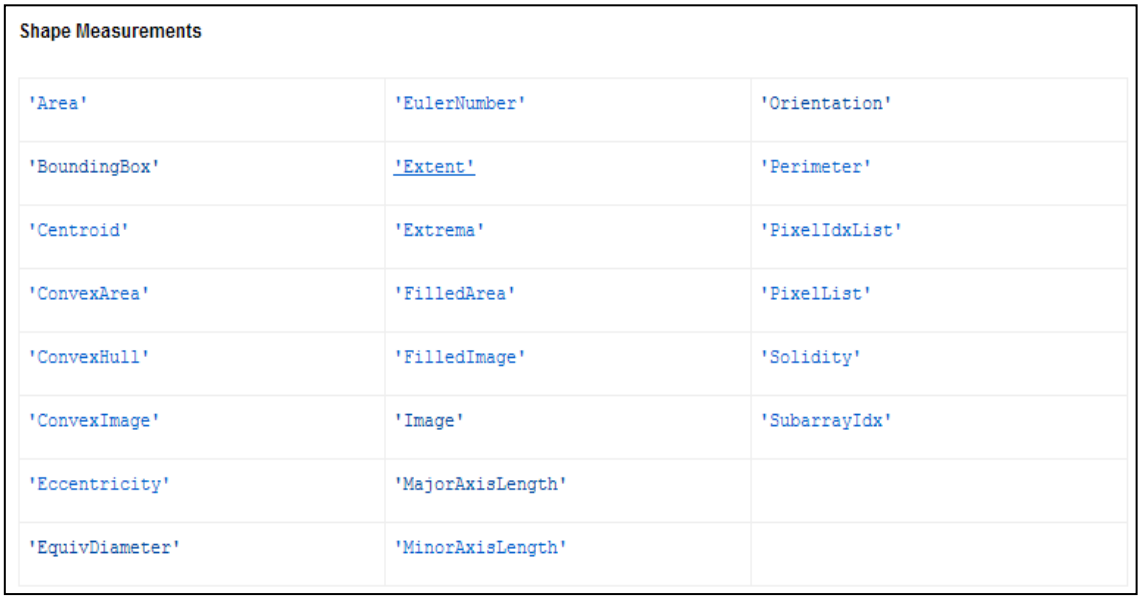

Shape Measurements

'Area'	'EulerNumber'	'Orientation'
'BoundingBox'	'Extent'	'Perimeter'
'Centroid'	'Extrema'	'PixelIdxList'
'ConvexArea'	'FilledArea'	'PixelList'
'ConvexHull'	'FilledImage'	'Solidity'
'ConvexImage'	'Image'	'SubarrayIdx'
'Eccentricity'	'MajorAxisLength'	
'EquivDiameter'	'MinorAxisLength'	

Figure B.9: regionprops() additional properties for extraction

If desired by the user, more properties may be extracted from the image. The MATLAB® function regionprops() allows for the following properties to be extracted.

Results and Cell Invasion Analysis

Following the extraction of these properties, the SCIA program calculates a handful of parameters of interest. Migration, being the most important, is calculated first. The Orientation angle with respect to the surface is calculated second. Lastly, the Aspect Ratio is also calculated.

- Migration: The distance between the cell/object's centroid and its horizontal intersection with the surface.
- Orientation with respect to the surface: The specific angle between the cell/object's major axis of alignment and the nearest segment of the surface.
- Aspect Ratio: The [0-1] ratio of the cell/object's minor/major axis of orientation.

Plotting and Saving Results

The program displays and stores the results discussed above. The two displayed figures and the data matrix named Results are then saved as specified by the original image's filename. Depending on the type of analysis, specified at the beginning, the program will either close the figures automatically (when multiple images are being analyzed) or leave them to be closed by the user (when a single image or the last image of a series is being analyzed). More information and examples are shown in the Output section of the report.

The Output(s)

The following images and graphs represent the outputs of the SCIA program (Figures B.10-B.12). All the following outputs are saved within the directory of the original image.

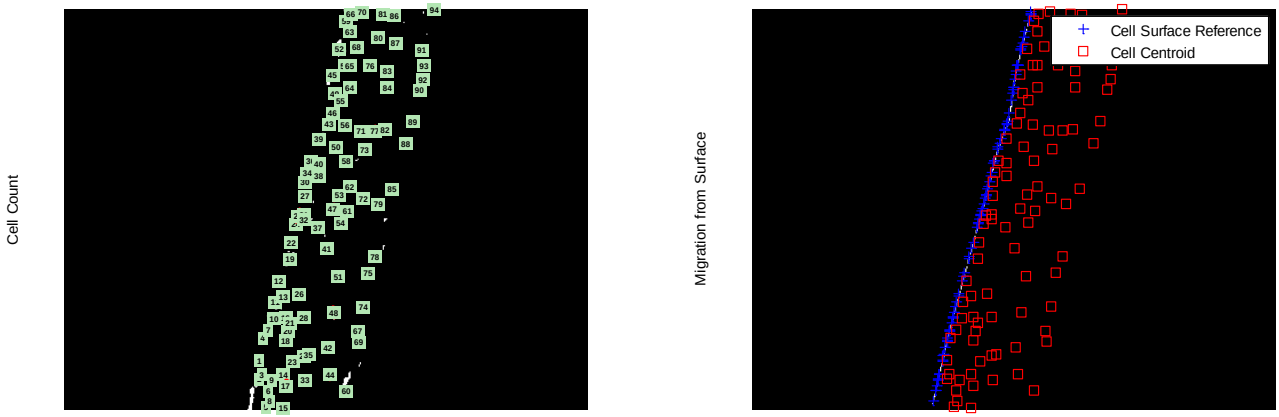

Figure B.10: Results Figure (1): Cell Count & Migration Analysis

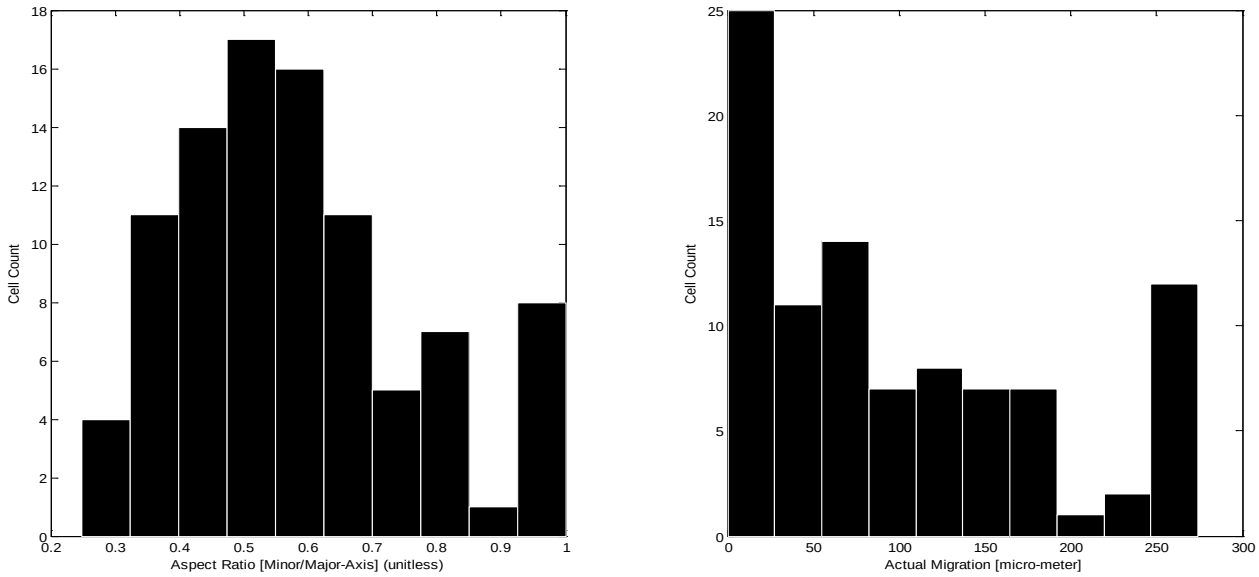

Figure B.11: Results Figure (2): Aspect Ratio & Migration Histograms

Surface Invasion Analysis

```
%% SURFACE CELL INVASION ANALYSIS [SCIA] - 2013 -
% -----------------------------------------------------------
% UNIVERSITY OF MINNESOTA - DEPARTMENT OF BIOMEDICAL ENGINEERING
% TRANQUILLO LAB - DEPARTMENT OF BIOMEDICAL ENGINNERING
% -----------------------------------------------------------
% Nathan Weidenhamer
% Fluvio Lobo
% ----------------------------------------------------------------------
% *The following program, in addition to the associated functions, has been
% developed to enhance the process of cell quantification and migration
% evaluation after the recellularization of TE-scaffolds*
% ----------------------------------------------------------------------
%
 format long
 close all;
```

	A	B	C	D	E	F	G	H	I	J
1	Cell Number	Cell Area	Centroid "X"	Centroid "Y"	Eccentricity	MajorAxis	MinorAxis	Actual Migration [micro-meter]	Orientation wrt Surface [degrees]	Aspect Ratio [Minor/Major-Axis]
2	1	18	257.6111111	456.7222222	0.70823969	5.809303732	4.101206089	12.3714	-0.758806525	0.705972054
3	2	5	258	481	0	2.780887149	2.780887149	22.6809	77.00538321	1
4	3	14	260.7857143	474.7857143	0.813157113	5.773502692	3.36043405	26.8047	32.00538321	0.582044251
5	4	69	262.7971014	428.4347826	0.798207109	12.27528754	7.394425885	8.2476	-3.565306107	0.60238311
6	5	21	267.7142857	517.9047619	0.663548583	6.156684327	4.60601992	0	0	0.748133196
7	6	11	270.6363636	496	0.798061088	5.100421681	3.073394503	57.7332	17.70015338	0.602576551
8	7	5	271	418	0	2.780887149	2.780887149	20.619	74.63838369	1
9	8	13	271.7692308	511.2307692	0.710197962	5.032996496	3.54323974	65.9808	6.799448632	0.704002028
10	9	44	274.5	482.5	0.846309618	10.3384234	5.507188285	59.7951	6.420295661	0.532691308
11	10	50	279.04	402.8	0.894938675	12.1619777	5.42654264	27.83565	6.214578555	0.446189162
12	11	20	280	380.5	0.908994602	7.933053216	3.306559138	17.52615	-15.36161631	0.416807886
13	12	38	285.2894737	353.7105263	0.842503936	9.694192273	5.222166246	12.3714	-13.25642534	0.538690187
14	13	64	289.5	373.9375	0.940856718	15.97807151	5.413446005	34.02135	26.34317337	0.338804718
15	14	36	289.9444444	475.9444444	0.832067021	9.176810323	5.090148238	86.5998	-2.21106225	0.554675106
16	15	6	289.5	519.6666667	0.833333333	4	2.211083194	0	0	0.552770798
17	16	71	292.5070423	401.084507	0.700363813	11.3379764	8.092889417	55.6713	-27.82371687	0.713786053
18	17	80	293.6	490.225	0.927812284	16.78376566	6.261140215	102.06405	12.33100509	0.373047404
19	18	46	[illegible]	[illegible]	[illegible]	[illegible]	[illegible]	[illegible]	[illegible]	[illegible]

Figure B.12: Results Excel File

```
 clc;
%
%%%%%%%%%%%%%%%%%%%%%%%%%%%%%%%%%%%%%%%%%%%%%%%%%%%%%%%%%%%%%%%%%%%%%%%%%%%%%%%%%%%%%%%%%%%%%%%%%%%%
%% (1) Locating and Importing the Image
%%%%%%%%%%%%%%%%%%%%%%%%%%%%%%%%%%%%%%%%%%%%%%%%%%%%%%%%%%%%%%%%%%%%%%%%%%%%%%%%%%%%%%%%%%%%%%%%%%%%
Analysistypequest = questdlg('How many images are being analyzed?', ...
'Analysis Type', ...
'Single','Multiple',[]);
switch Analysistypequest
   case 'Single'
   [filename,pathname] = uigetfile('*.*','Select the image to analyze');
   Nfile = 1;
   case 'Multiple'
```

```
    [filename,pathname] = uigetfile('*.*','Select the images to analyze','MultiSelect','on');
    Nfile = length(filename);
end
%%%%%%%%%%%%%%%%%%%%%%%%%%%%%%%%%%%%%%%%%%%%%%%%%%%%%%%%%%%%%%%%%%%%%%%%%%%%%%%%%%%%%%
%% (2) Begining-of-Analysis
%%%%%%%%%%%%%%%%%%%%%%%%%%%%%%%%%%%%%%%%%%%%%%%%%%%%%%%%%%%%%%%%%%%%%%%%%%%%%%%%%%%%%%
for h = 1:Nfile

    if Nfile == 1; % Control for the selection of a single image
        Xo = imread(fullfile(pathname, filename));
        im_name = strrep(filename,'.','');
    else % Control for the selection of multiple images
        Xo = imread(fullfile(pathname, filename{h}));
        im_name = strrep(filename{h},'.','');
    end

%%%%%%%%%%%%%%%%%%%%%%%%%%%%%%%%%%%%%%%%%%%%%%%%%%%%%%%%%%%%%%%%%%%%%%%%%%%%%%%%%%%%%%
%% (3) Treating the Scalebar
%%%%%%%%%%%%%%%%%%%%%%%%%%%%%%%%%%%%%%%%%%%%%%%%%%%%%%%%%%%%%%%%%%%%%%%%%%%%%%%%%%%%%%
% The scalebar is both a source of information and a source of noise.
% The SCIA program requests for the user to crop the area where the
% scale-bar is found in order to: 1) Obtain the conversion ratio, and 2)
% Eliminate the scale-bar from the original image.
    [scalebar, scalecoord] = imcrop(Xo); % Manual Cropping
    xmin = round(scalecoord(1));
    ymin = round(scalecoord(2));
    width = round(scalecoord(3));
    height = round(scalecoord(4));
% Once the scale-bar has been separated, the user is requested to either
% extract the conversion ratio from the image, or use a previously
% defined value for such ratio.
    Scalequest = questdlg('What is the Conversion Ratio (unit/pixel) of this Image?', ...
        'Pixel Scaling', ...
        'Scalebar','User Input',[]);

        switch Scalequest
%%%%%%%%%% Option 1: Extract the conversion ratio from the scale-bar
            case 'Scalebar'
            % The image is called for the user to draw a line parallel and
            % equal in magnitude to the scale-bar
            waitfor(imtool(scalebar));
            p1 = point1(1,1);
            p2 = point2(1,1);
            pixel_length = abs(p2-p1); % scale bar length
                % Once the scale bar magnitude is extracted, the
                % appropriate distance has to be specified.
                Scalequest2 = {'Enter the scale-bar dimension:','Specify the unit of the scale-bar:'};
                title = 'Magnitude and Unit'; lines = 1;
                def = {'200','micro-meter'};
                answer = inputdlg(Scalequest2,title,lines,def);
                scalebar_length = str2double(answer{1});
                scalebar_unit = answer{2};
```

```
        conversion_ratio = scalebar_length/pixel_length; % unit/pixel
        clear p1 point1 p2 point2 distance

%%%%%%%%%% Option 2: Using the ratio from the previous images. Implement
%%%%%%%%%% this option when analyzing a series of images.
        case 'User Input'
        close Figure 1
        Scalequest2 = {'Enter the unit/pixel ratio:','Specify the unit of measurement:'};
        title = 'Magnitude and Ratio';
        lines = 1;
        def = {num2str(conversion_ratio),'micro_meter'};
        answer = inputdlg(Scalequest2,title,lines,def);

        conversion_ratio = str2double(answer{1}); % unit/pixel
        scalebar_unit = answer{2};
    end

%%%%%%%%%%%%%%%%%%%%%%%%%%%%%%%%%%%%%%%%%%%%%%%%%%%%%%%%%%%%%%%%%%%%%%%
%% (4) Delimiting the Surface
%%%%%%%%%%%%%%%%%%%%%%%%%%%%%%%%%%%%%%%%%%%%%%%%%%%%%%%%%%%%%%%%%%%%%%%
  figure(1)
  imshow(Xo);
  xlabel('Select Surface Vertices');
  waitfor(figure(1));
  [dsur, Slopes, Intercepts, X, Y, Npoints, Nslopes] = detectsur(Xo, cursor_info);

%%%%%%%%%%%%%%%%%%%%%%%%%%%%%%%%%%%%%%%%%%%%%%%%%%%%%%%%%%%%%%%%%%%%%%%
%% (5) Marking the Surface
%%%%%%%%%%%%%%%%%%%%%%%%%%%%%%%%%%%%%%%%%%%%%%%%%%%%%%%%%%%%%%%%%%%%%%%
  [SUR] = fillingtheblanks(dsur); % Finilizing Surface in SUR
  [Yloc, Xloc] = find(SUR==1); % Finding the coordinates of the surface

%%%%%%%%%%%%%%%%%%%%%%%%%%%%%%%%%%%%%%%%%%%%%%%%%%%%%%%%%%%%%%%%%%%%%%%
%% (6) Manually taking the threshold && Scale-bar removal
%%%%%%%%%%%%%%%%%%%%%%%%%%%%%%%%%%%%%%%%%%%%%%%%%%%%%%%%%%%%%%%%%%%%%%%
  if length(size(Xo)) == 3
     Xo = rgb2gray(Xo);
%%%%%%% The following double for-loop removes the scale-bar before the
%%%%%%% thresholding
     for i = xmin:xmin+width
        for j = ymin:ymin+height
           Xo(j,i) = 0;
        end
     end
     [~,~,bw] = manual_thresh(Xo); % Thresholding
  else
%%%%%%% Similarly to above stated. In this case, the image is already a
%%%%%%% flat 2D matrix
     for i = xmin:xmin+width
        for j = ymin:ymin+height
```

```
            Xo(j,i) = 0;
        end
    end
    [~,~,bw] = manual_thresh(Xo); % Thresholding
end

%%%%%%%%%%%%%%%%%%%%%%%%%%%%%%%%%%%%%%%%%%%%%%%%%%%%%%%%%%%%%%%%%%%%%%%%%%%%%%%%
%% (7) Eliminating Noise before Migration Analysis
%%%%%%%%%%%%%%%%%%%%%%%%%%%%%%%%%%%%%%%%%%%%%%%%%%%%%%%%%%%%%%%%%%%%%%%%%%%%%%%%
  [~, ~, bw] = surfclear(Yloc, Xloc, bw);
%%%%%%%%%%%%%%%%%%%%%%%%%%%%%%%%%%%%%%%%%%%%%%%%%%%%%%%%%%%%%%%%%%%%%%%%%%%%%%%%
%% (8) Processing the Image:
%%%%%%%%%%%%%%%%%%%%%%%%%%%%%%%%%%%%%%%%%%%%%%%%%%%%%%%%%%%%%%%%%%%%%%%%%%%%%%%%
  [ResultsEMA] = EMA(bw);
%%%%%%%%%%%%%%%%%%%%%%%%%%%%%%%%%%%%%%%%%%%%%%%%%%%%%%%%%%%%%%%%%%%%%%%%%%%%%%%%
%% (9) Results & Cell Invasion Analysis
%%%%%%%%%%%%%%%%%%%%%%%%%%%%%%%%%%%%%%%%%%%%%%%%%%%%%%%%%%%%%%%%%%%%%%%%%%%%%%%%
%%% (9.1) Labeling
    Result_Labels = cell(1,9);

    % First, we tabulate the data obtained from regionprops() and the
    % EMA/AMA functions.
    Result_Labels(1,1) = { 'Cell Number' };
    Result_Labels(1,2) = { 'Cell Area' };
    Result_Labels(1,3) = { 'Centroid "X"' };
    Result_Labels(1,4) = { 'Centroid "Y"' };
    Result_Labels(1,5) = { 'Eccentricity' };
    Result_Labels(1,6) = { 'MajorAxis' };
    Result_Labels(1,7) = { 'MinorAxis' };

    % The results tabulated below consist of parameters calculated by
    % the SCIA program
    Result_Labels(1,8) = {strcat('Actual Migration [',scalebar_unit,']')};
    Result_Labels(1,9) = { 'Orientation wrt Surface [degrees]' };
    Result_Labels(1,10) = { 'Aspect Ratio [Minor/Major-Axis]' };

%%% (9.2) Initializing-Data-Arrays
    SNema = size(ResultsEMA);
    Nema = SNema(1);
    Results = zeros(Nema,10);
        Xsur = zeros(Nema,1);
        Ysur = zeros(Nema,1);
        Ycellcoords = round(ResultsEMA(:,4));
        Xcellcoords = round(ResultsEMA(:,3));

%%% (9.3) Populating-Data-Arrays
    for i = 1:Nema
        Results(i,1) = ResultsEMA(i,1); % Cell Number
        Results(i,2) = ResultsEMA(i,2); % Cell Area
        Results(i,3) = ResultsEMA(i,3); % Cell Centroid "X"
```

```
        Results(i,4) = ResultsEMA(i,4); % Cell Centroid "Y"
        Results(i,5) = ResultsEMA(i,5); % Eccentricity
        Results(i,6) = ResultsEMA(i,7); % Major Axis
        Results(i,7) = ResultsEMA(i,8); % Minor Axis

    %%% (9.3.1) Calculating Actual Migration
        Yindex = find(Yloc==Ycellcoords(i));
        for j = 1:length(Yindex)
           Xsur(i) = Xsur(i) + Xloc(Yindex(j))/(length(Yindex));
           Ysur(i) = Yloc(Yindex(1));
           %-------------------------------------------------------------------------%
           Results(i,8) = abs(Xsur(i)-Xcellcoords(i))*conversion_ratio; % Migration [unit]
           %-------------------------------------------------------------------------%
        end

    %%% (9.3.2) Calculating Orientation wrt the Surface
        % Calculating the Surface Angle
        vectorcompsur=zeros(Nslopes,2);
        anglesur=zeros(Nslopes,1);
        for j = 1:Nslopes
           vectorcompsur(j,1) =  X(j+1)-X(j) ;
           vectorcompsur(j,2) =  Y(j+1)-Y(j) ;
        % The following "if" statement arranges the angle based on the two
        % possible orientations of the surface.
           if vectorcompsur(j,1) > 0
              anglesur(j) = 180 - atand(vectorcompsur(j,2)/vectorcompsur(j,1));
           else
              anglesur(j) = atand(vectorcompsur(j,2)/abs(vectorcompsur(j,1)));
           end
        end
        % Calculating the Cell Angle
        Celltheta = zeros(Nema,1);
        % Final Orientation
        OrientationAngle = zeros(Nema,1);
        for j = 1:Nema
        % Defining the Angle of the Cell
           if ResultsEMA(j,6) >= 0
              Celltheta(j) = ResultsEMA(j,6);
           else if ResultsEMA(j,6) < 0
                 Celltheta(j) = 180 + ResultsEMA(j,6);
               end
           end
        % Subtracting the Angles
           for k = 1:Nslopes
              if Ycellcoords(j) <= Y(k+1) && Ycellcoords(j) > Y(k)
                 OrientationAngle(j) = anglesur(k) - Celltheta(j);
              end
           end
        end
        %-------------------------------------------------------------%
        Results(i,9) = OrientationAngle(i); % Orientation wrt Surface
        %-------------------------------------------------------------%

    %%% (9.3.3) Calculating the Aspect Ratio [Minor/Major-Axis]
        %---------------------------------------------%
        Results(i,10) = ResultsEMA(i,8)/ResultsEMA(i,7);
```

```
    %-------------------------------------------%
  end

%%%%%%%%%%%%%%%%%%%%%%%%%%%%%%%%%%%%%%%%%%%%%%%%%%%%%%%%%%%%%%%%%%%%%%%
%% (10) Plotting Results
%%%%%%%%%%%%%%%%%%%%%%%%%%%%%%%%%%%%%%%%%%%%%%%%%%%%%%%%%%%%%%%%%%%%%%%
  figure(1), % Migration
    % The first image labels every cell detected by the program.
    % Additionally, the code draws an elipsoid around the cell to
    % display its eccentricity. These two labeling techniques allow for
    %the user to validate the calculated results.
    subplot(1,2,1)
      imshow(bw)
      hold on
      phi = linspace(0,2*pi,50);
      cosphi = cos(phi);
      sinphi = sin(phi);
      for i = 1:Nema
        % Plots the Major Axis of Alignment of each Cell
        xbar = ResultsEMA(i,3); % centroidX
        ybar = ResultsEMA(i,4); % centroidY
        a = ResultsEMA(i,7)/2; % Major Axis
        b = ResultsEMA(i,8)/2; % Minor Axis
        theta = pi*ResultsEMA(i,6)/180; % Orientation
        R = [ cos(theta)   sin(theta)
            -sin(theta)   cos(theta)];
        xy = [a*cosphi; b*sinphi];
        xy = R*xy;
        x = xy(1,:) + xbar;
        y = xy(2,:) + ybar;
        plot(x,y,'r','LineWidth',2);

        % Showing the Cell Number
        text(Xcellcoords(i),Ycellcoords(i),num2str(i), ...
        'HorizontalAlignment', 'center', ...
        'VerticalAlignment', 'middle', ...
        'BackgroundColor',[.7 .9 .7], ...
        'FontSize',5, ...
        'FontWeight','bold');
      end
      ylabel('Cell Count');

    % The secondary figure displays the surface, the centroid of the
    % cells, and the point on the surface from which every cell is
    % tracked.
    subplot(1,2,2)
      imshow(SUR)
      hold on
      plot(Xsur,Ysur,'b+')
      plot(Xcellcoords,Ycellcoords,'rs')
      legend('Cell Surface Reference','Cell Centroid');
      ylabel('Migration from Surface');

  figure(2), % Data Histogram
```

```
        % The First histograms displays the Aspect Ratio of each cell in
        % the image. The ratio [# between 0-1] gives an approximation of
        % cell alignment.
        subplot(2,2,[1,3])

          hist(Results(:,10),10);
          h = findobj(gca,'Type','patch');
          set(h,'FaceColor','k','EdgeColor','w')
          xlabel('Aspect Ratio [Minor/Major-Axis] (unitless)');
          ylabel('Cell Count')

        % The second histogram shows the number of cells distributed
        % throughout the tissue.
        subplot(2,2,[2,4])

          hist(Results(:,8),10);
          h = findobj(gca,'Type','patch');
          set(h,'FaceColor','k','EdgeColor','w')
          xlabel(strcat('Actual Migration [',scalebar_unit,']'));
          ylabel('Cell Count')

%%%%%%%%%%%%%%%%%%%%%%%%%%%%%%%%%%%%%%%%%%%%%%%%%%%%%%%%%%%%%%%%%%%%%%%%%%%%%%%%
%% (11) Saving Files
%%%%%%%%%%%%%%%%%%%%%%%%%%%%%%%%%%%%%%%%%%%%%%%%%%%%%%%%%%%%%%%%%%%%%%%%%%%%%%%%
%   Clearing Variables
    clearvars -except Result_Labels Results im_name filename pathname Nfile h conversion_ratio;
%   MAT-file
    save(strcat(im_name,'.mat'))
    movefile(strcat(im_name,'.mat'),pathname);
%   Excel-File
    xlswrite(im_name,Result_Labels,'EMA','A1')
    xlswrite(im_name,Results,'EMA','A2')
    movefile(strcat(im_name,'.xls'),pathname);
%   Graph
    saveas(figure(1),strcat(im_name,'Fig1','.fig'));
    movefile(strcat(im_name,'Fig1','.fig'),pathname);
    saveas(figure(2),strcat(im_name,'Fig2','.fig'));
    movefile(strcat(im_name,'Fig2','.fig'),pathname);

    if Nfile > 1
       close all;
    end

end %End-of-program
```

Filling-the-blanks

```
%% FILLING THE BLANKS - 2013 -
% ---------------------------------------------------------------
% UNIVERSITY OF MINNESOTA - DEPARTMENT OF BIOMEDICAL ENGINEERING
% TRANQUILLO LAB - DEPARTMENT OF BIOMEDICAL ENGINNERING
% ---------------------------------------------------------------
% Nathan Weidenhamer
% Fluvio Lobo
% ---------------------------------------------------------------------
```

```
% *The following program, has the purpose of drawing the surface delimited
% by previously selected vortices or data points.
% ------------------------------------------------------------------------
%
function [Y] = fillingtheblanks(X)
% The input "X" is the binary image consisting of vortices that describe
% the surface of interest.
S = size(X); % S(1)=#rows; S(2)=#columns;
k = 1;
% The goal of the following loop is to obtain the location of each pixel
% that delimits the surface of interest. The loop scans the image for white
% pixels and records their location in the "yw" and "xw" arrays.
for i = 1:S(1)
   for j = 1:S(2)
      if X(i,j) == 1;
         yw(k,1) = i;
         xw(k,1) = j;
         k = k + 1; % The counter "k" keeps a logical order of the pixel
                    % coordinates
      end
   end
end
% The following loop draws the line between the delimiting points by
% printing white pixels.
for i = 1:length(xw)-1
   % The loop looks first at the difference, in the "y" direction, between
   % two points.
   dy = yw(i+1)-yw(i);
   % The program then prints white pixels for every unit difference,
   % defined by the "j" counter.
   for j = 1:dy
      X(yw(i)+j,xw(i))=1;
   end
   % The function then repeats the same idea in the "x" axis. However,
   % here the process is different.
   dx = abs(xw(i+1)-xw(i));
   % While "y" values may always increase, because of the standard
   % orientation of our sections, "x" coordinates may fluctuate and
   % therefore cannot be assume to increase/decrease. For this case, the
   % code implements and if statement to account for each case.
   if xw(i+1) > xw(i)
      for j = 1:dx
         X(yw(i),xw(i)+j)=1;
      end
   else
      for j = 1:dx
         X(yw(i),xw(i+1)+j)=1;
      end
   end

end
% The output "Y" is the binary image consisting of a line connecting the
% vortices or data-points used to delimit the surface of interest.
Y = X;
end % End-of-function
```

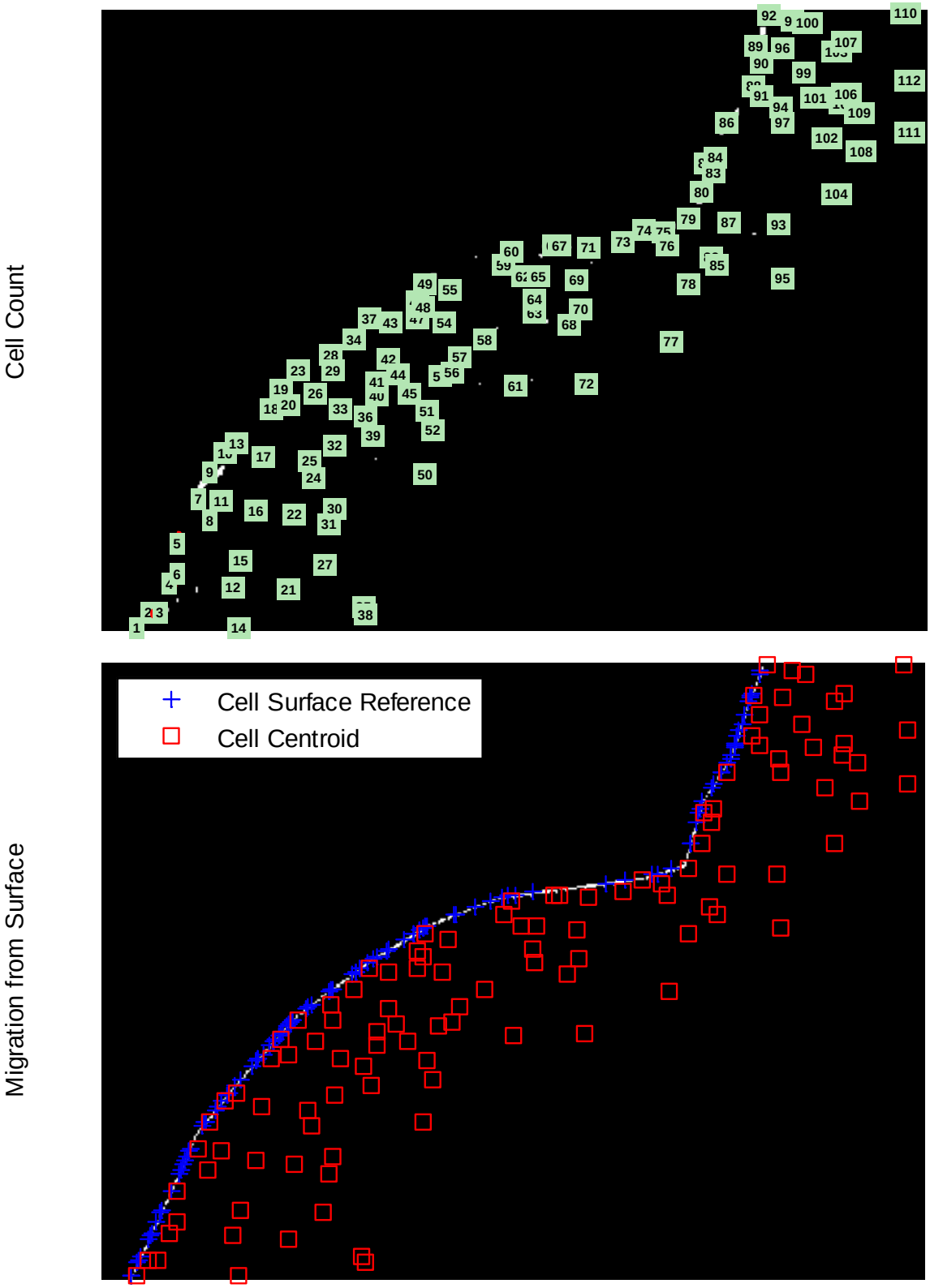

Figure B.13: Qualitative efficiency of fillingtheblanks.m

Manual Thresholding

```
function [level,level2,bw] = manual_thresh(im,cmap,defaultLevel) %mainfunction
%   manual_thresh  Interactively select intensity levels band for image thresholding.
%   manual_thresh launches a GUI (graphical user interface) for thresholding
%   an intensity input image, IM. IM is displayed in the top of the figure . A
%   colorbar and IM's histogram are displayed on the bottom. lines on the
%   histogram indicates the current threshold levels. The segmented image
%   (with the intensity levels between the low and high threshold levels is
%    displayed as a upper layer with tranperent background on the top of the image.  To change the
%   level, click and drag the lines or use the editable text or sliders. The output image updates
automatically.
%
%   There are two ways to use this tool.
%
% Mode 1 - nonblocking behavior:
%    manual_thresh  (IM) launches GUI tool.  You can continue using the MATLAB
%   Desktop.  Since no results are needed, the function does not block
%   execution of other commands.
%
%    manual_thresh  (IM,CMAP) allows the user to specify the colormap, CMAP.  If
%   not specified, the default colormap is used.
%
%    manual_thresh  (IM,CMAP,DEFAULTLEVEL) allows the user to specify the
%   default low threshold level. If not specified, DEFAULTLEVEL is determined
%   by GRAYTHRESH. Valid values for DEFAULTLEVEL must be consistent with
%   the data type of IM for integer intensity images: uint8 [0,255], uint16
%   [0,65535], int16 [-32768,32767].
%
%   Example
%       x = imread('coins.png');
%       manual_thresh(x)          %no return value, so MATLAB keeps running
%
% Mode 2 - blocking behavior:
%   [LOW LEVEL, HIGH LEVEL] =  manual_thresh (...) returns the user selected levels, LOW LEVEL $
HIGH LEVEL, and
%   MATLAB waits for the result before proceeding.  This blocking behavior
%   mode allows the tool to be inserted into an image processing algorithm
%   to support an automated workflow.
%
%   [LOW LEVEL, HIGH LEVEL,BW] = manual_thresh(...) also returns the thresholded binary
%   output image, BW.
%
%   Example
%       x = imread('coins.png');
%        [LOW LEVEL, HIGH LEVEL]  = manual_thresh(x')    %MATLAB waits for GUI tool to finish

% By Yishay Tauber JSC,Physics department,Bar Ilan University,Israel.
% Based on thresh_tool by Robert Bemis found in MATLAB CENTRAL



%defensive programming
error(nargchk(1,3,nargin))
error(nargoutchk(0,3,nargout))
```

```
%validate defaultLevel within range
if nargin>2 %user specified DEFAULTLEVEL
  dataType = class(im);
  switch dataType
    case {'uint8','uint16','int16'}
      if defaultLevel<intmin(dataType) | defaultLevel>intmax(dataType)
        error(['Specified DEFAULTLEVEL outside class range for ' dataType])
      elseif defaultLevel<min(im(:)) | defaultLevel>max(im(:))
        error('Specified DEFAULTLEVEL outside data range for IM')
      end
      case{ 'double','single'}
      %okay, do nothing
    otherwise
      error(['Unsupport image type ' dataType])
  end %switch
end

max_colors=1000;    %practical limit

%calculate bins centers
color_range = double(limits(im));
if isinteger(im)
  %try direct indices first
  num_colors = diff(color_range)+1;
  if num_colors<max_colors %okay
    di = 1;                          %inherent bins
  else %too many levels
    num_colors = max_colors;              %practical limit
    di = diff(color_range)/(num_colors-1);
  end
else %noninteger
  %try infering discrete resolution first (intensities often quantized)
  di = min(diff(sort(unique(im(:)))));
  num_colors = round(diff(color_range)/di)+1;
  if num_colors>max_colors %too many levels
    num_colors = max_colors;              %practical limit
    di = diff(color_range)/(num_colors-1);
  end
end
bin_ctrs = [color_range(1):di:color_range(2)];
%new figure - interactive GUI tool for level segmenting
scrsz = get(0,'ScreenSize');

h_fig = figure('Position',[ scrsz(3)/10 scrsz(4)/10 8*scrsz(3)/10 8*scrsz(4)/10]);
set(h_fig,'ToolBar','Figure')
if nargin>1 && isstr(cmap) && strcmp(lower(cmap),'jet')
  full_map = jet(num_colors);
elseif nargin>1 && isnumeric(cmap) && length(size(cmap))==2 && size(cmap,2)==3
  full_map = cmap;
else
full_map = gray (num_colors);
end
  h_ax1 = axes('unit','norm','pos',[0.1 0.25 0.8 0.7]);
setappdata(h_fig,'im',im)
%top  - input image
 colormap(full_map);
```

```
imagesc(im);
axis image
axis off
 hold on
sizeim=size(im);
layer=ones (sizeim(1),sizeim(2));
back=ind2rgb(layer,[1 0 0]);
threshimage=image(back);
axis image
axis off
setappdata (h_fig,'threshimage',threshimage);
% bottom - color bar
cbar=colorbar('location','southoutside');
set(cbar,'unit','norm','Position',[0.05 0.05 0.9 0.05]);
set(cbar,'xlim',[0 color_range(2)],'xtick',[0 color_range(2)])


%next to bottom - intensity distribution
h_hist = axes('unit','norm','pos',[0.05 0.1 0.9 0.1]);
n = hist(double(im(:)),bin_ctrs);
bar(bin_ctrs,n)

axis([[0 color_range(2)+1] limits(n(2:end-1))]) %ignore saturated end scaling
set(h_hist,'xtick',[],'ytick',[])
title('Intensity Distribution')
%threshold level - initial guess (graythresh)
lo = double(color_range(1));
  hi = double(color_range(2));
if nargin>2 %user specified default level
  low_level = defaultLevel;
else %graythresh default

  norm_im = (double(im)-lo)/(hi-lo);
  norm_level = graythresh(norm_im); %GRAYTHRESH assumes DOUBLE range [0,1]
  low_level = norm_level*(hi-lo)+lo;
end
high_level=hi;
%uicontrols (text edit & slider)
low_level_edit = uicontrol('Style','edit','unit','norm','Position',[0.055,0.8,0.05,0.03]);
set(low_level_edit,'BackgroundColor','white','String',num2str(floor(low_level)),'callback',@low_level_edit
_Callback);
setappdata(h_fig,'low_level_edit',low_level_edit);
high_level_edit = uicontrol('Style','edit','unit','norm','Position',[0.055,0.72,0.05,0.03]);
set(high_level_edit,'BackgroundColor','white','String',num2str(ceil(high_level)),'callback',@high_level_edit
_Callback);
setappdata(h_fig,'high_level_edit',high_level_edit);
low_level_slider=uicontrol('Style','slider','unit','norm','Position',[0.005,0.77,0.1,0.03]);
high_level_slider=uicontrol('Style','slider','unit','norm','Position',[0.005,0.69,0.1,0.03]);
set (low_level_slider,'Value',low_level,'Min',lo,'Max',hi,'SliderStep',[(1/(hi-lo))
0.1],'callback',@low_level_slider_Callback);
set (high_level_slider,'Value',low_level,'Min',lo,'Max',hi,'SliderStep',[(1/(hi-lo))
0.1],'callback',@high_level_slider_Callback);
setappdata(h_fig,'low_level_slider',low_level_slider);
setappdata(h_fig,'high_level_slider',high_level_slider);
uicontrol('Style','text','String','low:','unit','norm','Position',[0.005,0.8,0.05,0.03]);
uicontrol('Style','text','String','high:','unit','norm','Position',[0.005,0.72,0.05,0.03]);
```

```
%display level as vertical line
axes(h_hist)
h_lev = vline(low_level,'-');
h_lev2 = vline(high_level,'-');
set(h_lev,'LineWidth',2,'color',0.5*[1 0 0],'UserData',low_level)
set(h_lev2,'LineWidth',2,'color',0.5*[0 0 1],'UserData',high_level)
setappdata(h_fig,'h_lev',h_lev)
setappdata(h_fig,'h_lev2',h_lev2)
%attach draggable behavior for user to change level
move_vlines(h_lev,h_lev2,@update_plot);

update_plot

%add reset button
h_reset = uicontrol('unit','norm','pos',[0.0 0.95 .1 .05]);
set(h_reset,'string','Reset','callback',@ResetOriginalLevel)

if nargout>0 %return result(s)
  h_done = uicontrol('unit','norm','pos',[0.9 0.95 0.1 0.05]);
  set(h_done,'string','Done','callback','delete(gcbo)') %better
  %inspect(h_fig)
  set(h_fig,'WindowStyle','modal')
  waitfor(h_done)
  if ishandle(h_fig)
    h_lev = getappdata(gcf,'h_lev');
    level = mean(get(h_lev,'xdata'));
    h_lev2 = getappdata(gcf,'h_lev2');
    level2 = mean(get(h_lev2,'xdata'));
    if nargout>2
        thresh = getappdata(gcf,'threshimage');
      bw = logical(get(thresh,'AlphaData'));
    end
    delete(h_fig)
  else
    warning('THRESHTOOL:UserAborted','User Aborted - no return value')
    level = [];
  end
end

end %manual_thresh (mainfunction)


function ResetOriginalLevel(hObject,varargin) %subfunction
h_lev = getappdata(gcf,'h_lev');
init_level = get(h_lev,'UserData');
set(h_lev,'XData',init_level*[1 1])
h_lev2 = getappdata(gcf,'h_lev2');
high_level = get(h_lev2,'UserData');
set(h_lev2,'XData',high_level*[1 1])
update_plot
end %ResetOriginalLevel (subfunction)


function update_plot %subfunction
im = getappdata(gcf,'im');
h_lev = getappdata(gcf,'h_lev');
```

```
h_lev2 = getappdata(gcf,'h_lev2');
low_level = mean(get(h_lev,'xdata'));
high_level = mean(get(h_lev2,'xdata'));
text1=getappdata(gcf,'low_level_edit');
text2=getappdata(gcf,'high_level_edit');
slider1=getappdata(gcf,'low_level_slider');
slider2=getappdata(gcf,'high_level_slider');
 set (text1,'String',num2str(floor(low_level))); set (slider1,'Value',floor(low_level));
 set (text2,'String',num2str(ceil(high_level))); set (slider2,'Value',ceil(high_level));
h_ax1 = getappdata(gcf,'threshimage');
%segmented image using upper layer with tranperent background
bw = (((im>=low_level).*(im<=high_level)));
 set(h_ax1, 'AlphaData', bw);

end %update_plot (subfunction)


%function rgbsubimage(im,map), error('DISABLED')


%-----------------------------------------------------------------------
function move_vlines(handle1,handle2,DoneFcn) %subfunction
%move_vlines implements horizontal movement of two lines.
%
%
%Note: This tools strictly requires MOVEX_TEXT, and isn't much good
%      without VLINE by Brandon Kuczenski, available at MATLAB Central.
%<http://www.mathworks.com/matlabcentral/fileexchange/loadFile.do?objectId=1039&objectType=file>

% This seems to lock the axes position
set(gcf,'Nextplot','Replace')
set(gcf,'DoubleBuffer','on')

h_ax=get(handle1,'parent');
h_fig=get(h_ax,'parent');
setappdata(h_fig,'h_vline',handle1)
setappdata(h_fig,'h_vline2',handle2)
if nargin<3, DoneFcn=[]; end
setappdata(h_fig,'DoneFcn',DoneFcn)
set(handle1,'ButtonDownFcn',@DownFcn)
set(handle2,'ButtonDownFcn',@DownFcn2)
  function DownFcn(hObject,eventdata,varargin) %Nested--%
    set(gcf,'WindowButtonMotionFcn',@MoveFcn)          %
    set(gcf,'WindowButtonUpFcn',@UpFcn)                %
  end %DownFcn-----------------------------------------%
function DownFcn2(hObject,eventdata,varargin) %Nested--%
    set(gcf,'WindowButtonMotionFcn',@MoveFcn2)         %
    set(gcf,'WindowButtonUpFcn',@UpFcn)                %
  end %DownFcn-----------------------------------------%

  function UpFcn(hObject,eventdata,varargin) %Nested----%
    set(gcf,'WindowButtonMotionFcn',[])                %
    DoneFcn=getappdata(hObject,'DoneFcn');             %
    if isstr(DoneFcn)                                  %
      eval(DoneFcn)                                    %
    elseif isa(DoneFcn,'function_handle')              %
```

```
    feval(DoneFcn)                              %
  end                                         %
end %UpFcn-----------------------------------------%

function MoveFcn(hObject,eventdata,varargin) %Nested------%
  h_vline=getappdata(hObject,'h_vline');              %
  h_ax=get(h_vline,'parent');                       %
  cp = get(h_ax,'CurrentPoint');                     %
  h_fig=get(h_ax,'parent');
  high_level=get (getappdata(h_fig,'h_vline2'),'XData');
  xpos = cp(1);
  x_range=get(h_ax,'xlim');%
  x_range=[x_range(1) high_level(1)];                        %
  if xpos<x_range(1), xpos=x_range(1); end            %
  if xpos>x_range(2), xpos=x_range(2); end            %
  XData = get(h_vline,'XData');                     %
  XData(:)=xpos;                                  %
  set(h_vline,'xdata',XData)                        %


 end %MoveFcn-----------------------------------------%
function MoveFcn2(hObject,eventdata,varargin) %Nested------%
  h_vline=getappdata(hObject,'h_vline2');              %
  h_ax=get(h_vline,'parent');                       %
  cp = get(h_ax,'CurrentPoint');                     %
  h_fig=get(h_ax,'parent');
  low_level=get (getappdata(h_fig,'h_vline'),'XData');
  xpos = cp(1);
  x_range=get(h_ax,'xlim');%
  x_range=[low_level(1) x_range(2)];                        %
  if xpos<x_range(1), xpos=x_range(1); end            %
  if xpos>x_range(2), xpos=x_range(2); end
  XData = get(h_vline,'XData');                     %
  XData(:)=xpos;                                  %
  set(h_vline,'xdata',XData)                        %

 end %MoveFcn-----------------------------------------%

end %move_vlines(subfunction)



%---------------------------------------------------------------------
function [x,y] = limits(a) %subfunction
% LIMITS returns min & max values of matrix; else scalar value.
%
%   [lo,hi]=LIMITS(a) returns LOw and HIgh values respectively.
%
%   lim=LIMITS(a) returns 1x2 result, where lim = [lo hi] values

if nargin~=1 | nargout>2 %bogus syntax
  error('usage: [lo,hi]=limits(a)')
end

siz=size(a);
```

```
if prod(siz)==1 %scalar
  result=a;                    % value
else %matrix
  result=[min(a(:)) max(a(:))];     % limits
end

if nargout==1 %composite result
  x=result;                    % 1x2 vector
elseif nargout==2 %separate results
  x=result(1);                  % two scalars
  y=result(2);
else %no result
  ans=result                   % display answer
end

end %limits (subfunction)




%-----------------------------------------------------------------------------------------------------------
function hhh=vline(x,in1,in2) %subfunction
% function h=vline(x, linetype, label)
%
% Draws a vertical line on the current axes at the location specified by 'x'.  Optional arguments are
% 'linetype' (default is 'r:') and 'label', which applies a text label to the graph near the line.  The
% label appears in the same color as the line.
%
% The line is held on the current axes, and after plotting the line, the function returns the axes to
% its prior hold state.
%
% The HandleVisibility property of the line object is set to "off", so not only does it not appear on
% legends, but it is not findable by using findobj.  Specifying an output argument causes the function to
% return a handle to the line, so it can be manipulated or deleted.  Also, the HandleVisibility can be
% overridden by setting the root's ShowHiddenHandles property to on.
%
% h = vline(42,'g','The Answer')
%
% returns a handle to a green vertical line on the current axes at x=42, and creates a text object on
% the current axes, close to the line, which reads "The Answer".
%
% vline also supports vector inputs to draw multiple lines at once.  For example,
%
% vline([4 8 12],{'g','r','b'},{'l1','lab2','LABELC'})
%
% draws three lines with the appropriate labels and colors.
%
% By Brandon Kuczenski for Kensington Labs.
% brandon_kuczenski@kensingtonlabs.com
% 8 November 2001

% Downloaded 8/7/03 from MATLAB Central
% http://www.mathworks.com/matlabcentral/fileexchange/loadFile.do?objectId=1039&objectType=file

if length(x)>1  % vector input
```

```
    for I=1:length(x)
       switch nargin
       case 1
          linetype='r:';
          label='';
       case 2
          if ~iscell(in1)
             in1={in1};
          end
          if I>length(in1)
             linetype=in1{end};
          else
             linetype=in1{I};
          end
          label='';
       case 3
          if ~iscell(in1)
             in1={in1};
          end
          if ~iscell(in2)
             in2={in2};
          end
          if I>length(in1)
             linetype=in1{end};
          else
             linetype=in1{I};
          end
          if I>length(in2)
             label=in2{end};
          else
             label=in2{I};
          end
       end
       h(I)=vline(x(I),linetype,label);
    end
 else
    switch nargin
    case 1
       linetype='r:';
       label='';
    case 2
       linetype=in1;
       label='';
    case 3
       linetype=in1;
       label=in2;
    end



    g=ishold(gca);
    hold on

    y=get(gca,'ylim');
    h=plot([x x],y,linetype);
```

```
    if length(label)
        xx=get(gca,'xlim');
        xrange=xx(2)-xx(1);
        xunit=(x-xx(1))/xrange;
        if xunit<0.8
            text(x+0.01*xrange,y(1)+0.1*(y(2)-y(1)),label,'color',get(h,'color'))
        else
            text(x-.05*xrange,y(1)+0.1*(y(2)-y(1)),label,'color',get(h,'color'))
        end
    end

    if g==0
    hold off
    end
    set(h,'tag','vline','handlevisibility','off')
end % else

if nargout
    hhh=h;
end

end %vline (subfunction)
%callbacks for the uicontrols
function low_level_edit_Callback (hObject, eventdata)
      level=str2double(get(hObject,'String')) ;
      h_lev = getappdata(gcf,'h_lev');
      h_lev2 = getappdata(gcf,'h_lev2');
           high=get(h_lev2,'XData');
            slidermin=floor(get(getappdata(gcf,'low_level_slider'),'Min'));
     if (level<=slidermin)
        set(hObject,'String',num2str(slidermin));
        set(h_lev,'XData',slidermin*[1 1])
     elseif (level<high(1))
      set(h_lev,'XData',level*[1 1])
      else
      set(h_lev,'XData',high);
          end
       feval(@update_plot)
end
function high_level_edit_Callback (hObject, eventdata)
      level=str2double(get(hObject,'String')) ;
      h_lev = getappdata(gcf,'h_lev');
      h_lev2 = getappdata(gcf,'h_lev2');
     low=get(h_lev,'XData');
     slidermax=ceil(get(getappdata(gcf,'high_level_slider'),'Max'));
     if (level>=slidermax)
        set(hObject,'String',num2str(slidermax));
        set(h_lev2,'XData',slidermax*[1 1])
     elseif (level>low(1))
      set(h_lev2,'XData',level*[1 1])
          else
      set(h_lev2,'XData',low)
                end
       feval(@update_plot)
end
function low_level_slider_Callback (hObject, eventdata)
```

```
level=get(hObject,'Value') ;
      h_lev = getappdata(gcf,'h_lev');
      h_lev2 = getappdata(gcf,'h_lev2');
      high=get(h_lev2,'XData');
                if (level<high(1))
      set(h_lev,'XData',level*[1 1]);
           else
      set(h_lev,'XData',high);
     set (text,'String',num2str(ceil(high(1))));
         end
       feval(@update_plot)
end
function high_level_slider_Callback (hObject, eventdata)
      level=get(hObject,'Value') ;
      h_lev = getappdata(gcf,'h_lev');
      h_lev2 = getappdata(gcf,'h_lev2');
     low=get(h_lev,'XData');
          if (level>low(1))
      set(h_lev2,'XData',level*[1 1])
           else
      set(h_lev2,'XData',low)
            end
       feval(@update_plot)
end
```

Surface Clear

```
%% SURFACE CLEAR - 2013 -
% ---------------------------------------------------------------
% UNIVERSITY OF MINNESOTA - DEPARTMENT OF BIOMEDICAL ENGINEERING
% TRANQUILLO LAB - DEPARTMENT OF BIOMEDICAL ENGINNERING
% ---------------------------------------------------------------
% Nathan Weidenhamer
% Fluvio Lobo
% ------------------------------------------------------------------------
% *The following program, has the purpose of eliminating the noise
% generated by objects above the marked surface of the section.
% ------------------------------------------------------------------------
%
function [wnum1, wnum2, bw] = surfclear(Yloc, Xloc, bw)
% The following process seeks to eliminate all the information (cells)
% beyond the surface, in the opposite direction of migration.
% BW = zeros(size(bw));
S = size(bw);
Y1 = sort(Yloc); % Verical coordinates are flipped and aorted to allow for
              % looping
% White pixel counters to determine the level of noise.
wnum1 = 0;
wnum2 = 0;
% Outter loop goes through the vertical axis
for i = 1:length(Y1)
%%% The inner loops examine the horizontal axis in both sides of the
%%% surface
   yc = find(Yloc==Y1(i)); % Finds the index of the first value of the
                        % sorted "Y" array, to find the actual value in
```

```
                    % the original "Yloc" array.
   for j = 1:Xloc(yc) % Then, using the same index, we find the
                    % corresponding "Xloc" value
      wcoord1 = find(bw(Yloc(yc),j)==1);
      wnum1 = wnum1 + length(wcoord1);
   end
%%% Second inner loop
   for j = Xloc(yc):S(2)
      wcoord2 = find(bw(Yloc(yc),j)==1);
      wnum2 = wnum2 + length(wcoord2);
   end

end %This loop returns the wnum1 and wnum2 values which allow the code to
   %determine the region with noise.

for i = 1:length(Y1)
   % A similar strategy, as shown above, for indexing is used here
   yc = find(Yloc==Y1(i));
   % However, now we have a conditional
   if wnum1 < wnum2
      xc = 1:Xloc(yc); % From 1:Surface
   else
      xc = Xloc(yc):S(2); % From Surface:Image-far-edge
   end
   % Loop around the X values that follow the conditional direction above
   for j = xc
      % Printing!
      bw(Yloc(yc),j) = 0;
   end
end %This loops returns the updated image without the noise

 end % End-of-Function
```